Implementation of artificial neural network in predicting the mechanical properties of concrete at high temperatures

by

Sanaz Ramziaraghi

A thesis submitted to the Faculty of Graduate and Postdoctoral Affairs in partial fulfillment of the requirements for the degree of

Master of Applied Science

in

Civil Engineerings

Carleton University
Ottawa, Ontario

Abstract

Concrete might be exposed to high temperatures caused by fire that adversely affect its mechanical properties. Therefore, the ability to predict the mechanical properties of concrete exposed to high temperatures is necessary. In this study, Artificial Neural Network (ANN) models were developed to assess the mechanical properties of concrete exposed to high temperatures. For this purpose, 728 experimental results were collected from the available literature to predict mechanical properties of concrete at high temperatures, including compressive strength, tensile strength, and modulus of elasticity. The input database contains the volumes of coarse aggregate, fine aggregate, water, cement, water-cement ratio, coarse aggregate type, percentage of supplementary cementitious materials as the cement replacement, temperatures, and test methods. The mechanical properties were defined as the output variable. Proposed models are in good agreement with the experimental data and can predict the mechanical properties of concrete exposed to high temperatures.

Acknowledgments

First and foremost, I would like to express my sheer gratitude and appreciation for my supervisor Professor Hamzeh Hajiloo for his encouragement, patience, continuous support and invaluable guidance throughout this research and during my Master of Applied Science program at Carleton University.

I must express my profound gratitude to my husband, Sepher, for his patience, endless support and encouragement. Finally, I would like to thank my parents and my sister for their continuous encouragement and support.

Table of Contents

List of Tables

List of Illustrations

Chapter 1: Introduction

Concrete is one of the most common construction materials susceptible to fire attacks during its service life, resulting in serious damage to the structures while causing casualties and property loss [1]. Several mechanical and environmental factors can influence the deterioration of concrete when exposed to high temperatures, such as the level of high temperatures, humidity, the applied load, the heating time, the cooling method after heating, the aggregate type, the mineral admixtures, and the inclusion ratios [2]. Many experimental studies have been carried out to investigate the performance of concrete containing different types of aggregate and admixtures (silica fume, fly ash, and ground granulated blast furnace slag) under high temperatures effects. The results of these studies revealed that concrete exhibits a nonlinear mechanical behaviour at high temperatures. There are a number of temperature-dependent and highly complex properties that control its response under high temperatures [3]. Due to the extensive use of concrete, a comprehensive understanding of how fire impacts concrete is necessary [4].

There are many conventional types of linear and nonlinear regression models in the literature for the prediction of mechanical properties of concrete that were based primarily on empirical relationships derived from statistical analysis of experimental data [5]. Multiple drawbacks are associated with the development of these models. Conventional models perform poorly in the case of nonlinear and complex materials. Thus, to overcome the drawbacks of these conventional models, Machine Learning (ML) techniques can be used as an alternative method for predicting the mechanical properties of concrete. In recent years, the implementation of ML methods such as artificial neural networks (ANNs),

which are inspired by the human brain information process, acquired considerable attention in solving the complex and nonlinear problems of civil engineering, as in the case of concrete behaviour at high temperatures [6, 7].

The main objectives of the present study are as follows:

1. A comprehensive review of existing literature on the mechanical properties of concrete at high temperatures has been conducted. A meticulous data collection from experimental studies was performed to generate a database to enhance the understanding of the matter and to identify the key parameters influencing the degradation behaviour of concrete at high temperatures.
2. Reliable and accurate models were established to predict the mechanical properties (i.e., compressive strength, tensile strength, and modulus of elasticity) of concrete during and after exposure to high temperatures using artificial neural networks based on data collected from previous experimental studies existing in the literature.
3. The proposed model results can be implemented to predict the behaviour of concrete exposed to high temperatures for different ingredients under the effects of high temperatures and the test methods (i.e. Transient, steady-state and residual test).
4. This study covers past studies along with recent efforts to analyze fire resistance of materials that provide a basis for a better understanding of the behaviour of new construction materials, particularly concrete containing different amounts and types of supplementary cementitious materials (SCMs).

1.1 Research Methodology

The methodology for the development of the ANN models in this research is as follows:

1. A comprehensive literature review was conducted based on previous experimental studies to understand the behaviour of concrete and its constituents at high temperatures and identify the most influential parameters.
2. A large and reliable database was collected from available experimental research on the mechanical properties of concrete exposed to high temperatures for training, validation, and testing the artificial neural network models. All the data points were supplied to the model in the form of input and corresponding output variables.
3. The Levenberg-Marquardt backpropagation algorithm, as the fastest converging method, was used for training, whereas Tansig and Purlin activation functions were selected to provide better precision of predicted results of developed models.
4. The ANN models were developed for predicting the mechanical properties of concrete subjected to high temperatures using the MATLAB program R2021a.
5. The best configuration of ANN was selected using a trial-and-error approach. In other words, the models have run several times in the MATLAB program to find the optimal architecture of networks based on comparing the error values between the results of the ANN model and the actual results.

1.2 Organization of the thesis

Based on the scope of the investigation described earlier, this thesis was organized as follows:

Chapter 1 presents a general introduction of the present study and describes the main objectives to achieve. Chapter 2 provides a general literature review covering the behaviour of concrete produced by the different types of SCMs and aggregates and an overview of ML and ANN techniques that have been applied for predicting the mechanical characteristics of concrete at room temperature and high temperatures. Chapter 3 provides the process of developing artificial neural network models and evaluates the performance of the proposed networks to determine the optimum architecture for ANN models in this research. Chapter 4 presents the parametric analysis to show the generalization capability of the model in estimating the mechanical characteristics of concrete at high temperatures. Chapter 5 highlights the main conclusions and recommendations drawn from the present research and provides recommendations for future research.

Chapter 2: Literature review

This chapter provides a summary of the available literature on the influence of high temperatures on the mechanical properties of different types of concrete referenced in this thesis, along with an overview of the implementation of artificial neural networks in the civil engineering area to predict concrete properties.

2.1 Introduction

In most structures and buildings, fire is considered a serious potential risk [8]. This is due to the drastic microstructural thermo-physio-chemical degradations that occur in properties of construction materials under high temperatures and may never recover their pre-fire properties even after it has cooled to ambient temperature [9].

As a structural material, concrete is widely used in building construction because of its considerable advantages, such as durability, strength, and non-combustibility [10]. Concrete is possibly exposed to high temperatures caused by fire or other reasons. The mechanical properties such as compressive and tensile strength and modulus of elasticity of concrete are significantly decreased when exposed to high temperatures [11]. Concrete undergoes a series of chemical and physical changes, such as disintegrating of hydration products and aggregates, evaporation of water, increased porosity and microstructure coarsening exposed to high temperatures. The deterioration of the mechanical properties of concrete at high temperatures can be attributed to these changes at high temperatures [12]. Under high temperatures, the behaviour of concrete as a composite material is highly influenced by the properties of its constituents such as aggregates, water, and binder, including cement and supplementary cementing materials. Therefore, investigating the

influence of concrete constituents at high temperatures is of great significance. Several studies and experimental work have been conducted to investigate the properties of different types of concrete subjected to high temperatures. The present study aims to provide an analytical review and discussion of the existing findings regarding the residual compressive and tensile strength as well as modulus of elasticity at high temperatures. This study mainly focuses on the effects of cement replacement with different SCMs and aggregate types on the performance of concrete after high-temperature exposure. In addition, the mechanical behaviour of concrete at room temperature is also highlighted to better understand the response of concrete at high temperatures.

The properties of concrete exposed to high temperatures are typically measured through three different test methods: transient, steady-state, and residual tests. In the case of the transient test, the specimens are first pre-loaded (typically 20–40% of the ultimate compressive strength) and then subjected to high temperature to failure [13]. Figure 2-1 illustrates the failure of a concrete specimen during the transient test [14]. In the steady-state test, the concrete specimens are heated (without a pre-load) until they reach a uniform temperature, and then the specimens are loaded to failure. The concrete specimens in the residual test method are heated at a constant rate of temperature (without a pre-load) until specimens reach a thermal steady state. Then the load is applied at the specified rate after specimens are cooled to room temperature until failure occurs [13]. The residual test under two cooling methods (air-cooled and water-cooled) is shown in Figure 2-2.

The first two types of tests are suitable for evaluating the properties of concrete during high temperatures, while the residual test, which the researchers widely adopt, is excellent for determining the post-fire concrete properties [14].

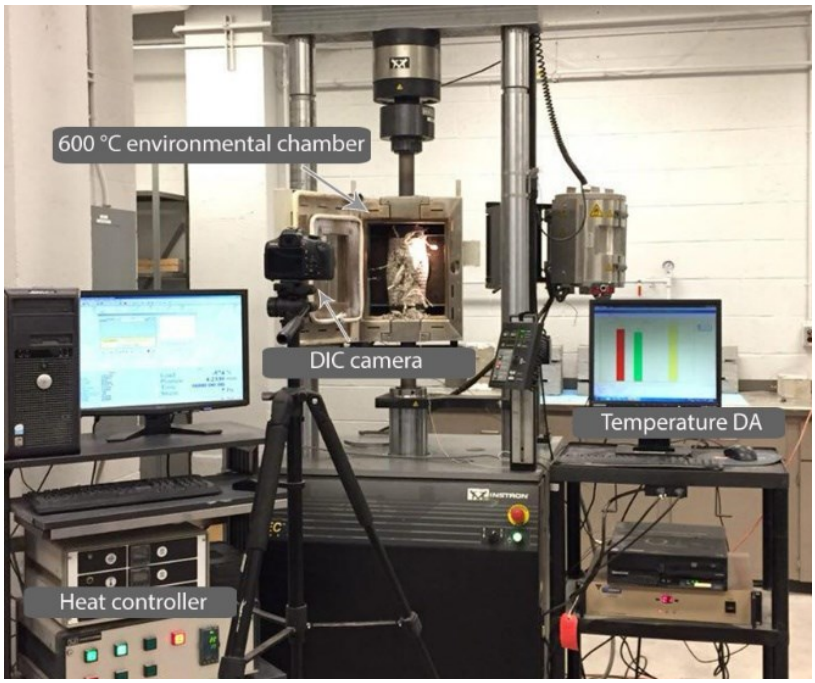

Figure 2-1. The test setup at high temperatures [15]

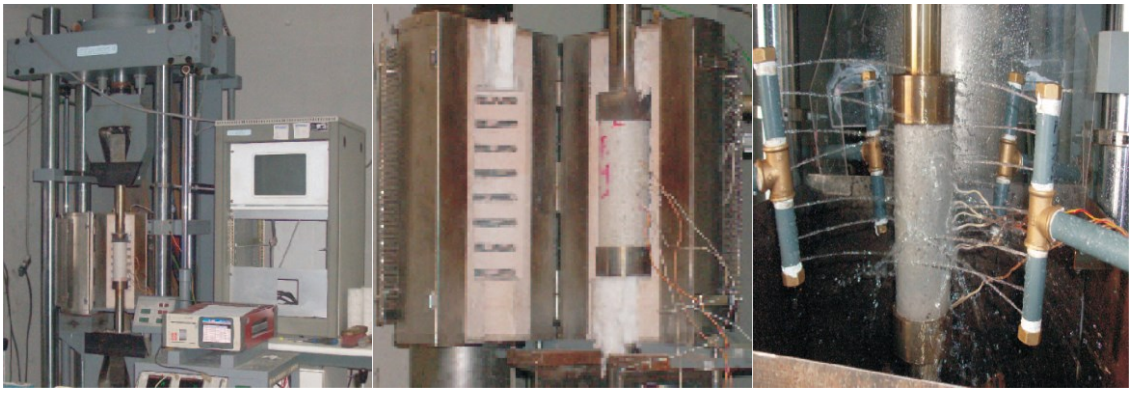

a) b) c)

Figure 2-2. Residual compressive strength testing: a) test setup; b) cooling in the air; c) cooling with water jets [16]

2.2 Supplementary Cementitious Materials (SCMs)

The manufacturing process of cement as the primary component of concrete requires a high level of raw materials of natural resources as well as produces huge amounts of CO_2

emission [17]. Replacement of cement with supplementary cementitious materials is one of the most effective alternative preventive solutions for reducing the environmental impact of cement production [17, 18]. Moreover, using the SCMs as the by-product material results in reducing industrial waste, and in some cases, this can reduce the cost of the concrete by reducing the cement content in concrete. Nowadays, supplementary cementitious materials such as silica fume, fly ash, and blast furnace slag are extensively used in concrete as partial cement replacement materials due to their ability to improve concrete properties [19]. The influence of different types of supplementary cementing materials on the mechanical behaviour of concrete at room and high temperatures are discussed in detail in the following sub-sections. Table 2-1 and Table 2-2 summarize the investigations conducted on the effect of supplementary cementitious materials on the mechanical properties of concrete at room temperature and high temperatures, respectively.

Table 2-1. Summary of research on the effect of SCMs on mechanical properties of concrete at room temperature

Year	Source	SCMs	Replacement levels (%)	Curing age (days)	w/b	Mechanical properties tested
2008	[20]	SF	0, 6, 10	7, 28	0.3, 0.4	*f'c*
2010	[21]	SF	0, 6, 10	28	0.3, 0.4	*f'c,ft*
2019	[22]	SF	10	3, 7, 28, 56	0.4	*f'c,ft*
2004	[23]	SF	0,6, 10, 15	7, 14, 28, 42, 90, 365, 400	0.35	*f'c,E*
1987	[24]	SF	0,5,10, 15, 20, 25	7, 28, 56, 91	0.28, 0.34	*f'c*
2005	[25]	SF	0,5,10, 15, 20, 25, 30	28	0.26, 0.30, 0.34, 0.38, 0.42	*f'c,ft*
1993	[26]	SF	0,5,10, 15, 20	28, 91, 182, 1-5 years	0.25, 0.36	*f'c,ft,E*
1994	[27]	SF	0, 10, 20, 25	1, 7, 28, 56	0.3, 0.4, 0.57	*f'c,E*
2018	[28]	FA	0, 20, 30	3, 7,28, 90, 180, 365	0.4	*f'c*
2004	[29]	FA	0, 40, 45, 50	7, 28, 91, 35	0.4, 0.41	*f'c,ft,E*
2018	[30]	FA	0, 10, 25, 50	7, 28, 60, 90	0.35, 0.45	*f'c*
2011	[31]	FA	0,10, 20, 30	1, 3, 7, 14, 28, 90, 180, 365	0.28	*f'c,E*
1998	[32]	FA	0, 15, 25, 45, 55	3, 7, 28, 90, 180	0.3, 0.4, 0.5	*f'c,ft*
2008	[33]	S	1, 3, 7, 28	0, 25, 40, 50, 60	0.31, 0.38	*f'c*
2011	[31]	S	0, 20, 40, 60	1, 3, 7, 14, 28, 90, 180, 365	0.28	*f'c,E*
2008	[34]	S	0, 50, 60, 70, 80	28, 90	0.4	*f'c,ft*
2005	[35]	S	0, 20, 30, 40, 50, 60,70	1, 7, 14, 28, 90	0.5	*f'c,E*
2000	[36]	S	0, 25, 50, 75	28	0.42	*f'c,ft*
2012	[37]	S	0, 20, 40, 60	28	0.45	*f'c,ft*
1990	[38]	S	0, 50, 65	1, 3, 7, 28	0.4,0.43, 045, 0.46, 0.5	*f'c,E*

Table 2-2. Summary of research on the effect of SCMs on mechanical properties of concrete exposed to high temperature

Year	Source	SCMs	Replacement levels (%)	Temperatures (°C)	w/b	Mechanical properties tested
2008	[20]	SF	0, 6, 10,	20-600	0.3, 0.4	*f'c*
2010	[21]	SF	0, 6, 10,	20-600	0.3, 0.4	*f'c,ft*
2008	[44]	SF	0, 5, 10	20-1000	0.42, 0.45, 0.53, 0.55, 0.58	*f'c*
2001	[45]	SF	0, 20, 30, 40	20-800	0.3	*f'c*
2008	[47]	SF	0, 10, 20, 30	20-800	0.77	*f'c, ft*
2001	[46]	SF	0, 10	25-450	0.22, 0.33, 0.57	*f'c,E*
2017	[57]	FA	0, 30	20-550	0.53,0.56	*f'c*
2017	[58]	FA	0, 30, 50, 70, 90	20- 800	0.35	*f'c*
2015	[59]	FA	0, 40, 50, 60	35- 800	0.35	*f'c, ft*
2003	[60]	FA	0, 25, 55	23-800	0.3, 0.5	*f'c ft*
2014	[61]	FA	0, 20, 40, 60	27-800	0.33	*f'c*
2001	[45]	FA	0, 30, 40	20-800	0.3	*f'c*
2008	[62]	FA	0, 10, 20, 30	20-800	0.77	*f'c, ft*
1979	[63]	FA	25	21- 232	0.5	*f'c, E*
2012	[64]	S	0, 20, 40, 60	27-350	0.45	*f'c, ft*
2012	[67]	S	0,10,30,50	150- 700	0.41	*f'c,E*
2017	[58]	S	0, 30, 50, 70, 90	20-800	0.35	*f'c*
2019	[68]	S	30, 50, 70	20-800	0.47	*f'c*

2.2.1 The Effects of Silica Fume at room temperature

An electric arc furnace produces silica fume as a by-product of smelting of the silicon and ferrosilicon [39, 40]. At the temperature of 2000 °C, high-purity quartz reduction to silicon results in SiO_2 vapours, which oxidize and condense to form tiny particles of amorphous silica in the low-temperature zone. Silica fume is also referred to as condensed silica fume, micro silica, volatilized silica or silica dust. Over 95% of silica fume particles are finer than 1 μm [40, 41]. The influence of SF in concrete is physicochemical. The physical phase is related to extremely fine particles, which act as a filler to fill the spaces between the particles of cement. In the chemical phase, the SF reacts chemically with calcium hydroxide $Ca(OH)_2$, leading to calcium silicate hydrate (CSH) formation in the concrete.

2.2.1.1 Compressive Strength

Behnood et al. [20] investigated the compressive strength of high-strength concrete (HSC) that contained 0,6 and 10% of silica fume as the cement replacement at room temperature and after exposure to high temperature. Compared to the mixture without SF, the 28-day compressive strength of concrete mixtures containing 6 and 10% SF increased by 19% and 25%, respectively. This can be attributed to the reaction between SF and calcium hydroxide leading to the formation of calcium silicate hydrate (CSH), which increases the strength of concrete. However, the increasing rate of strength is lower at the early ages because of the lower calcium hydroxide content. A similar test was conducted by Ghandehari et al. [21]. They found that cement replacement by 6 and 10% SF increased the compressive strength at room temperature by 20 and 36%, respectively, compared to Ordinary Portland Cement (OPC) concrete. They observed that the higher strength of SF concrete was due to the reaction between the SF and $Ca(OH)_2$. As a result of these reactions, the secondary calcium silicate hydrates are formed and occupy the pores generated during hydration. This reaction provides a stronger matrix compared to OPC concrete.

Kim et al. [22] studied the effect of three types of coarse aggregates, granite, quartzite, and basalt, and the use of 10 % silica fume to replace cement on the compressive strength of concrete at curing ages of 3, 7, 28, and 56 days. It was observed that the specimens composed of basalt aggregate and silica fume showed higher compressive strength than those made with quartzite and granite aggregates. This is due to the higher strength of the basalt aggregate compared to the other aggregates and the improvement of the interfacial transition zone (ITZ) caused by the filling effect of fine particles of SF.

Mazloom et al. [23] examined the effect of replacing cement with 0, 6, 10, and 15% of SF on the compressive strength of high strength concrete at different ages between 7 and400 days. Once compared to OPC concrete, it was observed that silica fume caused an increase in compressive strength of concrete up to 90 days. However, there were no significant changes in the strength of concrete for long-term strength at 400 days. This was due to the formation of a layer that inhibits the further reaction between calcium hydroxide and silica fume at longer ages. Similar findings for concrete containing 0, 10, 15, and 20% up to 5 years were observed in the experimental study conducted by Hooton [26].

Yogendran et al. [24] examined the compressive strength of concrete prepared with substitution cement by 0, 5, 10, 15, 20, and 25% of SF with two different water to binder (cement and other binding materials) ratios (w/b) ratios of 0.28 and 0.34 at the age of 28, 56, and 91 days. The results revealed that at the w/b ratio of 0.34, maximum compressive strength was obtained for concrete of 15% silica fume replacement at all ages. However, at the w/b ratio of 0.28, equal or marginally lower compressive strength than the concrete mixture without SF was observed at 5, 10, and 15% replacement levels at 28 and 56 days. The lower strength was observed for concrete with 20% SF. They concluded that the influence of silica fume decreased with increasing SF content and declining w/b ratios.

Bhanja et al. [25] evaluated the compressive strength of SF concrete at room temperature. In concrete specimens, silica fume was replaced with cement at levels of 0, 5,10, 15, 20, 25, and 30%. The water to binder (w/b) ratio was between 0.26 and 0.42. It was observed that the incorporation of silica fume in concrete improved the concrete compressive strength. It was reported that the optimum replacement level of silica fume depends on the

w/b ratio and has varied from 15% to 25% replacement ratios. Similar observations have been reported by Katkhuda et al. [42].

Figure 2-3 shows the relative compressive strength of SF concrete versus the curing ages reported by Mazloom et al. [23] and Hooton [26]. As seen in Figure 2-3, replacing cement with SF increases the compressive strength of concrete compared to OPC concrete. This enhancement in compressive strength can be explained by transforming the weak crystals of calcium hydroxide $Ca(OH)_2$ into calcium silicate hydrate (CSH) because of the pozzolanic reaction. Thus, calcium silicate hydrate as a hydration product improves the strength of concrete [43]. The replacement of cement with SF mainly influences the short-term strength of concrete. However, SF concrete has very low long-term strength gain compared to concrete without silica fume at room temperature.

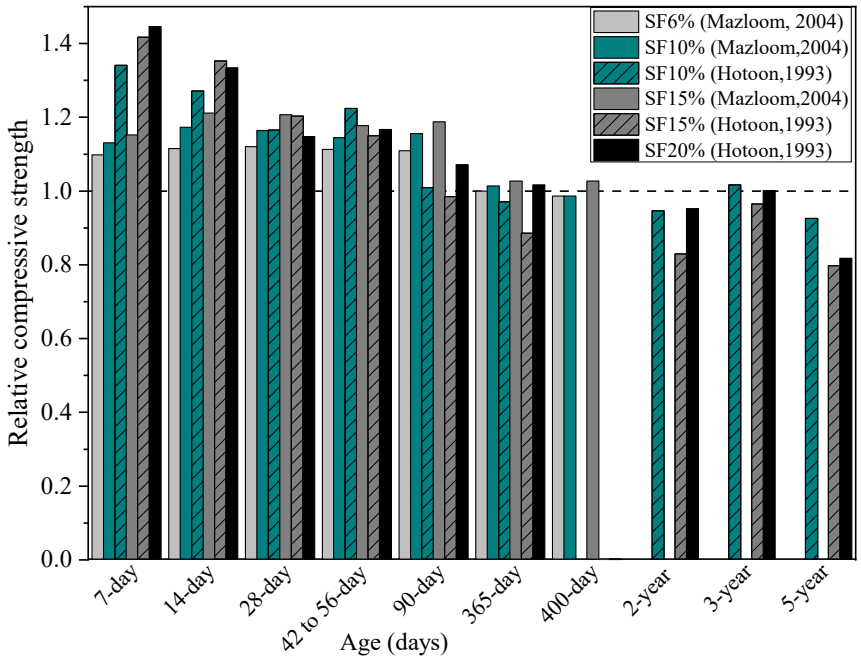

Figure 2-3. Relative compressive strength of SF- contained concrete at various curing ages [23, 26]

2.2.1.2 Splitting Tensile Strength

Bhanja et al. [25] evaluated the splitting tensile strength of concrete incorporating silica fume at the age of 28 days. The mixtures were prepared with 0, 5, 10, 15, 20, 25, and 30% silica fume at w/b ratios of 0.26, 0.30, 0.34, 0.38 and 0.42. The result indicated that the 5–10% replacements of silica fume caused a significant increase in the tensile strength in comparison to the control concrete for all w/b ratios. It was also observed that the enhancement of splitting strength for more than 15% replacement of cement with SF was insignificant.

Hooton et al. [26] studied the influence of cement replacement by 0, 10, 15, and 20% silica fume on the splitting tensile strength of concrete at the age of 28, 91, and 182 days. It was observed that the tensile splitting tensile strength for the SF mixes was not increased except for 28 days. The results demonstrated that the splitting strength of concrete with 10 and 15% SF was approximately equal but greater than concrete without SF at 28 days. However, the concrete with 20% SF exhibited the lowest splitting tensile strength at all ages.

2.2.1.3 Modulus of Elasticity

Khder et al. [27] examined the effect of cement replacement by 0, 10, and 20% silica fume on the modulus of elasticity of concrete. The results showed that the modulus of elasticity of concrete increased with the addition of SF. The best results were achieved from 20% silica fume. Similar findings for secant modulus of elasticity of high strength concrete with 0, 6, 10, and 15% silica fume until to 400 days were reported by Mazloom et al. [23]. They studied the effect of silica fume on the modulus of elasticity concrete at the testing ages

from 28 to 365 days. The results demonstrated that the elastic modulus of the Portland cement concrete and silica fume concretes was approximately equal at the age of 28 days. However, the modulus of elasticity of all specimens increased at advanced ages until one year.

Hooton [26] studied the effect of silica fume on the modulus of elasticity concrete at the ages of 28, 91, 182, and 365 days. The results demonstrated that the elastic modulus of the Portland cement concrete and silica fume concretes was approximately equal at the age of 28 days. However, the modulus of elasticity of all specimens continued to increase at later ages, up to one year.

2.2.2 The Effects of Silica Fume at high temperatures

2.2.2.1 Compressive Strength

Behnood et al. [20] reported how different content of silica fume affect the residual compressive strength of concrete after being exposed to temperatures up to 600 °C. Three concrete mixtures with 0, 6, and 10 % silica fume were prepared with the constant w/b ratio of 0.30. At 100 °C, the concrete compressive strength decreased significantly in comparison to strength at room temperature. A slight increase in residual compressive strength was observed between the temperature of 100 and 200 °C for all the concrete mixtures with or without silica fume. However, this strength recovery is higher in OPC concrete in comparison to SF concrete. This can be attributed to the filler role of extremely fine particles of SF and their pozzolanic reactions, which caused the microstructure of concrete containing Sf to become denser. This, in turn, results in the moisture content of SF concrete not being able to remove freely compared to OPC at 200 °C. In the range of

300–600 °C, the relative residual compressive strength was considerably reduced for all concrete specimens. It was noticed that the relative compressive strength was lower in SF concrete, especially for that containing 10% SF compared to OPC concrete. This was due to the denser transition zone between paste and aggregates formed in SF concrete. Thus, cement paste contraction and aggregate expansion led to higher levels of stress generated in the transition zone. This results in the bonding between cement paste and aggregate being more sensitive in concrete with silica fume than that of the OPC concrete. Similar results were observed by Ghandehari et al. [21].

Sancak et al. [44] determined the influence of the Portland cement replacement with SF at ratios of 0, 5, and 10% on the compressive strength of lightweight concrete (LWC) compared to normal weight concrete (NWC) after subjecting to temperatures of 20, 100, 400, 800, and 1000 °C. Half of the mixtures were prepared by adding the 2% superplasticizer (SP). The results indicated that the 0 and 10% SF specimens perform better than the 5% SF specimens and no SP. The reduction in compressive strength was quite fast at temperatures between 400 and 800 °C. At 1000 °C, no considerable strength was observed for all specimens. A similar response was reported for both LWC and NWC after being exposed to high temperatures. However, the rate of strength loss was lower in LWC than in NWC.

Poon et al. [45] evaluated the compressive strength of high-strength pozzolanic concrete incorporating silica fume as a cement replacement after being subjected to high temperatures up to 800 °C for 60 days. The silica fume content was 0, 5, and 10%. The compressive strength of high-strength concrete with SF decreased slightly at temperatures between 20 and 200 °C. Between temperatures of 200 and 400 °C, hairline cracks appeared

in SF concrete but no spalling. Beyond 400 °C, severe cracking and spalling occurred in SF concrete, and the residual strength of SF concrete was lower than the ordinary Portland cement concrete. This can be attributed to the buildup of vapour pressure produced by chemically and physically bound water evaporation because of the denser structure of SF concrete.

Phan et al. [46] determined the residual mechanical properties of high-performance concrete mixtures with 0 and 10% of silica fume as a replacement for cement and with w/b of 0.22, 0.33, and 0.57 exposed to high temperatures up to 450 °C. It was found that the mixture with similar w/b, cement replacement with 10 % SF, resulted in lower strength loss up to 200 °C. Furthermore, the mixtures with SF and lower w/b demonstrated less strength loss while they were more susceptible to explosive spalling.

There was only one study that investigated the combined effects of lightweight aggregate and SCM. Tanyildizi et al. [47] investigated the effects of SF on the compressive strength of lightweight concrete after being heated to temperatures of 200, 400, and 800 °C. The replacement ratios of SF in this study were: 0, 10, 20, and 30%. Test results revealed that a reduction occurred in the compressive strength for all mixes as the temperature increased. This is attributed to the formation of micro and macro cracks in the concrete because of high temperatures. However, the lightweight concrete containing SF performed better than the lightweight concrete without SF at high temperatures. The highest level of strength was reported in the concrete with 20% silica fume at all temperatures.

It can be concluded that the silica fume incorporation increased the concrete compressive strength at temperatures below 200 °C. However, the strength of SF concrete decreased at

further high temperatures. This was due to the ultra-fine particles and pozzolanic reactions of silica fume resulting in a very dense transition zone between paste and aggregates. Moreover, the concrete containing SF exhibited a denser microstructure which was more prone to severe cracking and spalling because of the accumulation of pore pressures produced by chemically and physically bound water evaporation [23]. The optimum content of silica fume as the cement replacement after exposure to high temperatures has been reported inconsistently by different researchers.

Figure 2-4 illustrates the compressive strength ratio at a particular temperature to concrete compressive strength at room temperature. While the findings by Behnood et al. [20] do not show a notable difference between the OPC and the SF-contained specimens, the results obtained by Poon [45] show that the specimens with higher SF have a slightly higher strength reduction after 400 °C.

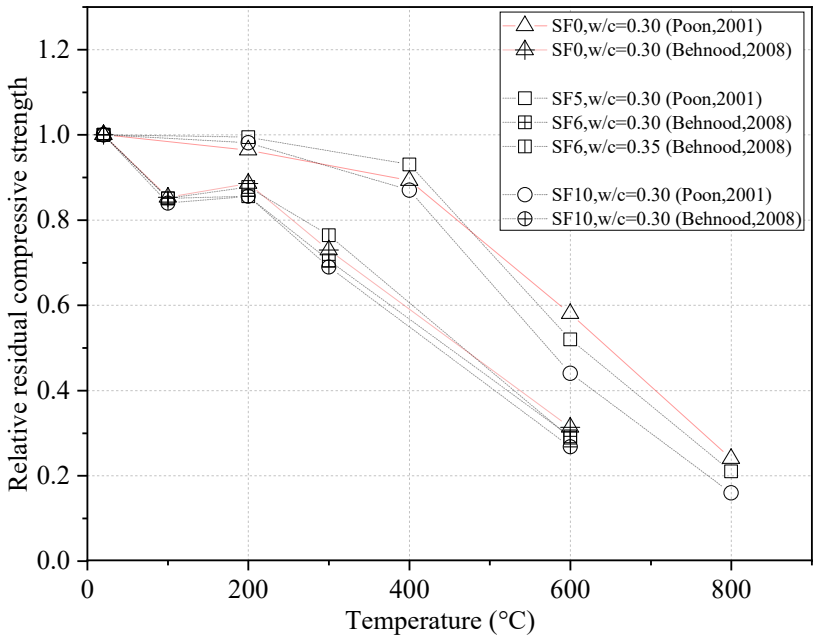

Figure 2-4. Effect of high temperatures on the residual compressive strength of SF-contained concrete [20, 45]

2.2.2.2 Splitting Tensile Strength

Ghandehari et al. [21] studied the splitting tensile strength of high-strength concrete containing SF (0, 6, and 10%) when subjected to high temperatures up to 600 °C. The splitting tensile strength of SF concrete decreased with temperature rise. It was observed that the tensile strength sharply declined for all concrete specimens after heating to 600°C. As the concrete temperature increased from 300°C to 600°C, the relative splitting tensile strength of concrete reduced from 71% to 25%. This considerable loss of strength was due to different thermal expansion of cement paste and aggregate as well as the decomposition of the hydration products in concrete. It was also found that a higher rate of tensile strength loss was observed compared to compressive strength loss at high temperatures. This can be attributed to the effects of crack coalescence being more significant in the tensile strength than the compressive strength. In addition, the cracks tend to close when subjected to compressive loads while opening under tensile loads.

Tanyildizi et al. [47] investigated the splitting tensile strength of lightweight concrete with 0, 10, 20, and 30% silica fume after being subjected to 200, 400, and 800 °C. It was found that the tensile strength declined by increasing the temperature. Moreover, lightweight concrete that contained 20% silica fume exhibited better performance at all temperatures.

The variation of the relative splitting tensile strength of concrete with temperatures is plotted in Figure 2-5. The relative splitting tensile strength of SF concrete decreases beyond 200 °C, and the residual tensile strength of SF concrete at the temperature of 800 °C is almost 20% of the original strength of concrete at room temperature.

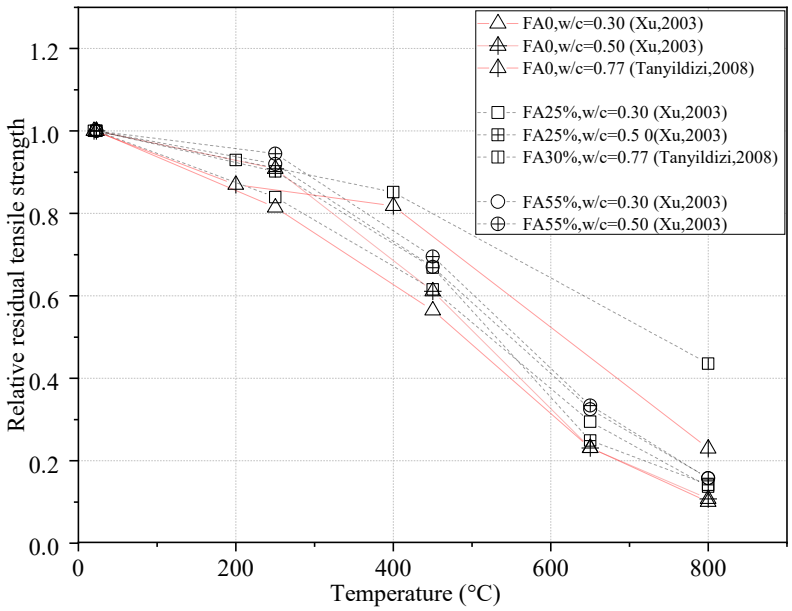

Figure 2-5. Effect of high temperatures on the residual tensile strength of SF-contained concrete [21, 47]

2.2.2.3 Modulus of Elasticity

Various techniques of high-temperature deformation measurement, including contact and non-contact approaches, have been developed to determine high-temperature deformation. Linear position transducer (LPT) and linear variable differential transformer (LVDT), Compressometer, High-temperature strain gauge, and Fiber-optic sensor are typical contact methods for strain measurement. On the other hand, Laser sensors and Digital image correlation (DIC) are the two key non-contact optical methods that have been increasingly used for measuring high-temperature deformation [48, 49]. However, there are still difficult technical problems in measuring the deformation-related properties such as modulus of elasticity despite the rapid development of various measurement techniques. Due to these difficulties and challenges, there is very limited reliable experimental data in the literature regarding the deformation-related properties such as the modulus of elasticity of different concrete mixtures exposed to high temperatures.

Phan et al. [25] examined the influence of high temperatures on the modulus elasticity of HPC concrete containing 0 and 10% silica fume with w/b of 0.22, 0.33, and 0.57 up to 450°C. It was observed that the modulus of elasticity of the HPC in this test program decreased for all mixtures with and without silica fume with increasing temperature. All mixtures demonstrated a 50% reduction in modulus of elasticity between room temperature and 300 °C. Modulus reduction was slower from 300 to 450 °C. However, all mixes lose more than 70 % of their initial modulus of elasticity at 450 °C.

2.2.3 The Effects of Fly Ash at room temperature

Fly ash, or pulverized fly ash, is the by-product generated from a fuel electricity-generating plant and is widely used as a cement replacement in the concrete industry [50, 51]. There are two main types of fly ash: low-calcium fly ash (Class F) produced by the combustion of anthracite or bituminous coal, and high-calcium fly ash (Class C) obtained from lignite or sub-bituminous coal burning. Class F is a material comprising silicate glass, modified with aluminum and iron, classified as a normal pozzolan. The calcium hydroxide is required by low-calcium fly ash to generate strength-developing products from the pozzolanic reaction. Therefore, it is combined with Portland cement, which produces calcium hydroxide in the hydration process [52, 53]. However, class C can significantly alter the hydration processes in cement due to higher reactivity, and more studies are needed to investigate the application of Class C of FA in concrete production [54]. Furthermore, fly ash has pozzolanic activity due to the presence of Al_2O_3 and SiO_2. The reaction of fly ash with calcium hydroxide results in the formation of additional calcium silicate hydrate (CSH) and calcium aluminate hydrate (CAH), which leads to forming of a denser matrix in concrete [51, 55].

2.2.3.1 Compressive strength

Golewski [28] evaluated the compressive strength of concrete containing 0, 20, and 30% fly ash as cement replacement at 3, 7, 28, 90, 180, and 365 days. The test results revealed the lower compressive strength of fly ash concrete at the early ages in comparison to control concrete (i.e., 0% FA). However, fly ash concrete exhibited higher strength compared to concrete without FA at later ages. A greater increase was reported for concrete with 20% fly ash replacement than control concrete after 28 days and subsequent curing ages. This was due to the sharp rise of pozzolanic reaction products at the longer curing time. The compressive strength of concrete with 30% FA was higher than the control concrete only after 180 and 365 days.

The influences of the inclusion of a high volume of Class F fly ash on compressive, splitting tensile, and modulus of elasticity of concrete at three ages of testing (28, 91, and 365 days) was investigated by Siddique et al. [29]. The dosages of replacing cement with fly ash were 0, 40, 45, and 50%. It was found that there was a reduction in the strength of concrete made with fly ash at the age of 28 days compared to the strength of mix without FA. However, beyond the 28 days, the compressive strength increased continuously in fly ash concrete. This increase can be attributed to the pozzolanic reaction of fly ash.

Abubaker et al. [30] determined the influence of cement replacement by 10, 25, and 50% fly ash on the mechanical properties of concrete until 90 days of curing. The mixes were prepared at the w/b of 0.35 and 0.45. The strength of concrete decreased with increasing the fly ash content due to the slow secondary hydration reaction at the early ages compared to concrete without fly ash. In the fly ash concrete, the compressive strength increased with

age. Moreover, it was observed that the concrete with a higher w/b exhibited a lower compressive strength.

Megat Johari et al. [31] examined the compressive strength of high-strength concrete that contained fly ash for up to 365 days. The concrete specimens were prepared with 0, 10, 20, and 30% fly ash. It was found that the strength of FA concrete decreased at early ages. Moreover, a considerable reduction was observed at higher substitution levels of FA. However, at later ages, the relative strength continued to exceed with increasing curing age. After 90 days, FA concrete showed higher strength than OPC concrete. At the age of one year, the relative compressive strength of the concrete with 10, 20, and 30% fly ash concrete was found as 104%, 111%, and 112%, respectively. Therefore, 30% is the optimum amount of fly ash that can be replaced with cement in high-strength concrete, which results in maximum long-term strength.

The variation of relative compressive strength of fly ash concrete versus the concrete age is shown in Figure 2-6. It is found that the FA-contained concrete showed lower relative strength at early ages because of the slow rate of pozzolanic reaction of fly ash and $Ca(OH)_2$ compared to OPC concrete. However, the compressive strength of FA concrete increased at later ages because of the additional formation of CSH due to the use of unreacted fly ash [30]. As the amount of FA increased, the strength of concrete decreased because of the slower rate of hydration with respect to cement [56].

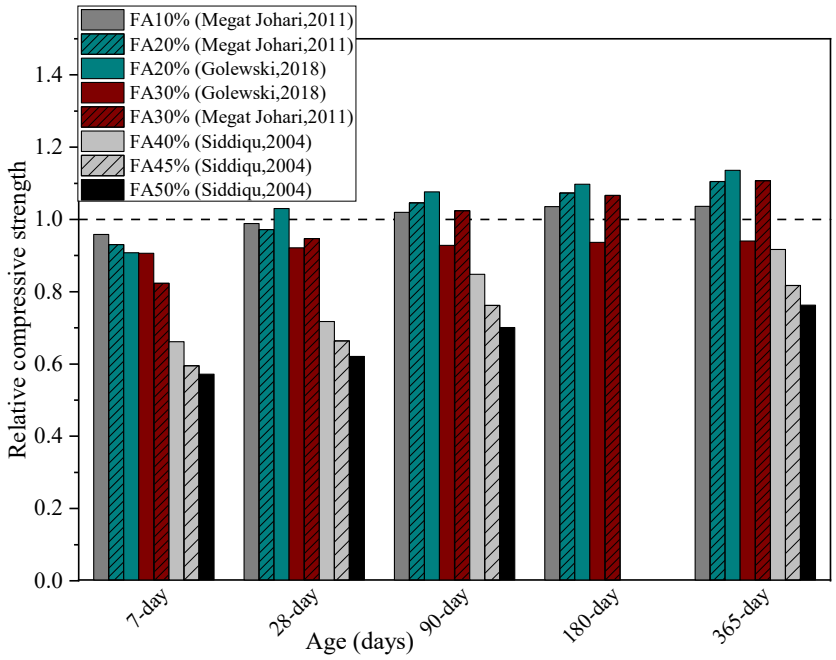

Figure 2-6. Relative compressive strength of FA-contained concrete at various curing ages [28, 29, 31]

2.2.3.2 Splitting Tensile Strength

Lam et al. [32] evaluated the splitting tensile strength of FA concrete at 28 and 56 days. The cement was partially substituted with 0,15, 25, 45, and 55% fly ash. The results revealed that 15 to 25% fly ash replacement improves the tensile strength of concrete. However, higher content of fly ash replacement caused slightly lower tensile strength at the ages of 28 and 56 days. This can be attributed to the lower concentration of cement hydration products, which required longer curing times to develop interfacial bonds in high-volume FA concrete.

A study by Siddique et al. [29] reported that the cement replacement with fly ash at 0, 40, 45, and 50% caused an enhancement in the concrete tensile strength at 91 and 365 days compared to tensile strength at the age of 28 days. However, increasing the FA content reduced the tensile strength at all ages.

2.2.3.3 Modulus of Elasticity

Siddique et al. [29] examined the modulus of elasticity of high-volume FA concrete made with 0 to 50% fly ash at the ages of 28, 91, and 365 days. The results revealed that beyond the 28 days, the modulus of elasticity of FA concrete increased with an increase in age. It was also observed that utilization of the higher content of fly ash decreased the modulus of the concrete in comparison to that of the control concrete mix.

2.2.4 The Effects of Fly Ash at high temperature

2.2.4.1 Compressive Strength

Wang et al. [57] evaluated the influence of the high temperatures on the compressive strength of concrete with 30% fly ash in comparison to control concrete without FA up to the temperature of 550 °C. The results demonstrated that (i) up to the temperature of 250 °C, the compressive strength decreased for all concrete mixtures with and without fly ash; (ii) in the range of 250-350 °C, compressive strength was improved and (iii) after 350 °C, the compressive strength of concrete continuously reduced due to the decomposition of $Ca(OH)_2$ and CSH crystal. After exposure to 550 °C, the strength of the control concrete and fly ash concrete was respectively 26.1% and 26.6 lower than the original strength at room temperature. Therefore, both FA concrete and ordinary concrete showed a similar trend after being subjected to high temperatures.

Karahan et al. [58] evaluated the compressive strength of the high volume fly ash concrete after being exposed to high temperatures (400, 600, and 800 °C). The mixes were made with 0, 30, 50, 70, and 90% fly ash. It was found that the compressive strength of concrete was remarkably decreased by increasing the fly ash replacement percentage after exposure

to high temperatures. It was also reported that the compressive strength of concrete with 30 and 50% FA was close to concrete without fly ash at 400, 600, and 800 °C. Accordingly, the optimal amount of FA as a cement replacement was 30–50% for exposure to high temperatures.

Khan et al. [59] examined the behaviour of fly ash concrete when exposed to high temperatures up to 900 °C. The mixes were prepared by replacing the cement with 0, 40, 50 and 60% FA. It was reported that with increasing test temperature up to 300 °C, the residual compressive strength of concrete increased. However, the strength of all the mixes decreased with a further increase in temperature. This reduction might be due to moisture evaporation and thermal expansion mismatch between the aggregate and cement paste. Furthermore, for a given temperature, concrete with a higher content of FA exhibited more reduction in compressive strength.

Xu et al.[60] investigated the deterioration of the mechanical properties of the concrete made with pulverized fly ash (PFA) dosages (0, 25, and 55%) after exposure to a series of high temperatures (250, 450, 650 and 800 °C) at 90 days. At 250 °C, an increase in compressive strength was observed in all specimens. This increase in strength is due to the occurrence of a relatively small amount of crack. At the temperature of 450 °C and higher temperatures, severe cracks were observed in concrete, resulting in reduced residual compressive strength in all specimens. The results also showed that the presence of PFA improved the relative residual compressive strength and resulted in the generation of a minor network of cracks in PFA concrete.

Nadeem et al. [61] studied the behaviour of high-performance concrete containing fly ash from 20 to 60%, exposed to high temperatures up to 800 °C, under two types of cooling

methods: slow cooling and quick cooling at the age of 180 days. At 200 °C, the compressive strength decreased continuously in mixes containing 20 and 40% fly ash, while a slight increase was observed in the strength of OPC concrete and concrete with 60% fly ash. This slight increase can be attributed to the additional hydration of the unhydrated cement grains due to the steam effect of internal autoclaving or free water evaporation, which resulted in greater van der Waals forces as the layers of cement gel moved closer together. After exposure to 400 °C, a major strength loss was observed for all concrete mixes. It was also found that the compressive strength loss under quick cooling in water was more significant than slow cooling due to the effect of thermal shock on concrete. This is due to the generation of microcracking caused by the difference in temperature between the inner and outer layers of concrete for water cooling conditions.

Poon et al. [45] conducted a comprehensive study on different SCMs and investigated the compressive strength of normal-strength concrete (NSC) and high-strength concrete (HSC) containing SF (5 and 10 %), FA (20, 30, and 40%), and GGBS (30 and 40%) exposed to temperatures up to 800 °C at 60 days. The compressive strength of FA and GGBS concrete increased up to 200 °C. At 400 °C, high-strength concrete retained its initial strength, while a significant reduction was reported in the strength of NSC. However, both types of concrete lost their strength due to the reduction of Ca $(OH)_2$ in concrete at temperatures above 400 °C. At the temperature of 800 °C, severe strength loss occurred because of the decomposition of CSH gel. It was also found that high-strength concrete exhibited higher relative residual compressive strength compared to normal strength concrete. Fly ash concrete showed the best performance in high-strength concrete, followed by GGBS, OPC, and SF concrete, whereas this order was GGBS, FA, and OPC in NSC. In addition, the

maximum relative residual strength was observed in concrete with a 30% FA replacement level in high-strength concrete and 40% slag replacement in NSC after high-temperature exposure.

Figure 2-7 represents the effect of high-temperature exposure on the behaviour of FA concrete as reported by multiple researchers. Generally, as seen in Figure 2-7, the compressive strength of concrete containing fly ash increased after exposure to high temperatures ranging from 250-300 °C. However, the strength decreased after the temperature reached 400 °C and higher temperatures. The addition of fly ash can improve the performance of concrete at high temperatures compared to OPC concrete. However, the literature shows contradictory results in determining the optimal content of FA in concrete subjected to high temperatures.

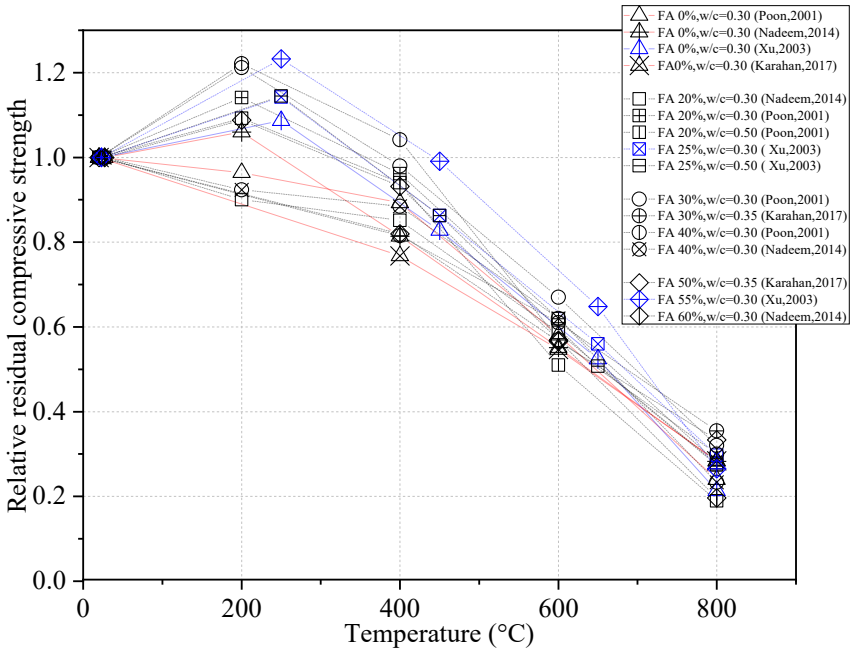

Figure 2-7. Effect of high temperatures on the residual compressive strength of FA-contained concrete [45, 58, 60, 61]

2.2.4.2 Splitting Tensile Strength

Xu et al. [60] studied the influence of PFA on the tensile strength of concrete after high temperatures exposure. The results revealed that at the temperature of 250 °C, the minor cracks observed in concrete and all the mixtures showed some losses of tensile strength. The tensile strength of concrete decreased as the temperature increased. However, the PFA concrete showed better performance at all high temperatures.

Tanyildizi et al. [62] studied the splitting tensile strength of lightweight concrete incorporating 0%, 10%, 20%, and 30% fly ash after being exposed to high temperatures. The splitting tensile strength of concrete decreased after exposure to high temperatures up to 800 °C. This was due to the occurrence of micro and macro cracks in lightweight structural concrete. It was found that a lower reduction in the tensile strength occurred in concrete with FA compared to OPC concrete. The highest tensile strength was observed with 30% FA in the concrete specimens.

Khan et al. [59] investigated the tensile strength of concrete with high-volume fly ash at replacement levels of 40, 50, and 60% exposed to high temperatures up to 900 °C. The tensile strength of FA concrete increased with increasing the exposure temperature, and maximum strength was reached at the temperature of around 300 °C. However, above the temperature of 300 °C, the splitting tensile strength decreased sharply. Moreover, it was found that the tensile strength of the fly ash concrete was reduced with an increase in the fly ash content.

The influence of high temperature on the splitting tensile strength of FA concrete is plotted in Figure 2-8. The tensile strength of concrete prepared with FA decreases almost linearly

with the temperature rise. However, the concrete that contained fly ash exhibited higher tensile strength values compared to OPC concrete.

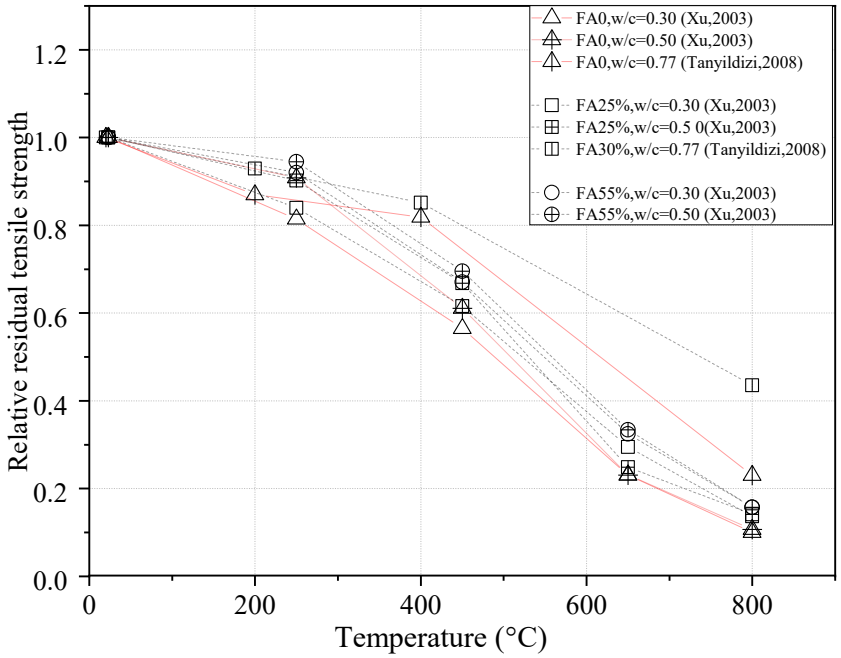

Figure 2-8. Effect of high temperatures on the residual tensile strength of FA-contained concrete [60, 62]

2.2.4.3 Modulus of Elasticity

Nasser et al. [63] examined the modulus of elasticity of concrete with 25% fly ash exposed to high temperatures up to 232 °C. It was observed that the modulus of elasticity remained constant in the temperature range of 121 °C to 149 °C. However, the modulus of elasticity decreased when the exposure temperature was 232 °C.

2.2.5 The Effects of Slag at room temperature

Blast furnace slag is a by-product of the iron and steel manufacturing industries in the blast furnace [64]. The mixture of limestone with iron ore is fed into blast furnaces and heated up to the temperature of around 1500 °C, producing molten slag and molten iron [65, 66]. The molten slag is quenched quickly in a pond or using powerful water jets, leading to the

formation of the fine and glassy form known as granulated slag [66]. Using ground granulated blast furnace slag (GGBFS) in concrete has attracted considerable attention because it improves the properties of the concrete and decreases the negative environmental effects [67]. GGBFS with latent hydraulic properties is hydrated with calcium hydroxide and water. This secondary pozzolanic reaction of hydrated lime $Ca(OH)_2$ results in a denser microstructure due to the consumption of $Ca(OH)_2$ and the CSH formation [33].

2.2.5.1 Compressive Strength

Chidiac et al. [33] investigated the compressive strength of concrete with GGBFS as cement replacement (0, 25, 40, 50, and 60%) and two different w/b ratios (0.31 and 0.38) at 1, 3, 7 and 28 days. The concrete with GGBFS exhibited lower strength at early ages than OPC due to the relatively slower initial hydration rate, while higher strength was observed for GGBFS concrete between 7 and 28 days with the formation of denser microstructure in concrete. The results also indicated that the compressive strength of GGBFS concrete improved with increasing the w/b ratio from 0.31-0.38 because of a higher degree of hydration.

Megat Johary et al. [31] investigated the properties of high-strength concrete made with 0, 20, 40, and 60% GGBS at the age of 1, 3, 7, 14, 28, 90, 180, and 365 days. The incorporation of GGBS in concrete decreased the initial age strength of the concrete compared to OPC concrete, especially at the higher replacement ratios. This was due to the slower GGBS reactivity as well as the diluting effect since part of the cement was substituted by GGBS. The compressive strength of GGBS concrete increased at advanced

ages up to one year. However, the later age strength of the HSC decreased gradually with the addition of slag content. It was also found that GGBS concrete exhibited higher long-term strength for the replacement ratio of 20% compared to 40% and 60% slag.

Güneyisi et al. [34] conducted an experimental study of high replacement levels of 0, 50, 60, 70, and 80% of blast furnace slag and different methods of curing (air and wet cured) on the mechanical properties of high-performance concrete during 28 and 90 days. The results revealed that the strength of concrete reduced gradually with increasing the slag content, particularly air-cured specimens. However, for concrete containing slag up to 60%, the compressive strength increased at 90 days under wet curing conditions.

Khatib et al. [35] investigated the compressive strength of concrete by replacing the cement with different ratios of GGBFS between 0 and 80% up to 90 days of curing. Compressive strength decreased as the content of GGBS increased at the initial stages of hydration. Beyond 28 days and up to at least 90 days, concrete containing 40 and 60% GGBS showed higher compressive strength compared to concrete without GGBFS. A considerable strength loss of GGBS concrete was observed in the replacement level of 80% at all ages.

The studies discussed above show that the compressive strength of the concrete containing GGBFS is inversely proportional to the GGBFS replacement ratios. Moreover, the compressive strength gain was more pronounced at longer ages compared to OPC concrete, as presented in Figure 2-9.

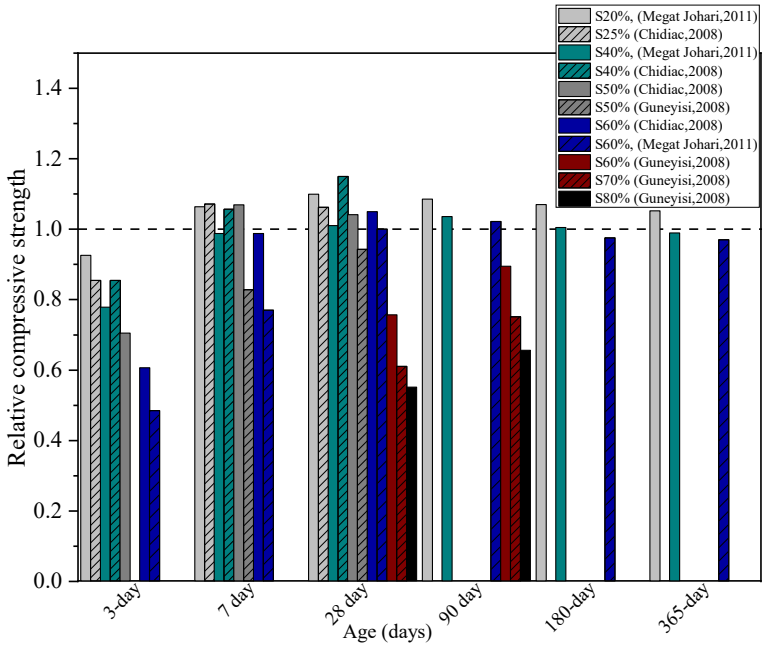

Figure 2-9. Relative compressive strength of slag-contained concrete at various curing ages [31, 33, 34]

2.2.5.2 Splitting Tensile Strength

Güneyisi et al. [34] evaluated the splitting strength of HPC high replacement levels from 50% to 80% of blast furnace slag at the ages of 28 and 90 days using two types of curing (air and wet cured). They observed that the tensile strength decreased with the augmentation of slag content except for concrete specimens with 50 and 60 % slag exposed to wet curing conditions at 90 days.

Aldea et al. [36] examined the effect of replacement cement by 25,50 and 75 % slag on the splitting tensile strength of concrete in comparison to control concrete mix without slag at two types of curing: steam curing and normal curing. The results indicated that the tensile strength improved for 25% and 50% slag replacement in concrete compared to the concrete without slag. In addition, it was found that cement replacement with the higher contents of

slag (i.e.,75% slag) decreased the tensile strength of concrete regardless of the type of curing.

2.2.5.3 Modulus of Elasticity

Siddique et al. [37] observed that the modulus of elasticity of concrete made with GGBFS (0,20, 40, and 60%) was lower than the OPC concrete at room temperature. Concrete containing 20%, 40% and 60% GGBFS had modulus of elasticity that were 22, 5, 39,98% and 41,7% less than control concrete. Furthermore, the results revealed that the increase in GGBFS content reduced the modulus of elasticity of concrete at room temperature for 28 days.

Swamy et al. [38] studied the modulus elasticity of concrete specimens made with 50 and 65% slag replacement by weight of cement using air and wet curing condition. It was found that there is a slight difference in the modulus of elasticity of slag concrete and OPC concrete when concrete is exposed to wet curing conditions. However, a considerable reduction in elastic modulus was observed under air curing.

Khatib et al. [35] examined the modulus of elasticity of GGBFS concrete up to 90 days of curing. The results revealed that the modulus elasticity decreased up to 28 days. However, above 28 days, the modulus of elasticity of concrete with 40 and 60% GGBFS increased slightly. It was also found that compared with the differences in compressive strength, there are little differences in modulus of elasticity values for all concrete mixtures.

2.2.6 The Effects of Slag at high temperature

2.2.6.1 Compressive Strength

Siddique et al. [37] studied the mechanical properties of concrete with 0, 20, 40, and 60% GGBFS when exposed to high temperatures up to 350 °C. At 100 °C, the compressive strength of concrete containing 0% and 20% GGBFS decreased because of thermal incompatibility between cement paste and aggregates, and then the strength increased with increasing temperatures. However, no significant change occurred in residual strength for the GGBFS concrete at replacement ratios of 40% and 50% with the increase in temperature. It was also found that the strength decreased as the GGBFS replacement ratio increased at room temperature and 350 °C.

Shumuye et al. [68] investigated the compressive strength of concrete containing 30, 50, and 70% GGBFS when exposed to high temperatures between 200 and 800 °C. The compressive strength of concrete with 30% and 50% slag replacement decreased at 200 °C and then increased at 400 °C. However, after heating to 400 °C, the compressive strength continuously decreased for all specimens. The most rapid strength loss was observed for concrete made with 70% slag. However, the concrete with 30% slag exhibited better performance in comparison to other concrete mixes at high temperatures.

Li et al. [67] examined the properties of concrete incorporating GGBFS after exposure to high temperatures up to 700 °C. The cement was replaced with three percentages of 0, 10, 30, and 50% of GGBFS. The compressive strength decreased with the temperature raised from 150 to 700 °C. The obtained amount of relative compressive strength of 10% GGBFS replacement was similar to OPC concrete. However, concrete containing 30 and 50%

GGBFS exhibited lower compressive strength than 10% of GGBFS and OPC concrete at heating range from 300 to 700 °C.

Karahan et al. [58] determined the compressive strength of the concrete prepared with replacement of cement by 0, 30, 50, 70%, and 90% of slag compared to the control concrete at 200, 400, and 800 °C. The results revealed that the compressive strength declined with increasing temperatures for all concrete mixtures. The concrete containing slag up to 70% showed lower or similar compressive strength compared to the control mix at high temperatures. It was also observed that the optimum amount of slag was 50–70% as a cement replacement.

The relative compressive strength of concrete containing slag after exposure to high temperatures is shown in Figure 2-10. The results indicate that generally, the slag concrete exhibits similar or lower compressive strength than the OPC concrete. However, slag may improve the relative residual strength of HSC exposed to high temperatures, according to the results reported by Poon et al. [45]. The aforementioned studies show contradictory findings regarding the optimal percentage of slag as a cement replacement when concrete is exposed to high temperatures.

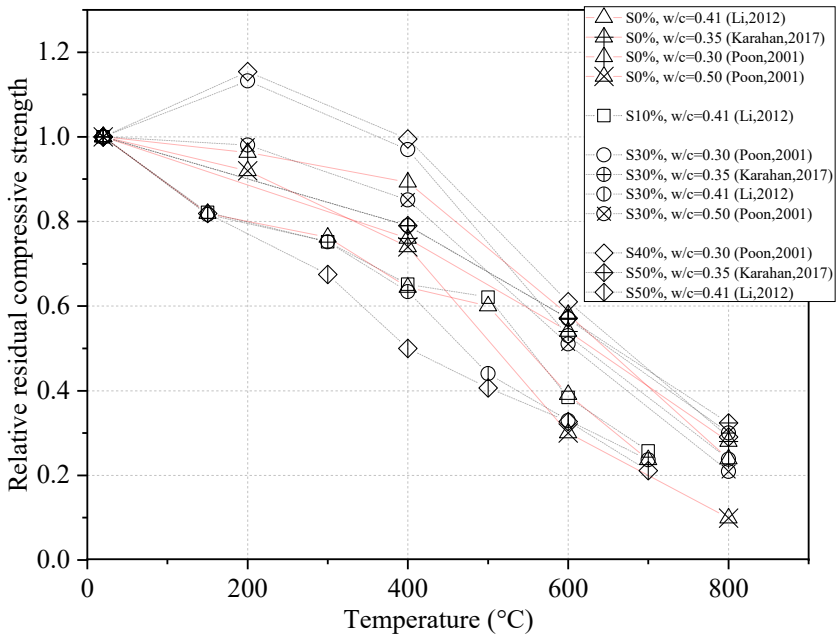

Figure 2-10. The residual compressive strength of slag-contained concrete [45, 58, 67]

2.2.6.2 Splitting Tensile Strength

The literature review demonstrated that very limited research had been carried out to study the tensile strength of slag concrete after exposure to high temperatures. Siddique et al. [37] evaluated the influence of GGBFS on the splitting tensile strength of concrete at high temperatures up to 350 °C. It was observed that the splitting tensile strength of concrete decreased as the temperature raised from 100 to 350 °C for all replacement levels of GGBFS. It was also reported that there is a very pronounced loss in splitting tensile strength, which contrasts with the gradual decline in compressive strength at high temperatures. This is due to the fact that the tensile strength is more susceptible to micro and macro cracks induced by high temperatures. The results of this study are presented in Figure 2-11.

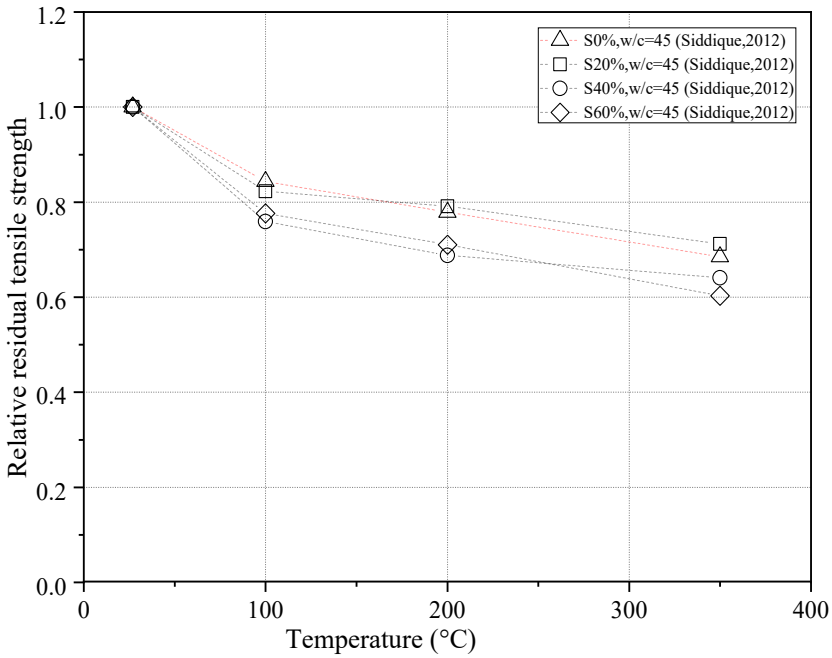

Figure 2-11. The residual splitting tensile strength of slag-contained concrete [37]

2.2.6.3 Modulus of Elasticity

Li et al. [67] studied the properties of GGBFS concrete with replacement levels of 10, 30, and 50% when subjected to high temperatures up to 700 °C. The results indicated that incorporating GGBFS caused a reduction in the relative modulus of elasticity of concrete.

Siddique et al. [37] examined the modulus of elasticity of concrete with 0, 20, 40 and 60% GGBS when subjected to high temperatures up to 350 °C at the ages of 28 and 56 days. The modulus of elasticity of concrete decreased as the exposure temperature increased for all GGBFS replacement levels by cement weight at 28 days. Furthermore, it was observed the modulus elasticity of GGBS concrete is lower than control mix concrete at all temperatures. Test results at 56 days exhibited a similar trend. The variation of modulus of elasticity as a function of temperature for slag-contained concrete is illustrated in Figure 2-12.

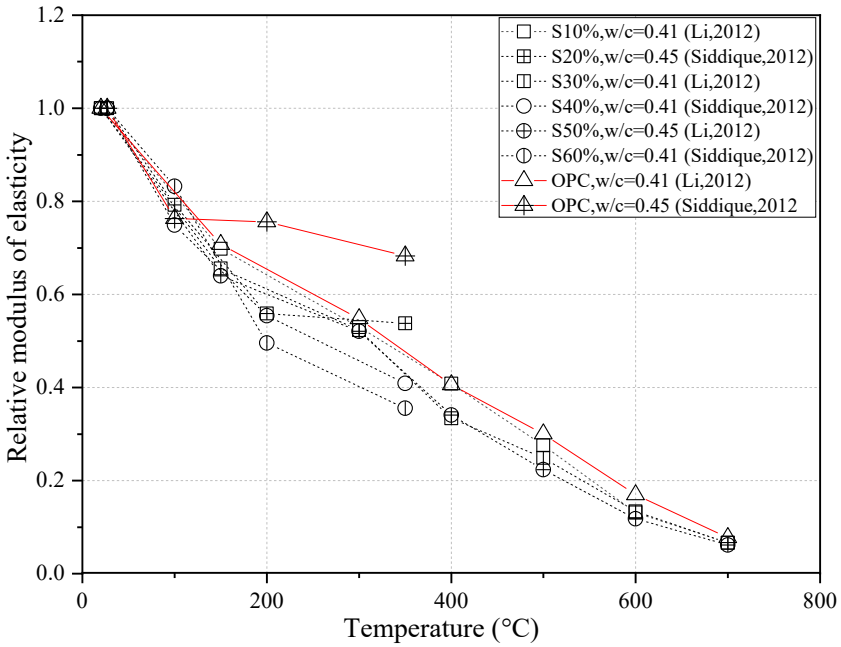

Figure 2-12. The residual modulus of elasticity of slag-contained concrete [37, 67]

2.3 Aggregate

Aggregate makes up 60-75% of the volume of concrete. Therefore, aggregate has a critical role in concrete behaviour at room and high temperatures. The coarse aggregate used in concrete can be classified into three groups according to its chemical composition and mineralogical nature: calcareous (Ca) aggregates (e.g., limestone, dolomite, basalt, and diabase), siliceous (Si) aggregate (e.g., quartzite, sandstone, and granite), and lightweight aggregates (LWA) (e.g., diatomite, pumice, scoria, clay ash, slate, perlite, and shale). The mechanical properties of concrete with three different types of aggregate at high temperatures are investigated in the following sections. Table 2-3 gives the summary of the effect of different types of aggregates on the mechanical properties of concrete after high-temperature exposure.

Table 2-3. Summary of research on the influence of different types of aggregate on mechanical properties of concrete after high exposure to high temperatures

Year	Source	Coarse aggregate type	Test temperature (°C)	w/c	Mechanical properties tested
2007	[11]	Limestone, River gravel.	200-1200	0.4, 0.5,0.6	f'_c
2005	[99]	Limestone, Siliceous	20-750	0.6	f'_c,E
2017	[70]	Limestone, Quartzite, Granite	25-650	0.55	f'_c,f_t,E
2018	[71]	Quartzite, Granite, Basalt	25-600	0.5	f'_c
2011	[72]	Silico-calcareous, Calcareous, Siliceous	150-750	0.3, 0.6	f'_c,f_t
2014	[16]	Granite, Calcareous	20-700	0.52, 0.56	f'_c,f_t,E
2004	[76]	Granite, Limestone	20- 800	0.22, 0.23, 0.25	f'_c,E
2007	[77]	Lightweight volcanic pumice	400,600, 800	0.45	f'_c,f_t,E
1971	[75]	Lightweight, Calcareous, Siliceous	21-871	0.4, 0.42, 0.54, 0.51, 0.58, 0.77	f'_c
2021	[78]	Lightweight expanded clay, Lightweight expanded shale	150- 600	0.45	f'_c,f_t,E

2.3.1 The Effects of Calcareous and Siliceous Aggregate at high temperature

2.3.1.1 Compressive Strength

Arioz et al. [11] examined the influence of high temperatures on the compressive strength of four concrete mixes prepared by two aggregate types (river grave aggregate and limestone aggregate) and different water to portlan cement ratios of 0.4, 0.5, and 0.6. The relative compressive strength of concrete reduced as high temperatures increased between 200-1200 °C. It was found that the strength loss was more significant for concrete with river gravel aggregate than crushed limestone aggregate. This can be explained by the composition of the siliceous river gravel aggregates. The relative strength of river gravel concrete decreased gradually but substantially as the temperature increased. In the limestone concrete mixture, relative strength was slightly reduced up to 600 °C. However, the relative strength sharply decreased at temperatures above 600 °C.

Savva et al. [69] studied the residual mechanical characteristics of concrete containing different types of Pozzolans, two lignite fly ashes, and one natural pozzolan as cement replacements when concrete was exposed to high temperatures of 100, 300, 600, and

750 °C. Two series of concrete specimens were made with limestone and siliceous aggregate, respectively. An increase was observed in the compressive strength of siliceous concrete at 300 °C. This can be attributed to the higher bond strength between siliceous aggregate and cement paste. Between 300 and 600 °C, the compressive strength decreased in both aggregate types, which was more significant for siliceous concrete. At temperatures above 600 °C, compressive strength deterioration was observed for all concrete mixtures. However, the limestone concrete showed a slightly higher strength reduction due to the decarbonation of limestone at these temperatures.

Tufail et al. [70] investigated the mechanical properties of three different concrete mixtures with granite, quartzite, and limestone aggregates exposed to temperatures up to 650 °C. The granite concrete showed the lowest strength loss value, followed by quartzite and limestone concrete after exposure to high temperatures. This was due to the high temperature-induced partial decomposition of calcite and inner fractures and cracks of mineral particles in limestone aggregates. Masood et al. [71] contradicted these observations by stating that concrete containing quartzite aggregate exhibited higher residual compressive strength than granite and basalt at temperatures ranging from 200 to 600 °C.

Xing et al. [72] evaluated the influence of the three types of aggregate (calcareous, siliceous, and semi crushed silico-calcareous) on the residual mechanical properties of normal strength and high-performance concrete at 20, 150, 300, 450, 600, and 750 °C. Similar behaviour was observed for normal concrete with three different aggregate types up to 300 °C. After heating to 300 °C, normal concrete with calcareous aggregate presented a lower strength loss as compared to normal concrete with silico-calcareous and siliceous

aggregates. This result is partially adapted to Eurocode [73] predictions. However, in high-performance concrete, the siliceous aggregate concrete exhibited better performance than other aggregate types, which was inconsistent with that predicted in Eurocode [73].

In contrary with the studies discussed above, Santos et al. [16] carried out an experimental study on the mechanical properties of two types of concrete specimens with calcareous and granite aggregates under two loading levels (0.3 f′c and 0.7 f′c) and different cooling methods (cooling in air and water jet) and exposed to high temperatures (300, 500 and 800 °C). For the loading level of 0.3 f′c, the strength of calcareous aggregate concrete decreased significantly in comparison to granite aggregate concrete, regardless of the cooling process. A similar trend was found for 0.7 f′c loading conditions up to 300 °C. However, at above 300 °C, calcareous aggregate concrete exhibited higher compressive strength than the granite aggregate concrete. Furthermore, for both types of concrete, the cooling by water jet induced a greater reduction in compressive strength at temperatures between 20 to 800 °C.

The residual compressive strength of siliceous and calcareous aggregate compared with the ACI 216.1 [74] predictions is illustrated in Figure 2-13 (a,b). Residual compressive strength of calcareous aggregate concrete collected from the literature proved to be almost equal to values in ACI 216.1 [74], particularly above 400 °C. The relative residual compressive strength of calcareous concrete generated from existing research is higher than the prediction of ACI 216.1 [74] up to 600 °C. Beyond this temperature, the ACI 216.1 [74] results indicated slightly higher strength.

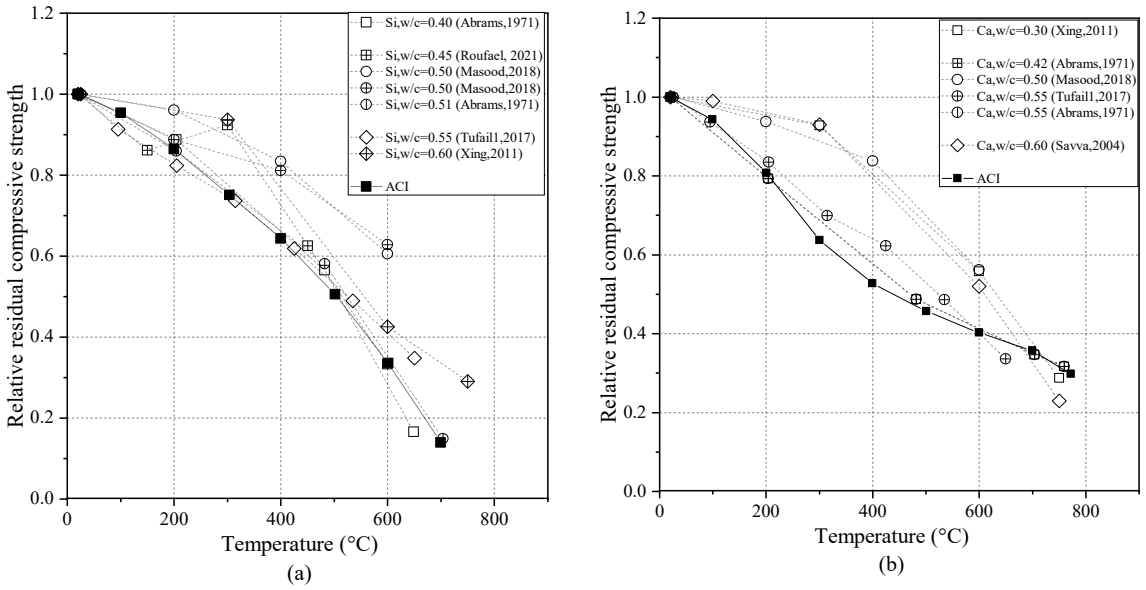

Figure 2-13. The residual compressive strength: a) siliceous aggregate concrete [69-71, 75], b) calcareous aggregate[69-72, 75]

2.3.1.2 Splitting Tensile Strength

Santos et al. [16] studied the tensile strength of granite aggregate concrete (GC) and calcareous aggregate concrete (CC) at high temperatures with different cooling approaches, including in air and water jet. It was found that both CC and GC showed similar behaviour up to 300 °C. However, above 300 °C, GC displayed lower residual splitting tensile strength compared to the calcareous concrete.

Xing et al. [72] indicated that the concrete with calcareous aggregates showed better residual tensile strength compared to silico-calcareous and siliceous aggregates up to 600 °C. However, due to the dissociation of calcium carbonate, the reduction of tensile strength of calcareous became more considerable at temperatures higher than 600 °C.

Tufail et al. [70] investigated the tensile strength of three concrete mixes containing limestone, quartzite, and granite aggregates up to 650 °C. It was found that the tensile

strength reduced as the exposure temperature increased. The granite concrete showed the highest tensile strength at all temperatures compared to two other concrete mixes containing quartzite or limestone aggregate.

The influence of high temperatures on the residual splitting tensile strength of concrete containing siliceous and calcareous aggregate is presented in Figure 2-14 (a,b), respectively. It seems that the degradation of splitting tensile strength at high temperatures is quite linear despite the results captured at 300 °C by Xing et al. [72]. Tufail et al. [70] tested specimens with closer temperature intervals and verified a continuous degradation of splitting strength at high temperatures. While the results of Xing et al. [61] show better performance of concrete with calcareous aggregate, the results of Tufail [70] showed quite similar tensile strength behaviour at high temperatures for both aggregate types.

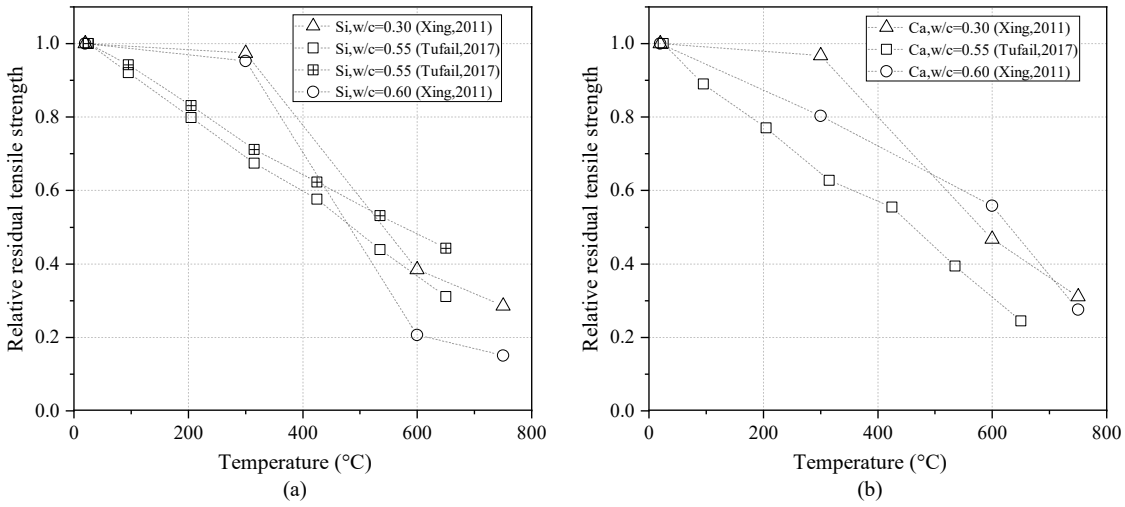

Figure 2-14. The residual tensile strength of concrete (a) concrete containing siliceous aggregate, (b) containing calcareous aggregate [70, 72]

2.3.1.3 Modulus of Elasticity

Santos et al. [16] found the reduction of residual modulus of elasticity was similar for calcareous and granite concrete up to a temperature of 400 °C. However, above 400 °C,

more reduction was observed for granite concrete compared with calcareous concrete. The results also indicated that the cooling methods have no considerable influence on the residual modulus of elasticity of both calcareous and granite concrete.

Savva et al. [69] examined the modulus of elasticity of limestone and ordinary concrete after exposure to high temperatures between 300 and 750 °C. The modulus of elasticity continuously decreased at all high temperatures for both aggregate types. However, the results indicated that this reduction was more substantial for concrete containing limestone aggregate.

Cheng et al. [76] examined the modulus of elasticity of two types of high-strength concrete made with carbonate and siliceous aggregate at temperatures of 100, 200, 400, 600, and 800 °C. It was observed that the modulus of elasticity decreased with increasing temperature. It was also found that the type of aggregate has a moderate effect on reducing the modulus of elasticity.

2.3.2 The Effects of Lightweight Aggregate at high temperature

2.3.2.1 Compressive Strength

Hossain et al. [77] determined the residual compressive strength of lightweight volcanic pumice concrete (VPC) compared to normal-weight concrete (NWC) with gravel aggregate at high temperatures up to 800 °C for different durations of 0, 0.5, 1, and 2 hours. The results indicated that the residual strength reduced in lightweight and normal-weight concrete as the temperature increased. However, lower strength loss was observed in VPC compared to NWC at a constant temperature for different durations or constant durations at different temperatures. The better residual strength of VPC was due to the less dense

pore structure of VPC in comparison with NWC. The denser pore structure in NWC results in water vapour buildup of higher pore pressure, leading to thermal crack formation, thus causing higher strength reductions at high temperatures than in VPC.

Abrams [75] investigated the residual compressive strength of three types of concrete made with carbonate, siliceous, and lightweight aggregates after being subjected to high temperatures up to 659 °C. The results indicated that the lightweight aggregate and carbonate aggregate concrete exhibited similar behaviour with higher strength retention than the siliceous aggregate concrete. Moreover, the original compressive strength has no significant influence on the residual compressive strength of the concrete at high temperatures.

Roufael et al. [78] examined the mechanical properties of lightweight concrete in comparison to normal-weight concrete subjected to high temperatures between 150 to 600 °C. It was observed that a slight reduction occurred in residual compressive strength at 150 °C, then an increase was observed at 300 °C for all mixtures. However, the strength decreased sharply for all concrete mixtures above this temperature. The lightweight aggregate concrete showed moderate strength loss compared to normal weight concrete. This can be attributed to the more resistant paste-aggregate bond with porous lightweight aggregates and better thermal deformation compatibility between the lightweight aggregate and the cementitious matrix. This better paste-aggregate bond was due to the paste penetration into the aggregate, causing interlocking sites between them. The variation of compressive strength of lightweight concrete exposed to high temperatures is plotted in Figure 2-15.

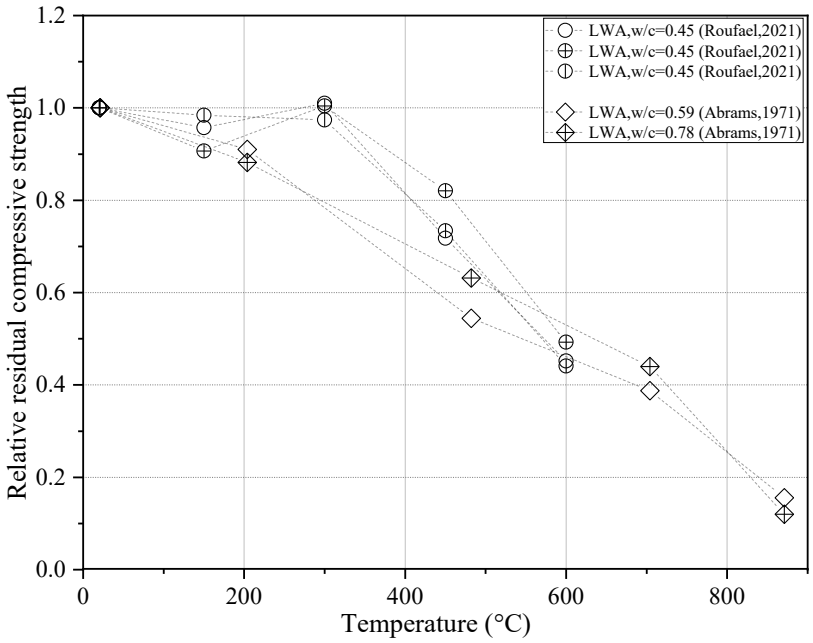

Figure 2-15. The residual compressive strength of concrete containing lightweight aggregate [75, 78]

2.3.2.2 Splitting Tensile Strength

Roufael [78] observed that the lightweight aggregate concrete showed a lower reduction of tensile strength with temperature increase than normal-weight concrete. Tensile strength loss was due to the expansion of aggregate, the dehydration of the cement paste, and the portlandite decomposition, which resulted in week ITZ at higher temperatures. The results of this study are shown in Figure 2-16.

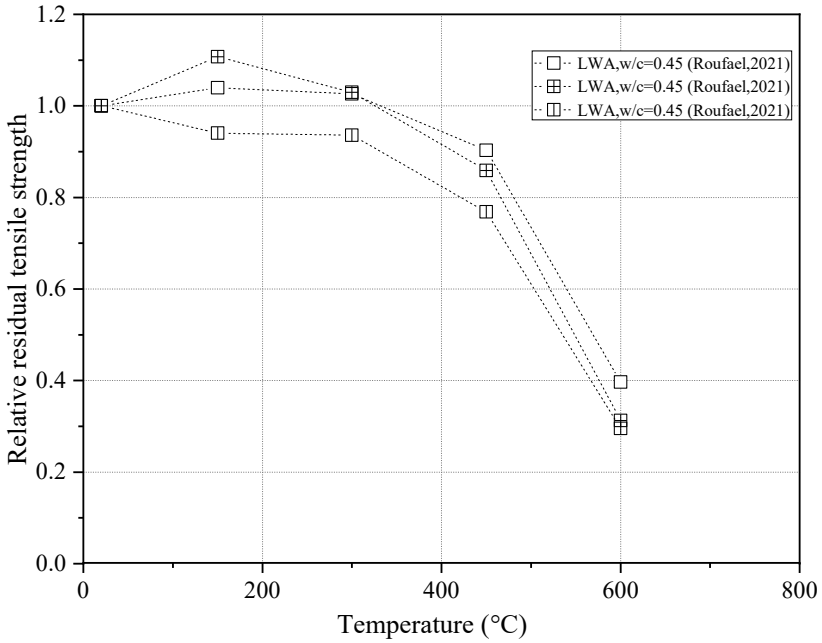

Figure 2-16. The residual tensile strength of concrete with lightweight aggregate [78]

2.3.2.3 Modulus of Elasticity

Roufael et al. [78] examined the modulus of elasticity of LWC exposed to high temperatures up to 600 °C compared to NWC made with calcareous aggregate. The lightweight aggregate concrete displayed a lower elastic modulus reduction than normal-weight concrete, particularly between 150 and 450 °C. The available relationships for residual mechanical properties of concrete at high temperatures.

2.3.3 The available relationships for mechanical properties of concrete at high

2.3.3.1 Compressive strength

ACI 216.1 [74] presents the reduction factor for compressive strength of concrete exposed to high temperature under three test conditions: transient, steady-state and residual test separately for three aggregate types (siliceous, calcareous and lightweight aggregate)

generated from the results of only one research conducted by Abrams [75],as shown in respectively.

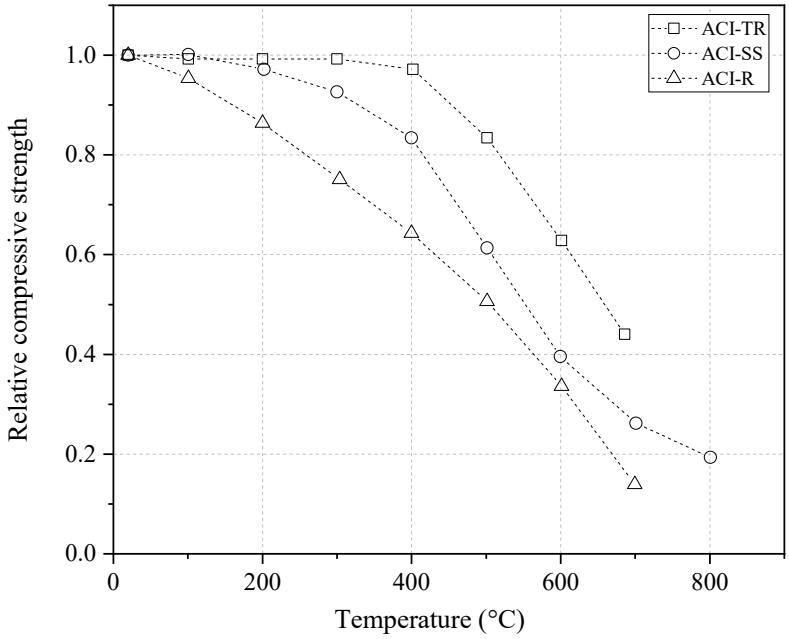

Figure 2-17.Relative compressive strength of siliceous aggregate concrete exposed high temperatures presented by ACI 216.1 [74]

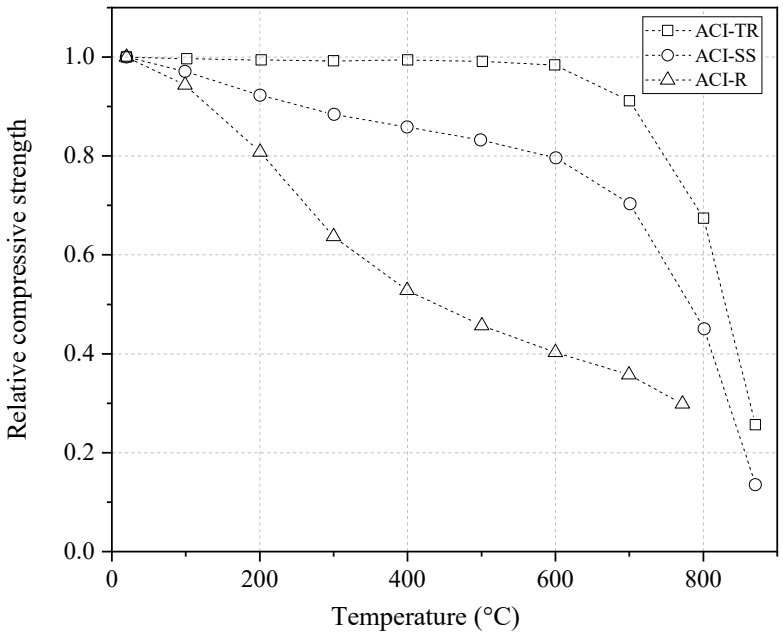

Figure 2-18. Relative compressive strength of calcareous aggregate concrete exposed to high temperatures presented by ACI 216.1 [74]

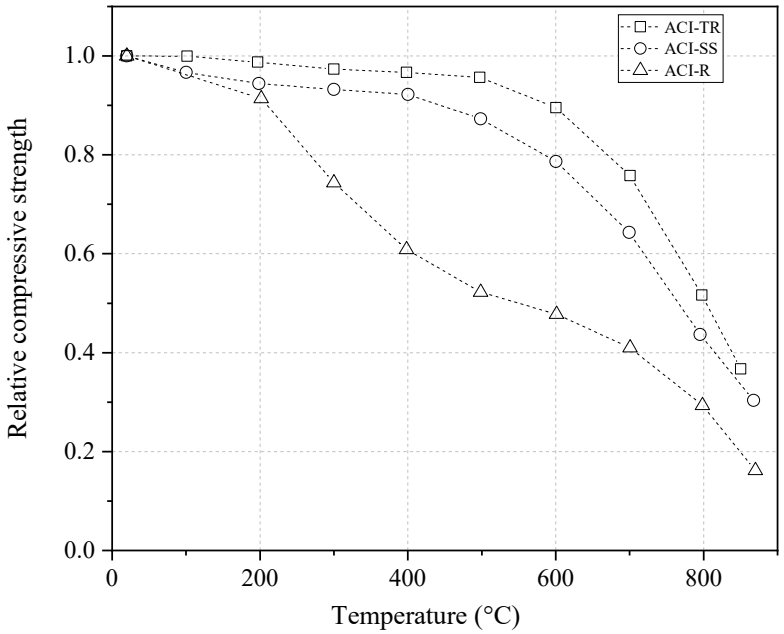

Figure 2-19. Relative compressive strength of lightweight aggregate concrete exposed to high temperatures presented by ACI 216.1 [74]

On the other hand, the Eurocode [73] shows the effect of high temperature on the compressive strength of siliceous aggregate concrete and calcareous aggregate concrete only for transient and steady-state test conditions. In addition, there is no data for lightweight concrete. In accordance with Eurocode [73], about 20% of the compressive strength of concrete is reduced at 400 °C, and concrete loses 80% of its strength compressive strength at the temperature of 800 °C. The decrease in compressive strength of concrete is obtained using the reduction factor of compressive strength identified on Eurocode [73], as shown in Figure 2-20.

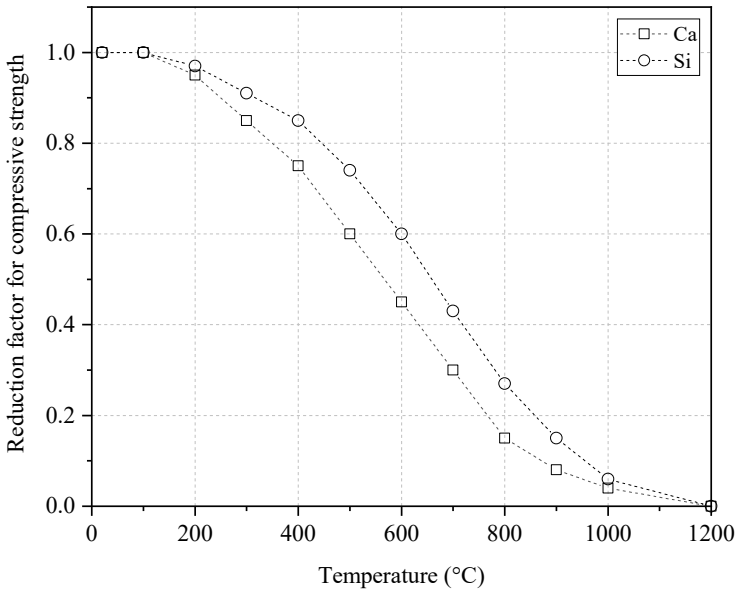

Figure 2-20. Reduction factor of compressive strength for siliceous concrete nad calcareous concrete presented by Eurocode [73]

2.3.3.2 Tensile strength

There has been less research on the tensile strength of concrete exposed to high temperatures than on the compressive strength and modulus of elasticity which is often disregarded. However, it plays a crucial role in susceptibility to spalling and cracking of concrete exposed to high temperatures. In other words, tensile strength resists the thermal stresses caused by internal vapour pressures at high temperatures [79, 80]. The Eurocode [73] provision has not taken to account the concrete residual test conditions and presented a simplified equation for the tensile strength of concrete under transient and steady-state test conditions. It shows that the deterioration of the tensile strength of concrete occurred above 100 °C. Furthermore, both NSC and HSC are considered the same when calculating the tensile strength of concrete exposed to high temperatures using the following equation (Equation 2-1):

$f_{ck,t}(\theta) = k_{c,t}(\theta)\, f_{ck,t}$ **Equation 2-1**

$k_{c,t}(\theta) = 1.0$ for 20 °C ≤ θ ≤ 100 °C

$k_{c,t}(\theta) = 1.0 - 1.0\,(\theta - 100)/500$ for 100 °C < θ ≤ 600 °C

where $f_{ck,t}$ tensile strength of concrete, $f_{ck,t}(\theta)$ reduced value of tensile strength of concrete at temperature of θ, and $k_{c,t}(\theta)$ reduction coefficient for tensile strength of concrete at temperature θ.

ACI 216.1 [74] does not provide a reduction factor or guidelines for the tensile strength of concrete subjected to high temperatures [81].

2.3.3.3 Modulus of elasticity

Despite extensive studies carried out on the compressive strength of concrete exposed to high temperatures, there is less investigation on the modulus of elasticity of concrete under fire conditions in the literature. The modulus of elasticity exposed to high temperature is not explicitly modeled in Eurocode [73]. The values of compressive strength or tensile strength and their corresponding strain as a function of temperature for concrete containing siliceous or calcareous aggregate are presented in Eurocode [73]. ACI 216R [82] has reproduced the data of only one research conducted by Cruz [83] for variation of modulus of elasticity of concrete exposed to high temperatures for three types of aggregate. The calcareous aggregate concrete exhibited a lower reduction in modulus of elasticity compared to siliceous and lightweight aggregate concrete [83].

There is inconsistency in the design curves of ACI 216.1 [74] and Eurocode [73], and their results are not applicable for the novel types of concrete containing SCMs. Moreover, as discussed earlier, the behaviour of concrete at high temperatures is nonlinear and affected

by several parameters such as physical and chemical changes in its ingredients, variations in heating and cooling regimes, type of aggregates and water to cement ratio. Therefore, the application of modern evaluating tools such as the machine learning approach is required to predict the mechanical properties of concrete at high temperatures.

2.4 An Overview of Machine Learning and Artificial Neural Network

Artificial Intelligence (AI) was first introduced at a workshop at Dartmouth College in the summer of 1956 [84]. AI is defined as the ability of a machine or system to exhibit behaviours associated with human intelligence, including planning, reasoning, perception, problem-solving, recognition of patterns, and creativity [85]. Several disciplines such as computer science, cybernetics, linguistics, information theory, and neurophysiology interact in order to develop artificial intelligence [86]. Machine learning is a subfield of AI that applies algorithms to synthesize the relationships between data and information [87]. Machine learning methods are divided into unsupervised, supervised, and semi-supervised learning. In supervised learning, a data set including both input and output variables is available. The algorithm learns by mapping the relationship between the supplied input and corresponding output variables [85, 88]. The supervised algorithm can predict the output of a new set of input data points, and this algorithm requires a large amount of data [89]. The Supervised algorithm is classified into two methods: the classification method is applied for discrete (categorical) output parameters, and regression is used for continuous output parameters**.**

On the other hand, in unsupervised learning, the input variables exist, and no output variables are provided. In this case, an algorithm tries to identify the underlying unknown

structure among inputs to fully understand the nature of the problem [78]. Semi-supervised learning is a type of learning that falls between unsupervised and supervised learning and has been shown to be able to learn from a small amount of training data and label (or test) unknown data [89].

The most common machine learning approaches are artificial neural networks (ANN), decision trees, support vector machines (SVM), and evolutionary algorithms (EA), as reported in the literature. There are significant differences in the structure of algorithms and strategies for finding the patterns in these models. The size of the dataset and the number of input variables influence the selection of the most suitable method [5, 88].

The artificial neural network (ANN) technique is popular and useful for a number of different purposes, including classification, pattern recognition, clustering and prediction [90]. One of the advantages of the ANN models is their ability to simplify the model to use and increase their accuracy in complicated natural systems with large inputs [90, 91].

2.4.1 Artificial neural network application in civil engineering

In recent years, ANN, as a subfield of ML, has been widely applied to solve many engineering problems [92]. The main property of ANNs is their ability to learn from examples directly. In addition, the other important features of ANNs are their capability to respond correctly or almost correctly to incomplete tasks, their ability to extract information from noisy or insufficient data, produce generalized results by analyzing new cases. These capabilities make ANNs highly effective tools for solving many civil engineering problems, in particular ones with complex or insufficient data. Neural networks have been successfully used in civil engineering to identify structural systems,

detect structural damage, material behaviour modeling, structural control, structural optimization, groundwater monitoring and predict experimental studies [93, 94].

The ANN method has been increasingly used to predict the mechanical properties of concrete at room temperature. However, relatively few research studies have been carried out on modeling the effect of high temperature on the mechanical properties of concrete. A review of the application of ANN-based models to predict the mechanical properties of concrete at room and high temperatures from literature is presented in the following subsections.

2.4.1.1 Prediction model for mechanical properties of concrete at room temperature

Behnood et al. [95] proposed an ANN-based model to estimate the compressive strength of concrete containing silica fume with acceptable error. Eight parameters including binder content, the percentage of silica fume to binder ratio, water to binder ratio, the ratio of coarse aggregate to the binder, the ratio of coarse aggregate to total aggregate, superplasticizer to binder ratio in percentage, age of concrete and maximum aggregate size were selected as input variables. The capability of the ANN model to predict the compressive strength of concrete based on the changes in the input parameter was examined using sensitivity analysis. It was found that when the percentage of silica fume to binder increased between 0 and 30%, the compressive strength of concrete with silica fume increased linearly. In addition, the maximum aggregate size significantly influences the compressive strength of silica fume concrete.

Atici [96] developed an ANN and multiple regression analysis (MRA) to estimate the compressive strength of concrete containing different amounts of fly ash and blast furnace

slag at various 3, 7, 28, 90, and 180-day curing times. The performance of the ANN model was compared to the MRA model using performance indices. It was concluded that the nonlinear functional relationships in inverse problems such as design concrete mix could be calculated using the ANN model, which is not possible with classical regression methods.

Chopra et al. [97] predicted the compressive strength of concrete with and without fly ash at different curing ages, including 28, 56, and 91 days using two computing techniques, Genetic Programming (GP) and Artificial Neural Networks. It was found that the ANN model using the Levenberg-Marquardt algorithms for training the network is the most reliable prediction tool for this purpose compared to the GP model.

Roshani et al. [91] developed the ANN model to investigate the mechanical properties of fly ash concrete. The database consists of 296 data points gathered from the literature. The parameters such as water content, fly ash, gravel, sand, cement, and SiO_2 content of fly ash were considered as the inputs of the network. The outputs of the network included the compressive strength, tensile strength, and modulus of elasticity. It was found that experimental results and predicted outputs of the ANN models agreed well. In addition, based on the ANN results to use the outputs of the network, simple and practical equations were derived to predict the mechanical properties of concrete with fly ash.

Boğa et al. [92] used an ANN model to predict the mechanical properties and durability properties of concrete that contained ground-granulated blast furnace slag (GGBFS) and calcium nitrite-based corrosion inhibitor (CNI). A total of 162 tests were conducted for

compressive strength, tensile strength and chloride ion permeability. It was found that the ANN model can estimate the experimental data with a notable degree of accuracy.

Bilim et al. [66] used an artificial neural network model to estimate the compressive strength of concrete made with GGBFS considering ingredients and age of concrete. ANN model was developed using 212 test data collected from laboratory work. The concrete specimens were prepared with three different w/b ratios (0.3, 0.4, and 0.5), three different cement dosages (350, 400, and 450 kg/m^3) and four different levels of partial GGBFS replacement (20%, 40%, 60%, and 80%). Compressive strengths were reported at six different ages (3, 7, 28, 90, and 360 days). The ANN model has been developed using six input parameters, including concrete age and ingredients. It was found that artificial neural networks can be used as an alternative method for predicting the compressive strength of slag concrete. They concluded that among the different ANN learning algorithms tested in this study, the Levenberg- Marquardt algorithm was determined to be the best algorithm.

2.4.1.2 Prediction model for mechanical properties of concrete at high temperature

Mukherjee et al. [3] evaluated the behaviour of concrete under three load conditions, including varying load under isothermal conditions, the varying temperature under constant load, and varying temperature under total restrain, by developing three separate feedforward artificial neural networks. The results indicated that the prediction results of the proposed ANN models indicated close agreement with the experimental results in all these situations.

Ahmad et al. [98] evaluated the compressive strength of concrete at high temperatures using different machine learning techniques, namely ANN and the decision tree gradient

boosting and bagging, based on 207 data points from the published articles in the literature. It was found that the ML algorithms are quite effective in predicting concrete performance at high temperatures. The ANN model showed a better performance compared to the decision tree. However, the bagging model correlation coefficient indicated a better level of accuracy in comparison to the ANN, decision tree, and gradient boosting.

Abbas et al. [99] investigated the residual strength of HSC after exposure to high temperatures using the ANN model. Three different ANN models were developed for concrete containing siliceous, calcareous, and combined aggregate. A total of 460 data sets was collected from the literature, of which 177 data points were for calcareous aggregate, 228 data points were for siliceous aggregate, and the rest were either silico-calcareous or unknown aggregate. According to the results of the sensitivity analysis, among various variables, the water to binder ratio, elevated temperature, and the compressive strength of concrete at room temperature were the most affecting variables to develop the models for all aggregate types. The ANN-based models showed small errors and high correlation consistently.

Türkmen et al. [100] used an ANN model to evaluate the compressive strength of lightweight concrete containing Pumis aggregate after high temperatures exposure. An experimental test was conducted, and the experimental results were used to establish the ANN model database. The ratio of Pumis and the temperature target was considered as inputs of the network. The prediction results of the ANN model were in good agreement with experimental data. As a result, the compressive strength can be predicted using the ANN model. Based on the sensitivity analysis for the model, it can be concluded that the target temperature has the most influence on the ANN model of compressive strength.

As seen from the above literature, the existing studies are restricted to a specific type of concrete and many affecting critical factors in the mechanical properties of concrete at high temperatures are ignored. Moreover, some studies have been conducted based on the own experimental data of the researchers, while they may not be reliable and accurate in predicting the results of other researchers.

Therefore, to overcome these drawbacks, the present study has employed the artificial

neural network model to predict the mechanical properties of concrete exposed to high temperatures based on a comprehensive database collected from previous experimental studies considering all the possible influencing parameters. The procedure for developing the ANN models are described in the following sections.

Chapter 3: Developing artificial neural network (ANN) models

The artificial neural network learns from past experiments, identifies the pattern of the collected data, and predicts the behaviour of the study subject [101]. Generally, a neural network is developed through the acquisition and analysis of data and creating a database, determining the architecture, training of the network, and evaluating the model's performance after training [102]. Three different ANN models were developed for predicting the compressive strength, tensile strength and modulus of elasticity of concrete exposed to high temperatures. The process of development of proposed ANN models is presented in the following subsections.

3.1 Development of the ANN model

The topology of artificial neural networks is similar to the human brain in two aspects: (1) the neural network acquires the knowledge from its environment using a learning process, and (2) acquired knowledge is stored in inter-neuron connections strengths or (synaptic) weights [85, 103].

ANN models are comprised of large numbers of neurons, which serve as data processing units. As seen in Figure 3-1, the general configuration of the neural network is composed of an input layer, one or more hidden layers and an output layer. The neurons of each layer are connected to all neurons of the next layers with numerical values known as weights. Weights could be adjusted for every new input data [104]. The input information received by neurons of the input layer is multiplied by the modifiable weights. The sum of the weighted inputs is obtained using the following function (Equation 3-1) :

$$(net)_j = \sum_{i=1}^{n}(\boldsymbol{x}_i \boldsymbol{w}_{ij}) + \boldsymbol{b}$$ **Equation 3-1**

where (net)j is the weighted sum of the jth neuron for the input received from the preceding layer with n neurons, x_i represents the input value of the in input neuron, w_{ij} is the weight between i neuron of the input layer and j neuron in the next layer; and b is a fixed value as internal addition called bias. The summation results are then transmitted to neurons in the hidden layer. Each hidden neuron processes information through an activation function and sends its output to the neurons of the output layer. This data is multiplied by the corresponding weights between the hidden layer and output layer, and then their sum is calculated and transmitted to the output layer [92, 105]. Then another activation function is applied to this data, and the output of the network is computed in the output layer. The ANN model outputs are then compared to the desired outputs to determine the error of the network. In order to minimize training error, the output layer passes the error back to the input layer, and the network weights and biases are adjusted using an error backpropagation algorithm. This training cycle, known as an epoch, is repeated until the error is decreased to an acceptable level [106, 107]. Various algorithms have been used for training ANN models, including the back-propagation algorithm, simulating annealing algorithm, genetic algorithm, and particle swarm optimization algorithm [108]. The backpropagation algorithm is one of the most common training algorithms using the gradient descent approach that modifies the weights for a particular training pattern in order to minimize the error.

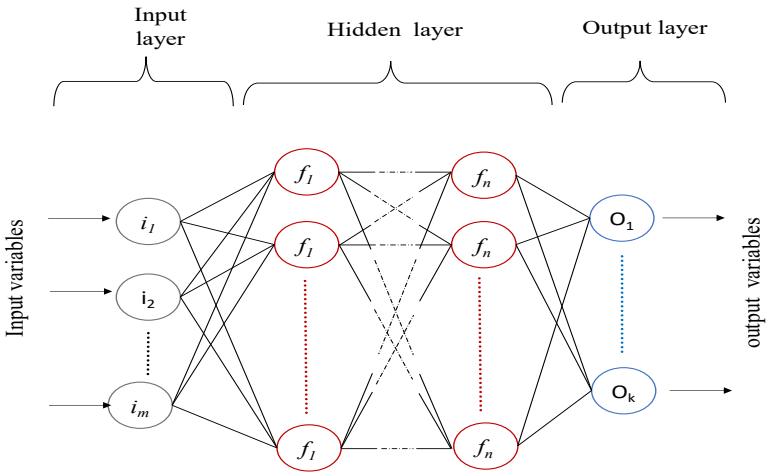

Figure 3-1. Typical architecture of the artificial neural network with n hidden layer

3.1.1 Database of materials tests at high temperatures

In the first step, it is extremely important to select the proper database for training neural networks. There are two important criteria: (i) the database should contain complete information regarding the relationship between the inputs and outputs, and (ii) the training data must be sufficiently large for the training process [109]. Generally, an in-depth literature review or a comprehensive testing program is conducted to develop the database. In order to accelerate the learning process and achieve faster convergence as well as generate values in the 0-1 range by the activation functions, the content of the database before the training process must be normalized within the 0-1 range using the linear Equation 3-2 [110, 111]:

$$x_{normalized} = \frac{x - x_{min}}{x_{max} - x_{min}} \qquad \textbf{Equation 3-2}$$

where $x_{normalized}$, x_{min} and x_{max} denotes the normalized, minimum, and maximum values of x from input or output variables, respectively.

In the present study to construct the database, the following criteria were considered:

1. Due to the abundance of residual material tests on concrete in the database, the focus of this research has been placed on the residual properties of concrete.
2. The database only contained air-cooled concrete after the heating period for the residual test method.
3. The data covers concrete specimens containing no fibres.

3.1.1.1 Compressive strength model

An optimized ANN model for predicting the compressive strength of concrete exposed to high temperature was developed by collecting a comprehensive database containing 500 experimental results from the published literature. Fourteen parameters, including temperature level, aggregate type (Si, Ca and LWA), percentage of SCMs (SF, FA, and GGBFS) as the cement replacement, the amount of cement, coarse and fine aggregate, water content, and test method, namely transient (T), steady-state (SS) and residual (R), were selected as input variables. The ratio of compressive strength of concrete at a given temperature to the initial strength of concrete at room temperature was considered the output of the ANN-based model.

It should be noted that the variation of heating rate in the collected experimental records was between 0.77 and 25. However, the degradation of mechanical properties had no significant differences with varying the heating rate. As a result, the heating rate is not very influential in the degradation of mechanical properties of concrete other than in the case when it impacts the spalling occurrence. As the heating rate increases, concrete is more prone to spalling [112]. Furthermore, some studies have not reported the heating rate. Therefore, the heating rate was not included in the input parameters of the ANN model because the mentioned studies with a good number of data (105 data points) should have

been discarded. The statistical properties of collected data sets are represented in Table 3-1. The distribution of each quantitative input parameter in the data set is shown in Figure 3-2. In addition, the frequency of different SCMs (SF, FA and GGBS) and various test methods for three types of aggregate (Si, Ca and LWA) are represented in Figure 3-3 and Figure 3-4, respectively. The studies on lightweight aggregate are considerably limited compared to other types of aggregate, and there is no investigation of the calcareous aggregate concrete containing GGBFS exposed to high temperatures.

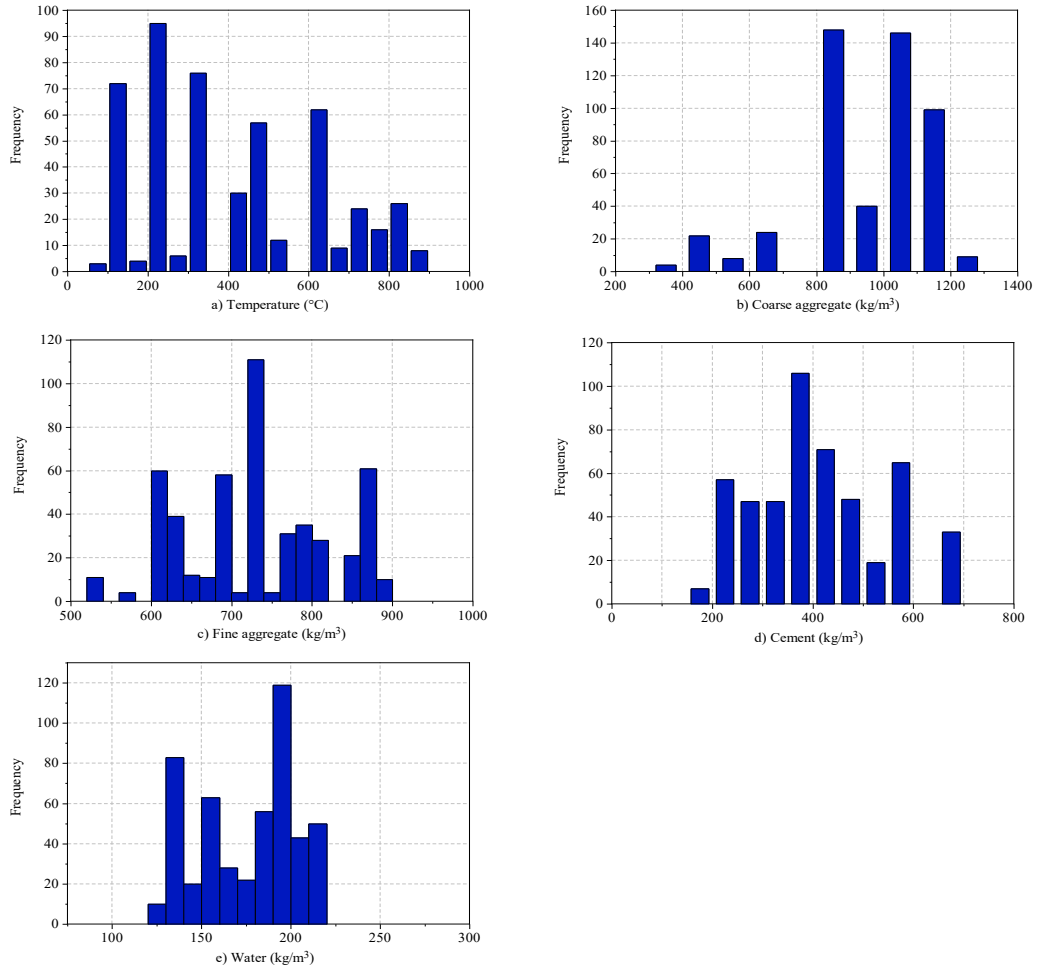

Figure 3-2. Distribution of input parameters for prediction of compressive strength: a) level of Temperature, b) coarse aggregate, c) fine aggregate, d) cement, and e) Water

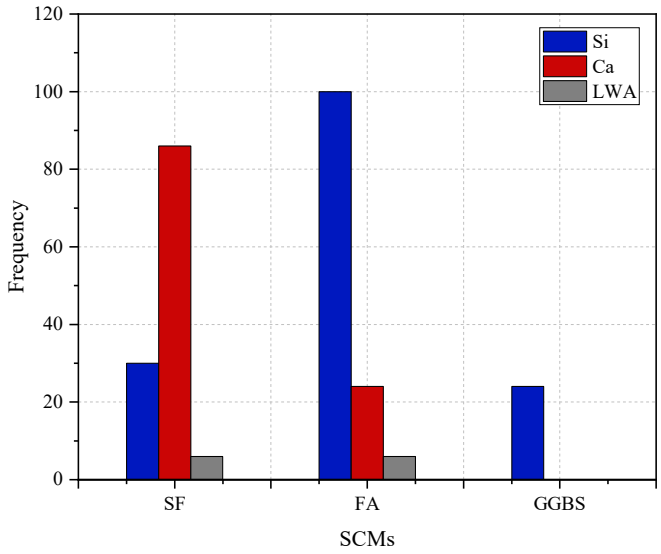

Figure 3-3. Distribution of different types of SCMs (SF, FA and GGBS) for prediction of compressive strength

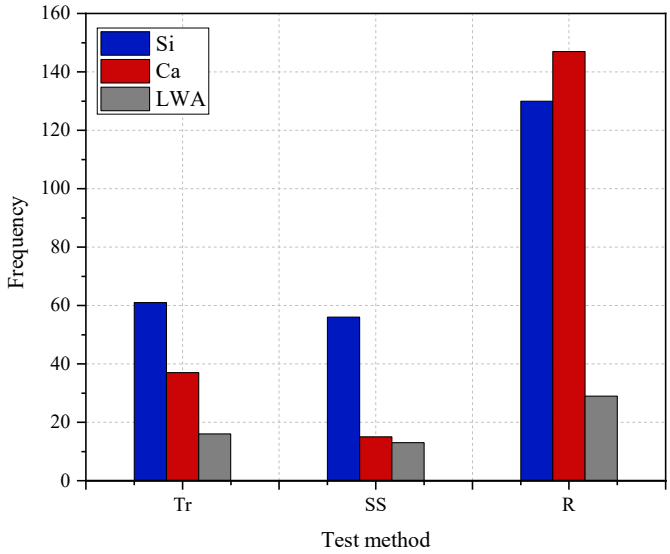

Figure 3-4. Distribution of different test methods (Tr, SS and R) for prediction of compressive strength

Table 3-1. Statistics of the quantitative input parameters used in the compressive strength ANN model

Attribute	Unit	Max	Min	Average
Temperature	°C	870	95	392
Coarse aggregate	kg/m^3	1200	369	950
Fine aggregate	kg/m^3	880	536	732
Cement	kg/m^3	662	180	406
Water	kg/m^3	250	127	175

3.1.1.2 Tensile strength

The tensile strength of normal strength concrete is only 10% of its compressive strength, and this ratio is even lower for high strength concrete. For this reason, in calculating strength at room and high temperatures, the tensile strength is often ignored. The literature is limited in reporting the tensile strength of concrete exposed to high temperatures. However, tensile strength is the main reason for cracks formation in concrete in fire conditions. In addition, spalling occurs in concrete when cracks form due to rapid temperature rising or under fire conditions. Thus, tensile strength plays a crucial role in the behaviour of concrete at high temperatures, particularly in spalling of concrete [10].

The database, including the results of 110 specimens reported in previous studies, was collected to predict the tensile strength of concrete exposed to high temperatures. The collected data is restricted to residual tests. The input variables include temperature level, aggregate type (Si, Ca and LWA), the percentage of SCMs (SF and FA) as the cement replacement, the amount of cement, coarse and fine aggregate, and water content. The relative residual tensile strength was selected as the output variable. Figure 3-5 represents the histogram of the input parameters used for developing the ANN model to predict the tensile strength. The descriptive statistics of the input parameters are given in Table 3-2. The distribution of different types SCMs for the prediction of tensile strength exposed to high temperatures is illustrated in Figure 3-6. It can be seen that the tensile strength of concrete containing SCMs has been less studied, particularly for GGBS.

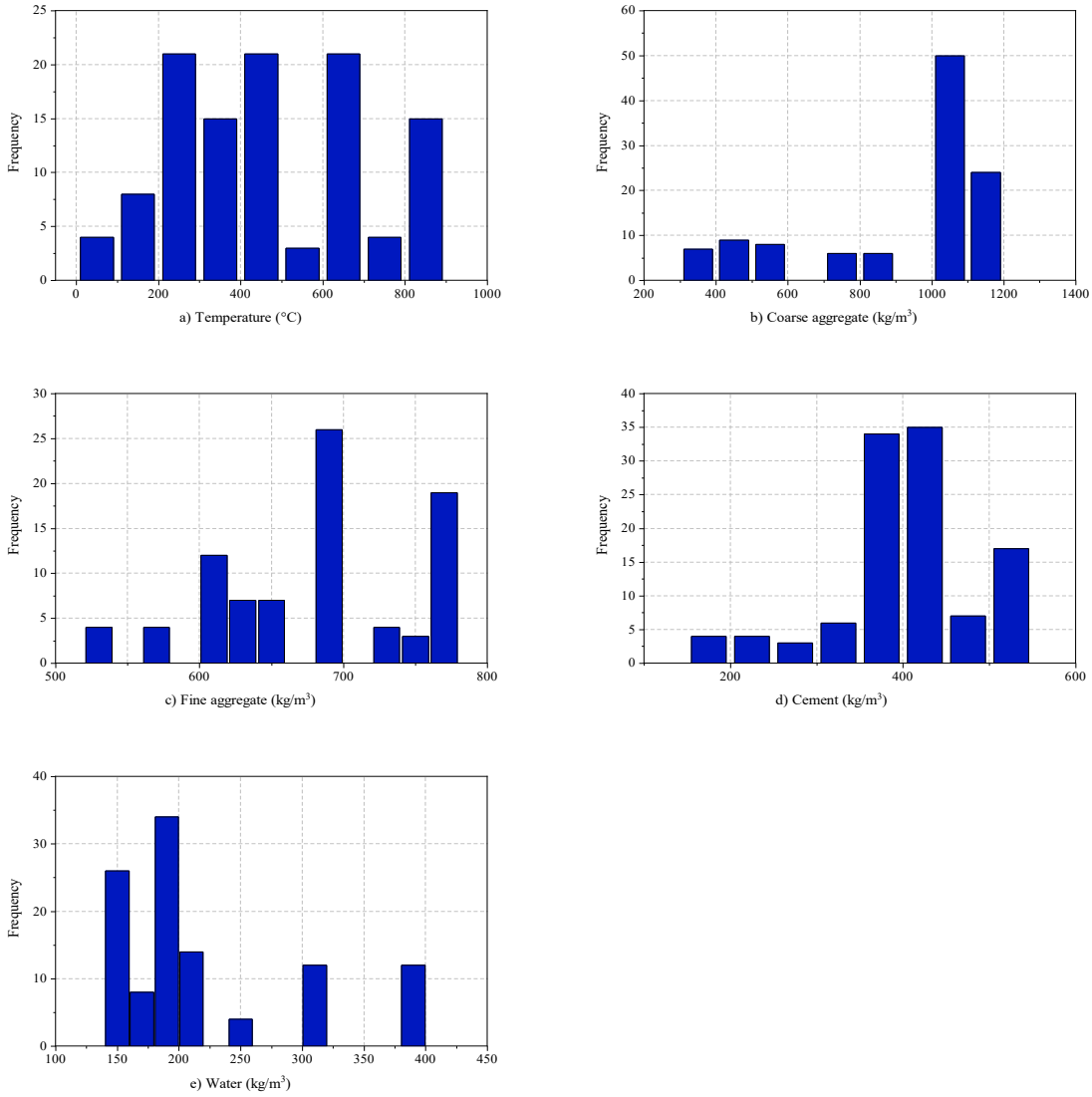

Figure 3-5. Distribution of input parameters for prediction of tensile strength: a) level of Temperature, b) coarse aggregate, c) fine aggregate, d) cement, and e) water

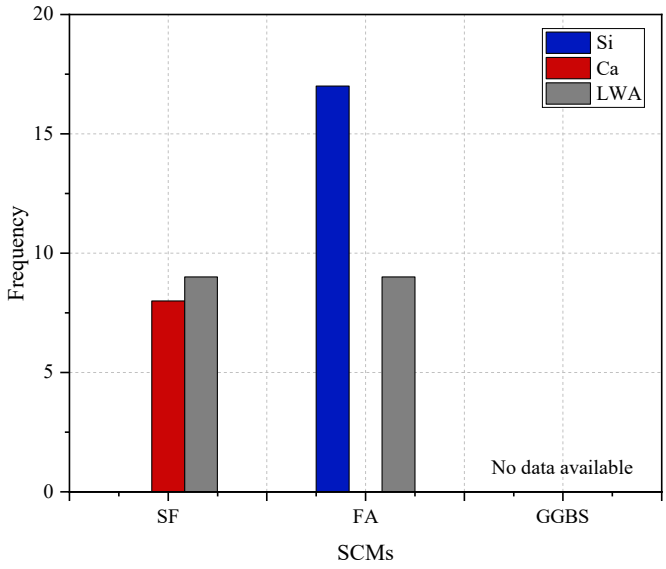

Figure 3-6. Distribution of different types of SCMs (SF, FA and GGBS) for prediction of tensile strength

Table 3-2. Statistics of the quantitative input parameters used in the tensile strength ANN model

Attribute	Unit	Max	Min	Average
Temperature	°C	800	95	484
Coarse aggregate	kg/m^3	1168	369	938
Fine aggregate	kg/m^3	777	536	666
Cement	kg/m^3	500	184	363
Water	kg/m^3	308	149	188

3.1.1.3 Modulus of elasticity

A total of 128 data points from the literature were compiled for the purpose of estimating the modulus of elasticity of concrete under high temperatures. The parameters such as temperature level, aggregate type (Si and Ca), the percentage of SCMs (SF and FA) as the cement replacement, amount of coarse and fine aggregate, the amount of cement, water content and test methods (Tr and R) were considered as the input parameters. The distribution of input variables to develop an ANN model to predict the modulus of elasticity of concrete exposed to high temperature is represented in Figure 3-7. The statistical

properties of collected data sets are represented in Table 3-3. Moreover, the distributions of different types SCMs (SF, FA and GGBS) and test methods are shown in

Figure **3-8** and Figure 3-9. It can be seen that the lack of data is highly apparent for transient and steady-state tests.

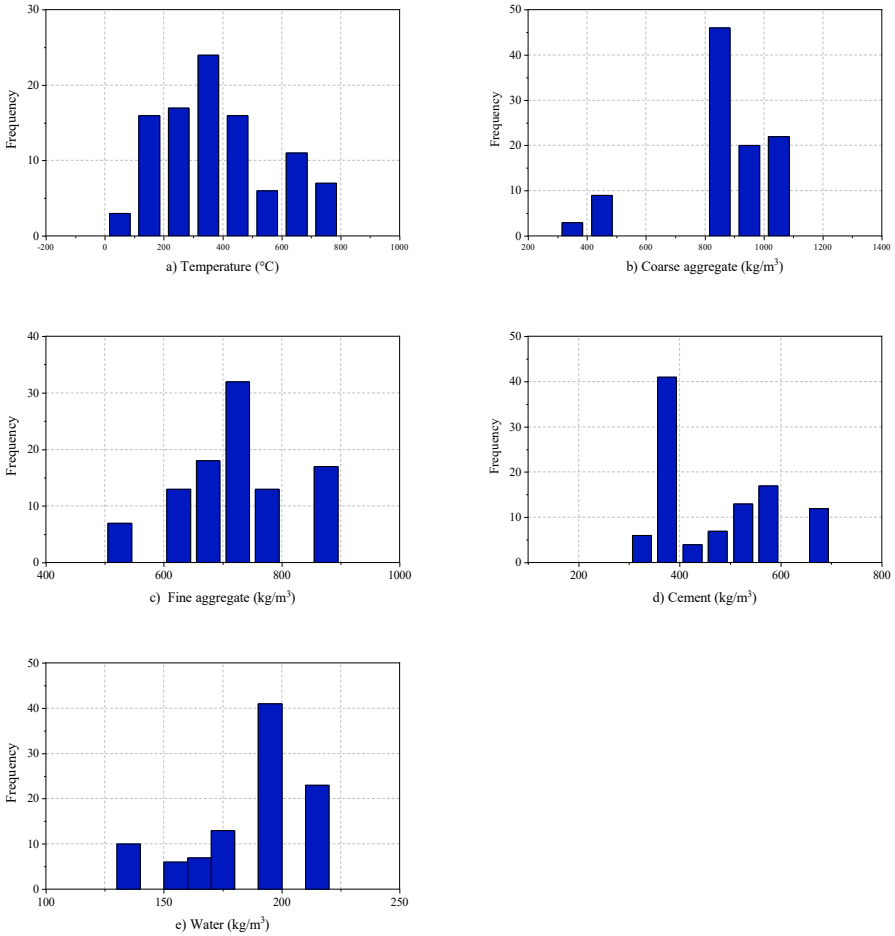

Figure 3-7. Distribution of input parameters for prediction of modulus of elasticity: a) level of Temperature, b) coarse aggregate, c) fine aggregate, d) cement, and e) Water

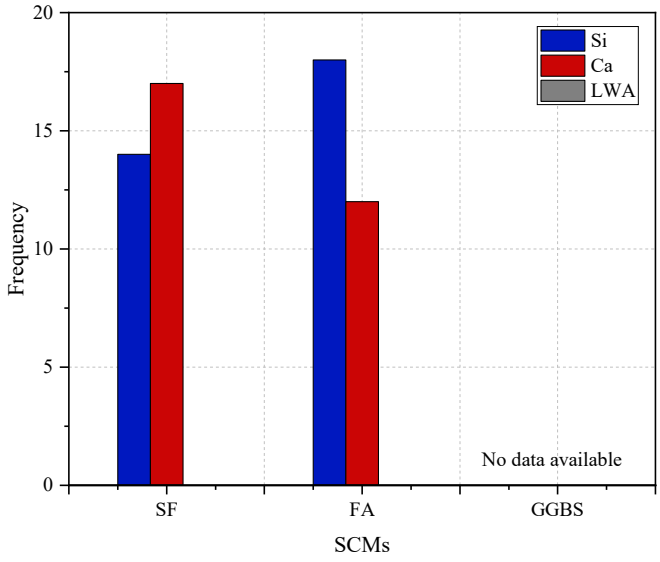

Figure 3-8. Distribution of different types of SCMs (SF, FA and GGBS) for prediction of modulus of elasticity

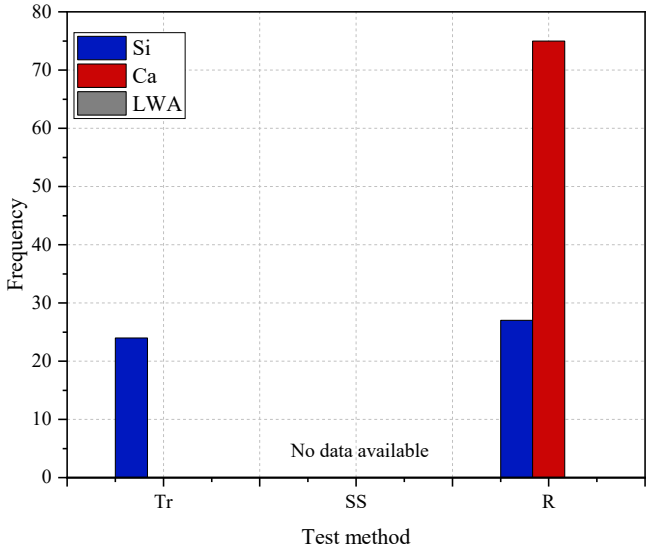

Figure 3-9. Distribution of different test methods (Tr, SS and R) for prediction of modulus of elasticity

Table 3-3. Statistics of the quantitative input parameters used in modulus of elasticity ANN model

Attribute	Unit	Max	Min	Average
Temperature	◦ C	750	95	385
Coarse aggregate	kg/m^3	1095	393	906
Fine aggregate	kg/m^3	868	537	746
Cement	kg/m^3	662	210	418
Water	kg/m^3	217	133	185

3.1.2 Modeling the network

After creating the database, the critical step is identifying the best architecture of the model. The architecture of the ANN model is comprised of four elements [112]:

1. The number of layers and neurons within each layer
2. The activation function
3. The training algorithm

3.1.2.1 The number of layers and neurons within each layer

Generally, the ANN model consists of the input, hidden, and output layers. Input and output parameters determined the number of neurons in input and output layers. Therefore, in order to achieve the best architecture of an artificial neural network, the number of hidden layers and their neurons should be chosen appropriately. There is no general method for selecting the number of neurons in the hidden layer to establish an ANN model for a particular problem. The number of neurons in the hidden layer is determined through the trial-and-error method. The design of a stable backpropagation network is conducted by changing the number of neurons in the hidden layer and evaluating changing stability of the ANN models [96]. Thus, the number of neurons in the hidden layers can be started with a small number and increasing it progressively while monitoring the error of the network. Finally, the optimum number of the hidden neurons is obtained based on the error criteria or performance of the network. The performance of the network is discussed in section 3.1.3.

In the present study, a source code was used in the MATLAB program to operate the trial-and-error process automatically. The model was run several times in the MATLAB environment to determine the best architecture of the neural network.

3.1.2.1 The activation function

Activation functions are selected based on the type of data and layer available. The neurons calculate their output using an activation function based on the weighted inputs that they receive. There are three different types of activation functions commonly used in artificial neural networks, namely hyperbolic tangent sigmoid (TANSIG), logarithmic sigmoid (LOGSIG), and linear transfer (PURLIN) function, as represented in Equation 3-3, Equation 3-4 and Equation 3-5 [113].

$$y = TANSIG = \frac{2}{1+e^{-2x}} - 1 \qquad \textbf{Equation 3-3}$$

$$y = LOGSIG = \frac{1}{1+e^{-x}} \qquad \textbf{Equation 3-4}$$

$$y = PURLIN = x \qquad \textbf{Equation 3-5}$$

This study employed Tansig and Purlin activation functions in the hidden layer and output layer, respectively.

3.1.2.2 The training algorithm

There are different training algorithms in the MATLAB environment, such as Scaled Conjugate Gradient back, Levenberg-Marquardt, Bayesian Regularization, etc. In this research, the backpropagation Levenberg Marquardt (LM) training algorithm was employed due to its accuracy in predicting the mechanical characteristics of concrete seposed to high temperatures.

3.1.2.3 Structure of ANN models

In the following sections, the optimum architecture of each model to predict the mechanical properties of concrete exposed to high temperatures is presented. Similar activation function and training function was used to develop the ANN models. The number of hidden neurons was achieved using a trial and error approach.

3.1.2.3.1 ANN Structure for prediction of compressive strength

The best configuration of the network is reached by trial and error. Different architectures with varying numbers of neurons in the hidden layer have been tested to achieve the best structure of the proposed model using the MATLAB program. The error values for each number of neurons in the hidden layer were checked. Finally, a model with a suitable error consisting of 12 neurons in one hidden layer was selected to estimate the relative compressive strength of concrete at high temperatures, as depicted in Figure 3-10.

It is worth mentioning that the number of neurons in the input and output layer equals the number of input and output variables for each ANN model.

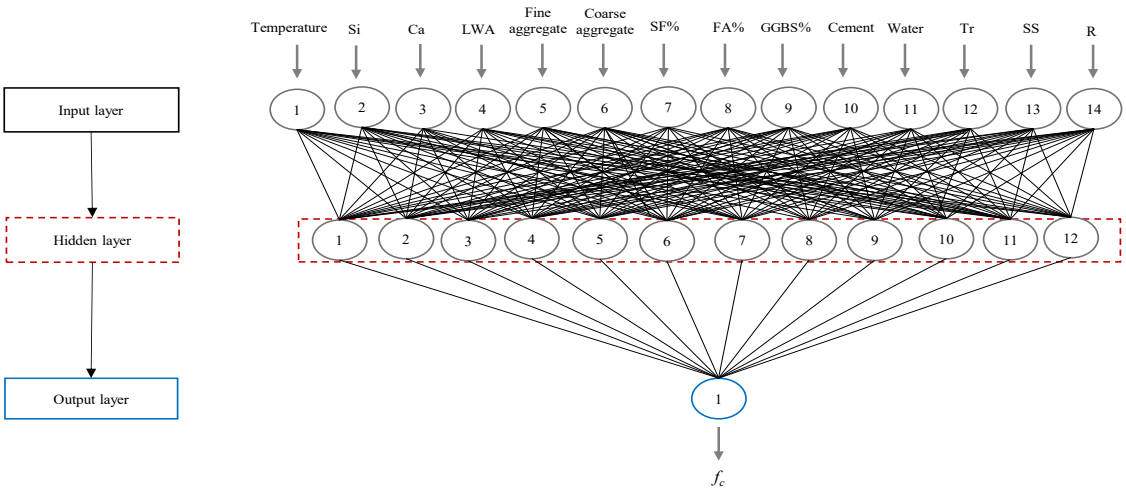

Figure 3-10. The architecture of the proposed compressive strength ANN model

3.1.2.3.2 ANN structure for prediction tensile strength

Figure 3-11 illustrates the selected structure of the network comprising a single hidden layer with 15 neurons to predict the tensile strength of concrete exposed to high temperatures based on the trial and error approach.

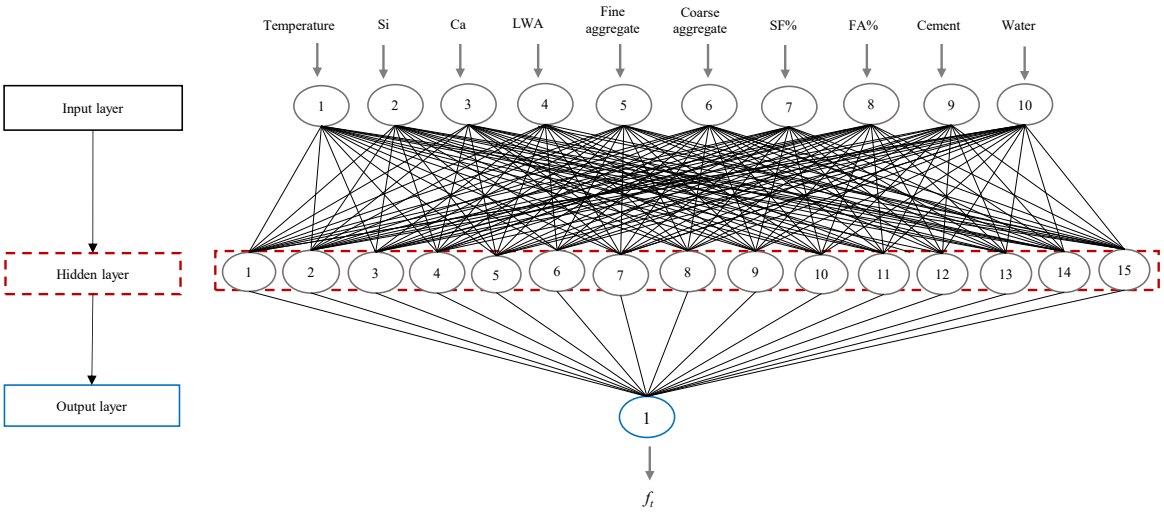

Figure 3-11. The architecture of the proposed tensile strength ANN model

3.1.2.3.3 ANN structure for prediction of modulus of elasticity

The ANN-based model with twelve neurons in a single hidden layer shows the best performance to predict the modulus of elasticity of concrete under high temperatures, as shown in Figure 3-12.

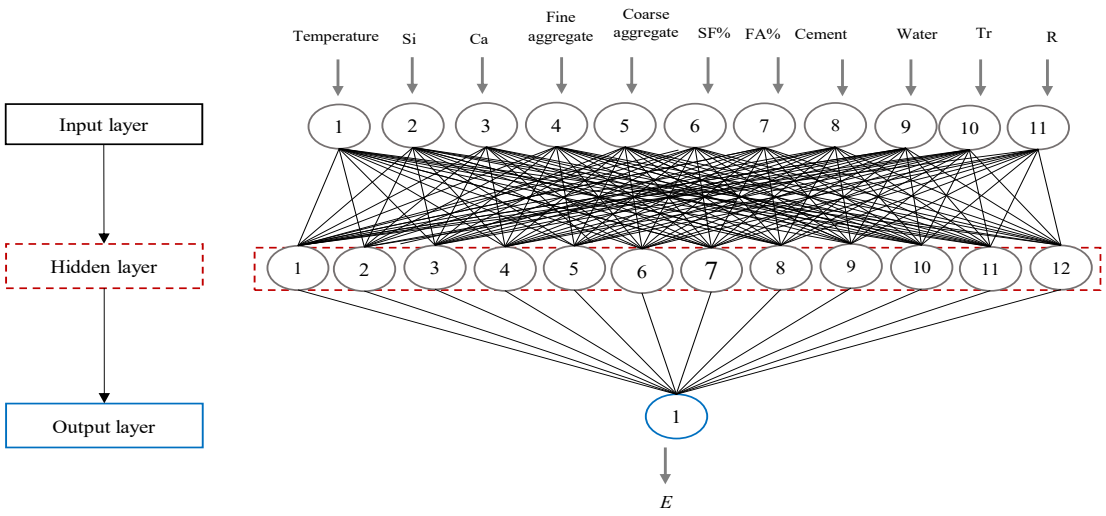

Figure 3-12. The architecture of the proposed modulus of elasticity ANN model

3.1.3 Performance of the ANN models

Statistical error estimation methods, including coefficient correlation (R), root mean square error (RMSE), mean square error (MSE), mean absolute error (MAE), etc., are used to evaluate the performance of the proposed model. In this study, R and MSE between the actual experimental output (target) and model output are employed to assess the adequacy and precision of the trained networks according to Equation 3-6 and Equation 3-7. The R-value close to 1 and MSE almost 0 demonstrates the reliability of the outcome of the network [114].

$$\boldsymbol{MSE} = \frac{1}{N}\sum_{i=1}^{N}(y_i - \hat{y}_i)^2 \qquad \textbf{Equation 3-6}$$

$$\boldsymbol{R} = \frac{\sum(\hat{y}-\bar{\hat{y}})(y-\bar{y})}{\sqrt{\sum(\hat{y}-\bar{\hat{y}})^2}\sqrt{\sum(y-\bar{y})^2}} \qquad \textbf{Equation 3-7}$$

where $\bar{y}$ and $\bar{\hat{y}}$ demonstrate the average values of the target and predicted outputs;y and the $\hat{y}$ are the target and predicted values of the network, respectively.

The evaluation of the performance of each suggested ANN model is presented in the following subsections.

3.1.3.1 Proposed ANN model of compressive strength

Generally, the ANN models are developed using three main datasets: training, validation, and testing. Therefore, the database was randomly divided into three subsets in order to achieve good generalization: training, validation, and testing sets. The training data is used for training the model by adjusting weight. As part of the training process, the validation data sets are used to evaluate the model fit on training data and refrain from overfitting by stopping the training. The testing data set is used to measure the generalization capability of the model [115].In the present study, by default in MATLAB, the database is randomly divided into three subsets: 70% of total data points for training, 15% for validation and 15 % for testing using the LM algorithm. These percentages are the most common ratios to split the data set. However, other portions to divide the data, such as (80%,10% and 10%) and (60%, 20% and 20%) can be used to determine the best performance for the network.

In order to assess the performance of data, plots of the mean square error (MSE) versus epoch (number of iterations) are used for training, validation, and testing [116]. Figure 3-13 shows the best performance of the networks in predicting the compressive strength established in the MATLAB program. The blue line represents the decreasing mean square error of the training data set. The green line shows the validation error, which monitors the overfitting of networks as the main feature to specify the ability of the ANN model to predict new data [117]. The overfitting occurs in the network when the validation error data begins rising [118]. The red line indicates the error of the test data used to determine the performance of the model after training. The circle shows the iteration at which the validation performance reached a minimum value.

The best performance is achieved at the lowest error of validation when there is no further increase in MSE error [116]. The best validation of the performance of the proposed compressive strength ANN model was obtained at epoch 18 with a mean square error (MSE) of 0.00477. The number of epochs indicates how many times the training cycle was repeated to achieve the MES error of 0.00477.

The coefficient correlation (R) indicating the correlation between the target and predicted values for all data is depicted in Figure 3-14. It can be seen that the coefficient correlation was 0.966 for the relative compressive strength ANN model. In terms of R, one is the optimal value, and on the other hand, the desired value for MSE is zero [91]. Thus, the obtained values of R and MSE indicated the satisfactory performance of the proposed network with a large number of input variables.

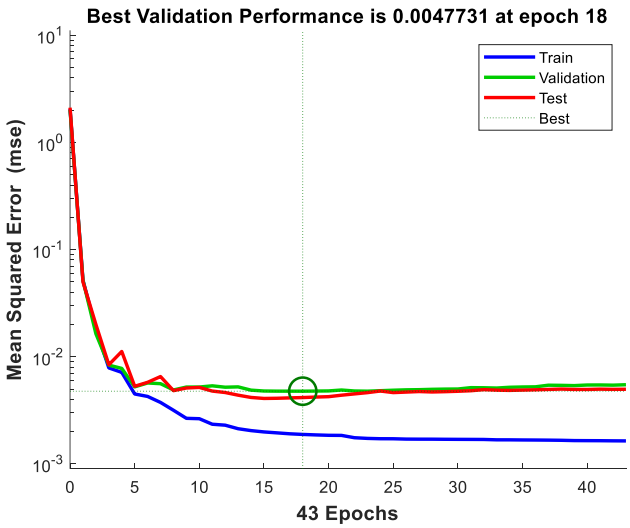

Figure 3-13. The performance of the proposed model of compressive strength

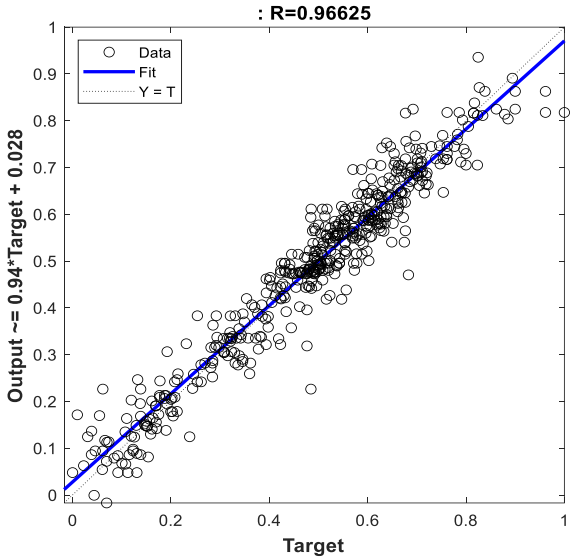

Figure 3-14. The regression of the proposed model of compressive strength

3.1.3.2 Proposed ANN model of Tensile strength

The values of min square error and coefficient correlation to estimate the tensile strength of concrete under high temperature were 0.0096 and 0.976, as shown in Figure 3-15 and Figure 3-16, respectively. These values were at an acceptable level indicating the accuracy of the model in predicting the tensile strength of concrete.

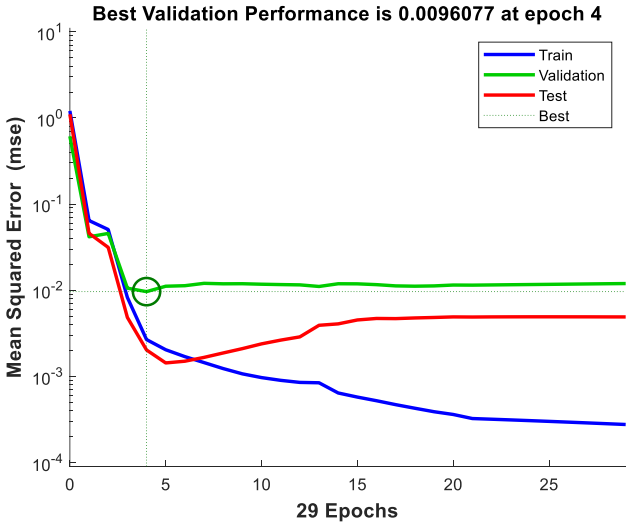

Figure 3-15. The performance of the proposed model of tensile strength

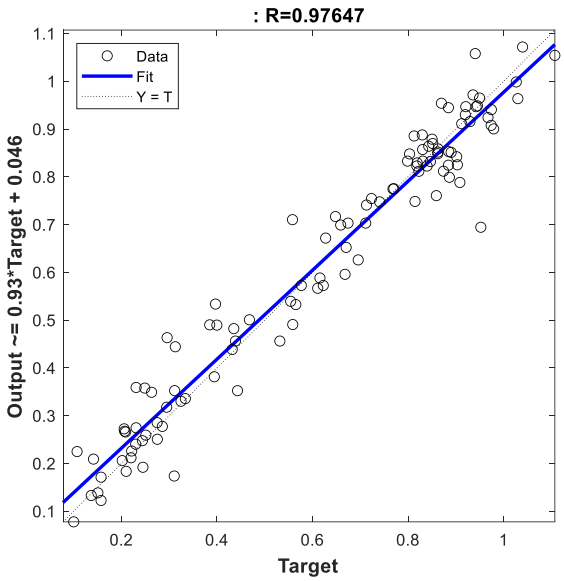

Figure 3-16. The regression of the proposed model of tensile strength

3.1.3.3 Proposed ANN model of Modulus elasticity

The suggested ANN model to predict the modulus of elasticity of concrete exposed to high temperature presents an MSE of 0.0089 and an R of 0.981, as illustrated in

Figure 3-17 and Figure 2-18, respectively. These values demonstrated the capability of the suggested ANN model to accurately predict the modulus of elasticity of concrete exposed to high temperatures.

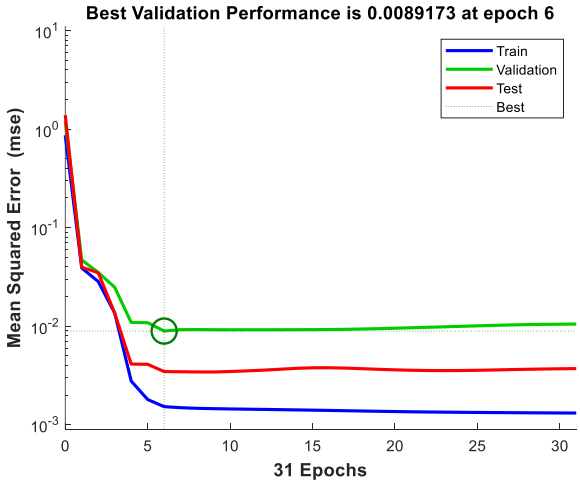

Figure 3-17. The performance of the proposed model of modulus of elasticity

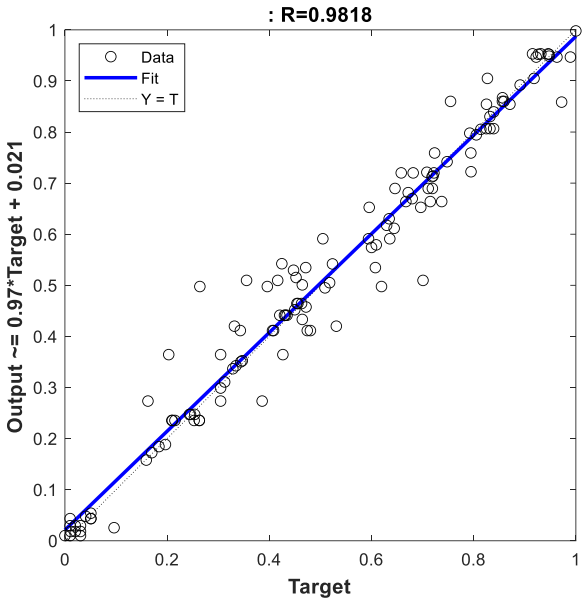

Figure 3-18. The regression of the proposed model of modulus of elasticity

3.2 Sensitivity analysis

The sensitivity analysis is used to determine how input variables contribute to the output of a network. In this way, the user can reduce the size of the network by eliminating insignificant input parameters [119]. This technique identifies the most important input parameters considered by the network. The weights determine the impact of a particular input on the output of the network. The relative significance of each parameter in the network is assessed by calculating Garson's factor as shown in Equation 3-8 [110]:

$$\boldsymbol{Q_{ik}} = \frac{\sum_{j=1}^{l}\left(\frac{w_{ij}}{\sum_{r=1}^{N} w_{rj}} v_{jk}\right)}{\sum_{i=1}^{N}\left(\sum_{j=1}^{L}\frac{w_{ij}}{\sum_{r=1}^{N} w_{rj}} v_{jk}\right)} \qquad \textbf{Equation 3-8}$$

where w_{ij} is the connection weight between the hidden neuron i and the input neuron j, v_{ik} is the connection weight of hidden neuron i, and the output neuron k and $\sum_{r=1}^{N} w_{rj}$ is the sum of the connection weights of N input neurons and hidden neuron j [110]. The algorithm of relative importance is represented in Figure 3-19.

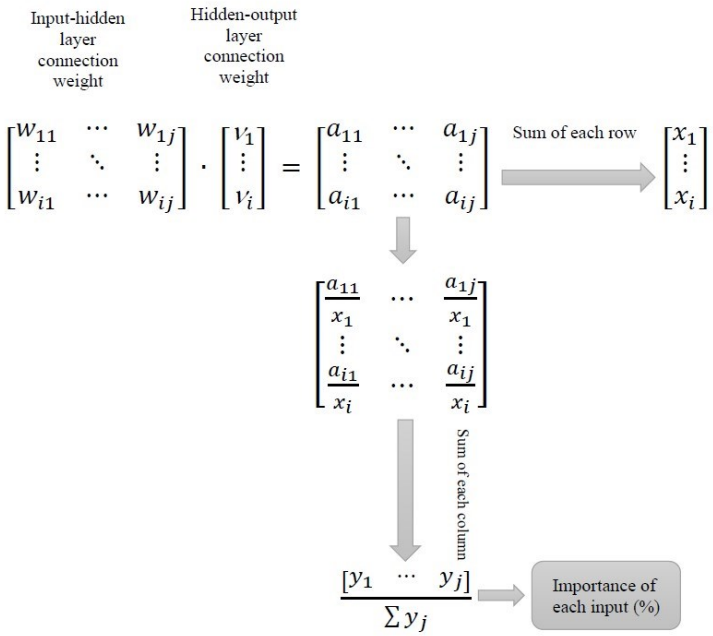

Figure 3-19. Algorithm of relative importance [110]

After training the model, the values connection weights between each layer can be generated. In this algorithm, i indicates the number of neurons in the hidden layer, and j shows the number of neurons in the input layer. The absolute value of the hidden-output layer connection weights is multiplied by the absolute value of the hidden-input layer connection weights. Then each element of the product matrix is divided by the sum of its corresponding row. In the new matrix, the sum of each column is calculated, which produces a matrix with one row. Then each element of this matrix is divided by the sum of its all elements. Expressed these values as a percentage, the relative importance of each input variable is obtained [120].

In the present study, the sensitivity analysis is conducted, and results for the compressive and tensile strength and modulus of elasticity of concrete are illustrated in Figure 3-20,

Figure **3-21** and Figure 3-22, respectively. Relatively comparable participation in predicting the mechanical properties of concrete exposed to high temperatures was observed for almost all input variables. Since no parameters have low importance, it can be concluded there are no excessive or irrelevant input parameters that were included [91]. The results of the sensitivity analysis revealed that the target temperature is the most important parameter in the results of the three developed ANN-based models compared to other input variables.

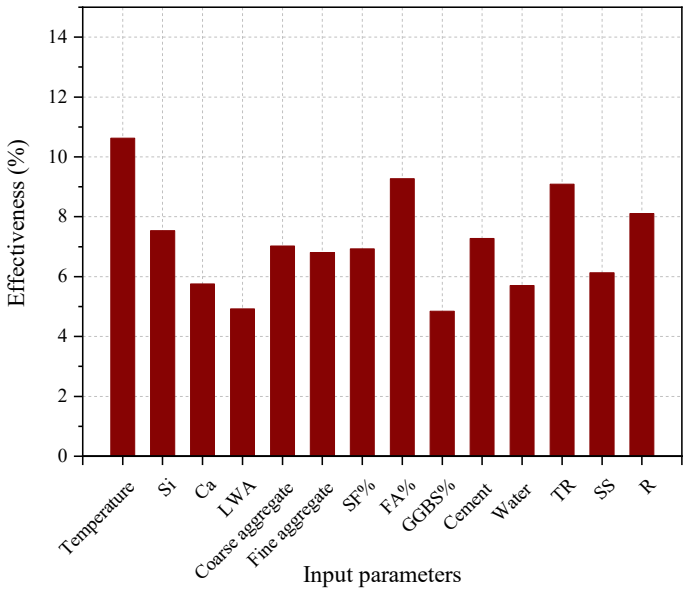

Figure 3-20. Sensitivity analysis of the selected model for compressive strength of concrete at high temperatures

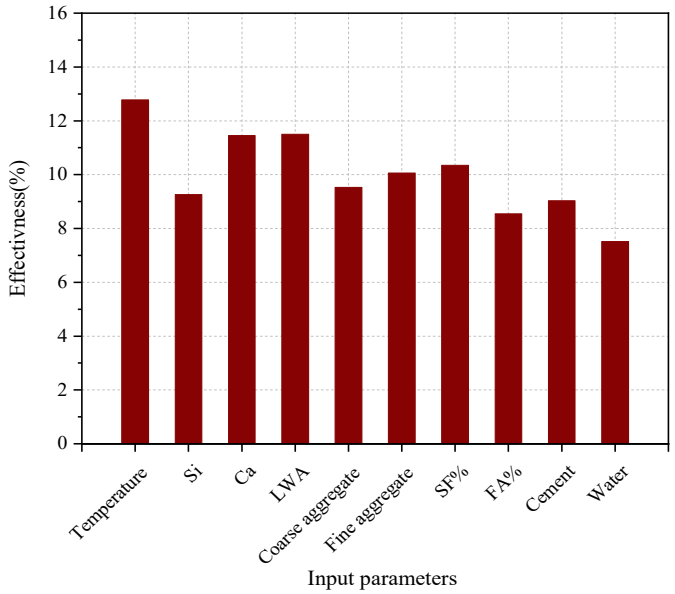

Figure 3-21. Sensitivity analysis of the selected model for tensile strength of concrete at high temperatures

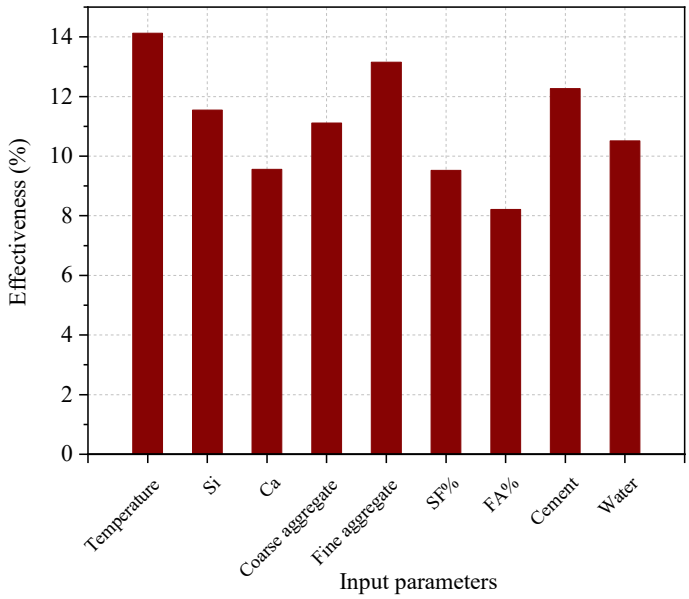

Figure 3-22. Sensitivity analysis of the selected model for modulus of elasticity of concrete at high temperatures

Chapter 4: Implementation of the ANN model to predict concrete properties at high temperatures

4.1 Parametric study

Three separate ANN-based models were developed to predict the mechanical characteristics of concrete exposed to high temperatures, and their performance was evaluated. Due to the generalization capability of the neural network, parametric studies can be conducted to examine the influence of the input variables on the output [120]. In the following subsections, the parametric analysis results are presented to evaluate the effect of input variables on the mechanical characteristic of concrete using suggested ANN models.

4.1.1 Compressive strength model

The variation of compressive strength due to changes in input parameters was determined in this section. Patterns similar but not identical to those with which ANN models have been trained can be recognized and answered by the models [112]. In other words, ANN models are able to be generalized effectively for new input data in the range for which they were trained. However, outside of this range, they are unable to extrapolate accurately. Therefore, a wide variety of concrete mixtures can be evaluated utilizing the network results of proposed ANN models. Table 4-1 and Table 4-2 list all the concrete mix designs for three aggregate types selected for a parametric study on compressive strength. Furthermore, the range of temperature was selected between 20 and 800 °C.

Table 4-1. The concrete mix designs employed for parametric analysis of the effect of the test method and water to cement ratios on the compressive strength

Number	Coarse Aggregate Type	Coarse aggregate (kg/m^3)	Fine aggregate (kg/m^3)	SF%	FA%	GGBS %	Cement (kg/m^3)	Water (kg/m^3)	w/c	Used in
1	Si	1080	855	0	0	0	249	127	0.5	Test method
2	Si	1080	855	0	0	0	249	127	0.5	
3	Si	1000	880	0	0	0	308	154	0.5	
4	Ca	1095.3	794.7	0	0	0	320	160	0.5	
5	Ca	1095.3	794.7	0	0	0	320	160	0.5	
6	Ca	1095.3	794.7	0	0	0	320	160	0.5	
7	LWA	482	678	0	0	0	370	185	0.5	
8	LWA	482	678	0	0	0	370	185	0.5	
9	LWA	482	678	0	0	0	370	185	0.5	
10	Ca	1168	615	0	0	0	495	149	0.3	Effects of w/c
11	Ca	853.8	868.2	0	0	0	392	196	0.5	
12	Ca	853.8	868.2	0	0	0	368.3	221	0.6	
13	Si	1086	724	0	0	0	500	150	0.3	
14	Si	1132	609	0	0	0	410	205	0.5	
15	Si	1050	699	0	0	0	343	205	0.6	

Table 4-2. The concrete mix designs employed for parametric analysis of the effect of different SCM on the compressive strength of concrete

Number	Coarse Aggregate Type	Coarse aggregate (kg/m^3)	Fine aggregate (kg/m^3)	SF %	FA %	GGBS%	Cement (kg/m^3)	Water (kg/m^3)	w/b	Used in
16	Ca	1168	615	0	0	0	495	149	0.3	Effects of SF
17	Ca	1168	615	5	0	0	495	149	0.3	
18	Ca	1168	615	10	0	0	495	149	0.3	
19	Si	1066	710	0	0	0	500	150	0.3	
20	Si	1066	710	5	0	0	500	150	0.3	
21	Si	1066	710	10	0	0	500	150	0.3	
26	Si	1196	643	0	0	0	450	135	0.3	Effects of FA
27	Si	1196	643	0	20	0	360	135	0.3	
28	Si	1196	643	0	30	0	315	135	0.3	
29	Si	1196	643	0	40	0	270	135	0.3	
22	Si	1095.3	794.7	0	0	0	300	180	0.6	
23	Si	1095.3	794.7	0	20	0	240	180	0.6	
24	Si	1095.3	794.7	0	30	0	210	180	0.6	
25	Si	1095.3	794.7	0	40	0	180	180	0.6	
26	Ca	845.8	733.6	0	0	0	661.6	198.6	0.6	
27	Ca	845.8	733.6	0	20	0	5929.3	198.6	0.6	
28	Ca	845.8	733.6	0	30	0	463	198.6	0.6	
29	Ca	845.8	733.6	0	40	0	396.6	198.6	0.6	
30	Si	1145	616	0	0	0	500	150	0.3	Effect of GGBS
31	Si	1145	616	0	0	30	350	150	0.3	
32	Si	1145	616	0	0	40	300	150	0.3	
33	Si	1135	626	0	0	30	273	195	0.5	
34	Si	1135	626	0	0	30	273	195	0.5	
35	Si	1135	626	0	0	40	234	195	0.5	

4.1.1.1 The effects of test methods

The variation of relative compressive strength of concrete as a function of temperature for concrete containing three different aggregate types: siliceous, calcareous, and lightweight aggregate, are discussed in this section.

In the case of concrete with a water to cement ratio of 0.5, the results of the network for three test methods (transient, steady-state and residual) are compared to ACI 216.1 [74] and Eurocode [73] prediction for siliceous, calcareous, and lightweight concrete, as shown in Figure 4-1, Figure 4-2 and Figure 4-3, respectively. It should be mentioned that the Eurocode [73] results are limited to the transient test; however, they are more similar to the results of the ACI 216.1 [74] for the steady-state test. Furthermore, the Eurocode [73] model does not cover the relative compressive strength of lightweight concrete.

Overall, the lowest relative strength loss was observed in the transient test, followed by the steady-state and residual test for all types of aggregate. The lower reduction of strength in the transient test was due to the friction caused by the pre-loading of specimens limiting the thermal stress in the expansion of the specimens, thereby preventing thermal cracking caused by the thermal gradient. Moreover, this might be attributed to the effect of preloading on the densifying of the coarse pore structure of concrete induced by high temperature [12, 121].

The results predicted by the proposed ANN model are fairly close to the results of A CI 216.1 [74], and Eurocode is sitting between, as shown in Figure 4-1. It can be seen in Figure 4-2 that in the case of calcareous aggregate concrete, In the case of calcareous aggregate concrete, there is a considerable difference between the results of ACI 216.1 [74] and the

prediction of the ANN model. However, the results of Eurocode [73] were close to ANN results.

The outcomes of the ANN model compared to the ACI 216.1 [74] result for lightweight concrete are plotted in Figure 4-3. It was found that the relative compressive strength was in close agreement with the ACI216.1 results for lightweight concrete for all test methods.

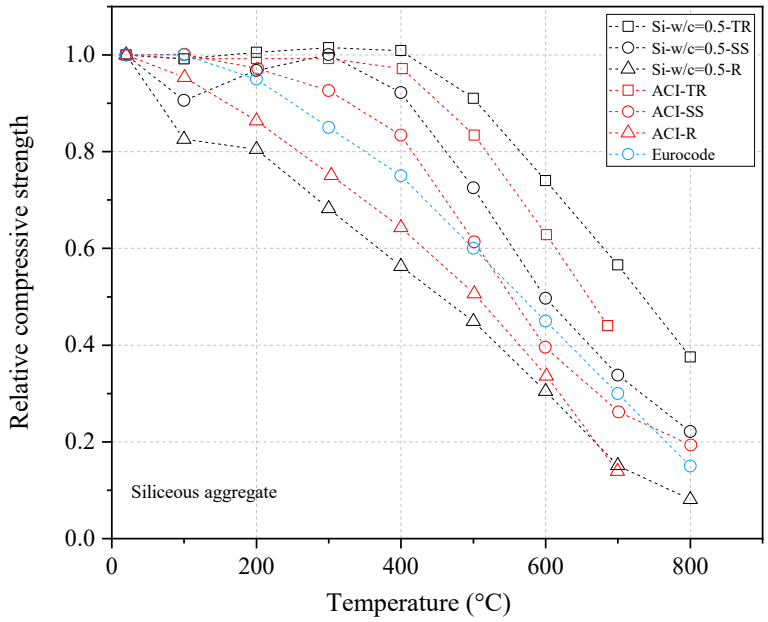

Figure 4-1. The comparison of the results of the ANN model for relative compressive strength of siliceous concrete for three test methods (TR, SS and R) exposed to high temperatures with ACI 216.1 [74] and of Eurocode [73] results

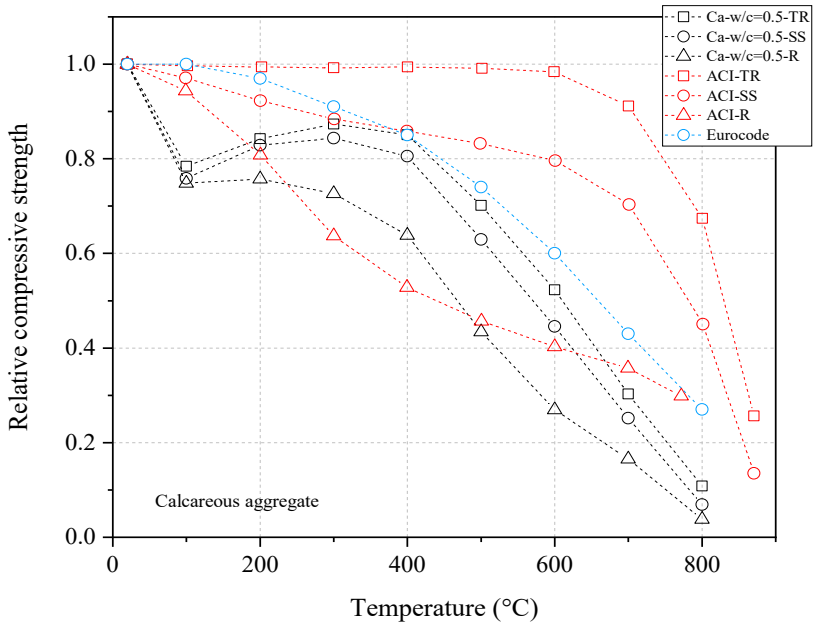

Figure 4-2. The comparison of the results of the ANN model for relative compressive strength of calcareous concrete for three test methods (TR, SS and R) exposed to high temperatures with ACI 216.1 [74] and of Eurocode [73] results

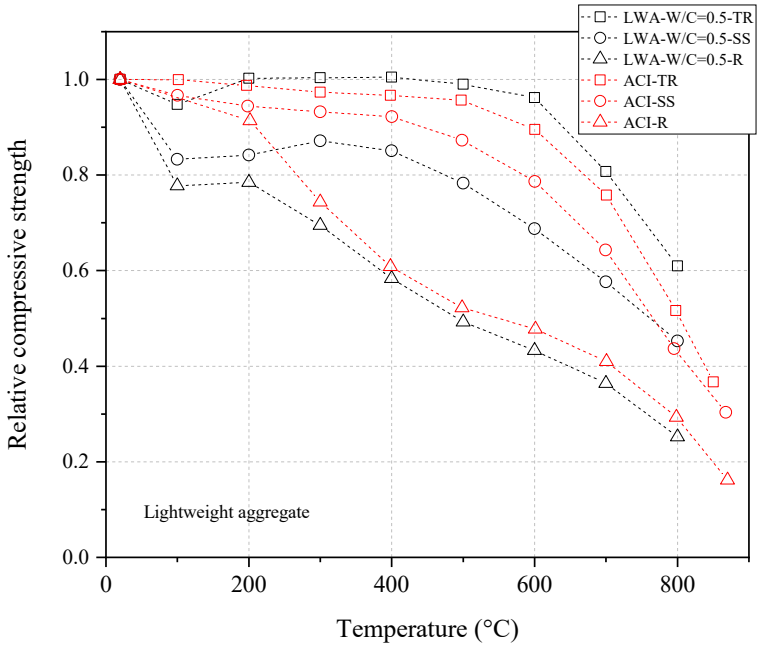

Figure 4-3. The comparison of the results of the ANN model for relative compressive strength of lightweight concrete for three test methods (TR, SS and R) exposed to high temperatures with ACI 216.1 [74] and of Eurocode [73] results

4.1.1.2 Effect of water to cement ratio

The relative compressive strength at three different water to portland cement ratios of 0.3, 0.5 and 0.6 for siliceous and calcareous concrete subjected to high temperatures up to 800 °C compared to the results of the ACI 216.1 [74] and Eurocode [73] is illustrated in Figure 4-4 and Figure 4-5, respectively. The estimation of the ANN model was only presented for the residual test due to a wide range of data in this test approach, as shown in Figure 3-4. At 100 °C, the residual compressive strength of siliceous aggregate concrete was reduced due to free water from concrete evaporation. Between 100 °C and 300 °C, the strength improved or remained constant. Beyond 300 °C, the compressive strength was reduced with temperature rise. Regarding calcareous aggregate concrete with w/c of 0.3, the compressive strength reduced continuously with increasing the temperature. However, in the case of higher w/c (0.5 and 0.6), the significant strength loss occurred up to 100 °C. Then a compressive strength recovery was observed after heating to 200 °C compared to 100 °C. Above 300 °C calcareous concrete presents severe strength loss, as shown in

Figure **4-5**.

The relative compressive strength was reduced by increasing the w/c ratios for both siliceous and calcareous aggregate. Poon et al. [38], Phan et al. [46], and Chan et al. [122] also reported similar conclusions about the residual compressive strength of concrete exposed to high temperatures. However, based on the finding of Kodour et al. [10] and Phan et al. [46], high-strength concrete with lower w/c is more susceptible to spalling due to its lower permeability compared to normal-strength concrete. In contrast, the prediction

of Eurocode [73] indicated that the reduction of compressive strength was lower in normal strength concrete (NSC) compared to high-strength concrete (HSC).

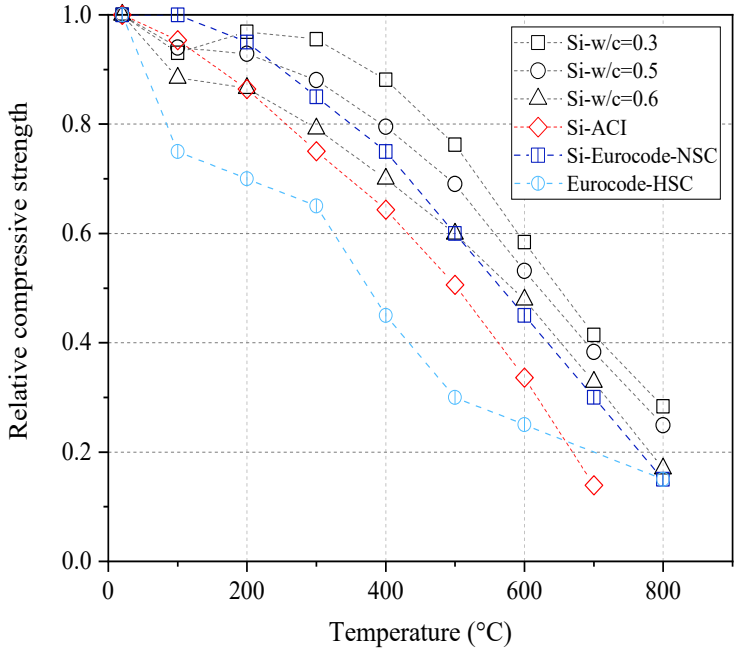

Figure 4-4. Comparison of prediction of ANN model for the relative compressive strength of siliceous concrete with three w/c: 0.3, 0.5 and 0. exposed to high temperatures with Eurocode [73] and ACI 216.1 [74] results

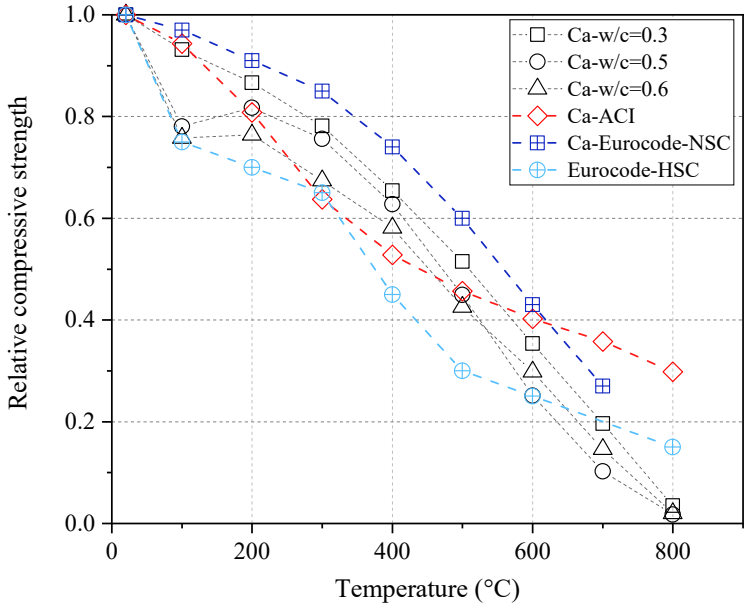

Figure 4-5. Comparison of prediction of ANN model for the relative compressive strength of calcareous concrete with three w/c: 0.3, 0.5 and 0.6 exposed to high temperatures with Eurocode [73] and ACI 216.1 [74] results

4.1.1.3 Effect of supplementary cementitious materials

In order to analyze the effect of replacement of cement with different SCMs, the compressive strength of concrete containing different content of silica fume (0, 5 and 10%), fly ash (0, 20, 30, and 40%), and ground blast slag (0, 30 and 40%) at high temperatures up to 800 °C was investigated. It is worthy to note that the provisions of both ACI 216.1 [74] and Eurocode [73] have not covered the effect of SCMs on the compressive strength of concrete at high temperatures. The selected mix designs are represented in Table 4-1.

4.1.1.3.1 The Effects of silica fume (SF)

The available research works are limited to high-strength concrete containing SF at 0-10% cement replacement ratios. Accordingly, this study examines incorporating silica fume at replacement levels of 0, 5%, and 10 % on the strength of concrete with the water to binder ratio of 0.3. The prediction of the network for siliceous concrete compared to calcareous concrete at high temperatures up to 800 °C is depicted in Figure 4-6.

It can be seen that the concrete without SF shows slightly better performance than the SF concrete, particularly at temperatures beyond 500 °C for both Ca and Si aggregate concrete.

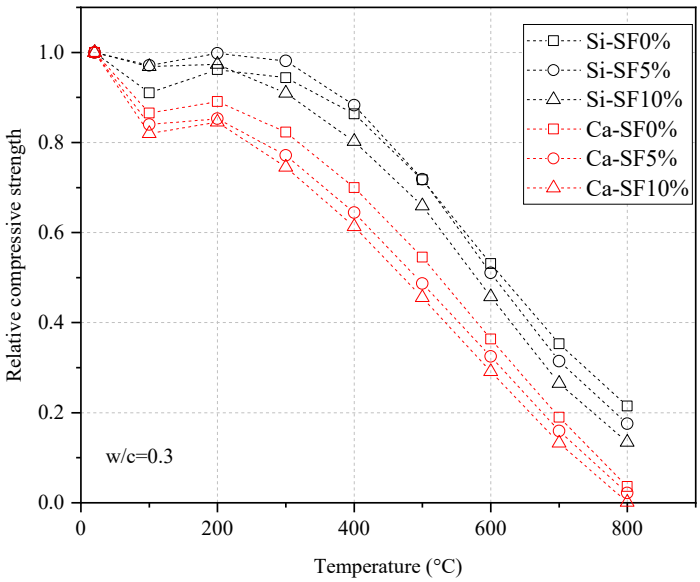

Figure 4-6. The influence of SF content on relative compressive strength of siliceous or calcareous concrete with w/b of 0.3 exposed to high temperature using the proposed ANN model

4.1.1.3.2 The Effects of fly ash (FA)

The influence of different content of fly ash (0, 20,30 and 40%) on the compressive strength of siliceous aggregate concrete at w/b of 0.3 and 0.6 are plotted in Figure 4-7 Figure 4-8.

It can be seen that the presence of FA improves the compressive strength of siliceous concrete up to 300 °C. Beyond this temperature, the strength decreased with temperatures rising in all concrete mixtures. The siliceous aggregate concrete with a higher percentage of FA exhibited higher values of relative compressive strength up to 500 °C for both levels of water-binder ratio. In contrast, beyond this temperature, the concrete with a lower content of FA showed slightly higher strength. In addition, the inclusion of FA increases the relative compressive strength of concrete compared to concrete without FA at all temperatures. The strength loss was higher in concrete with a higher w/b ratio.

The results were investigated only for calcareous concrete with the w/b ratio of 0.6 because there is insufficient data available in the literature for calcareous concrete with lower w/b ratios. As seen in Figure 4-9, calcareous concrete made with FA up to 30% FA shows better results compared to OPC concrete. The presence of FA increased the strength of concrete up to 300 °C. However, the compressive strength was reduced with temperature rise for all concrete mixtures. Between 300 and 800 °C, concrete loses more compressive strength with increasing the FA content. Similar results were reported in experimental research carried out by Savva et al. [69].

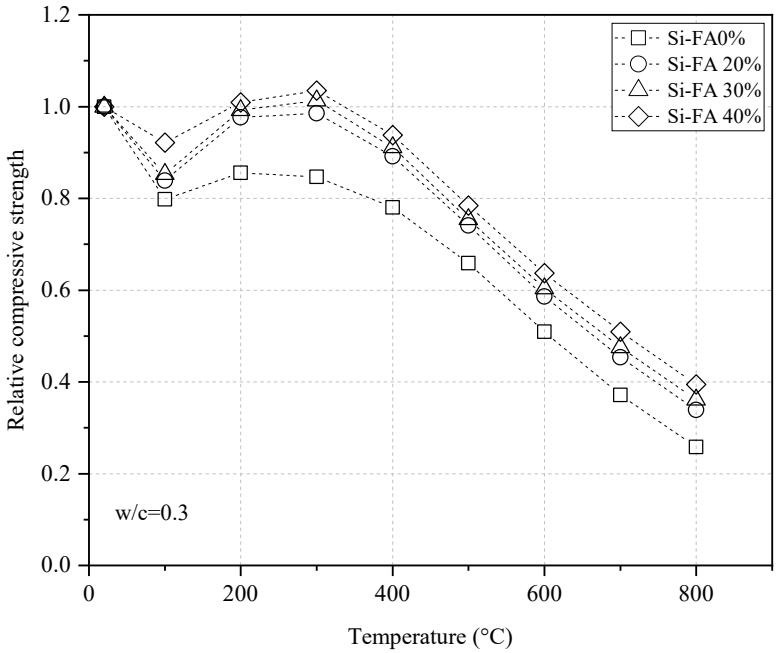

Figure 4-7. The influence of FA content on relative compressive strength of siliceous concrete with w/b of 0.3 exposed to high temperature using the proposed ANN model

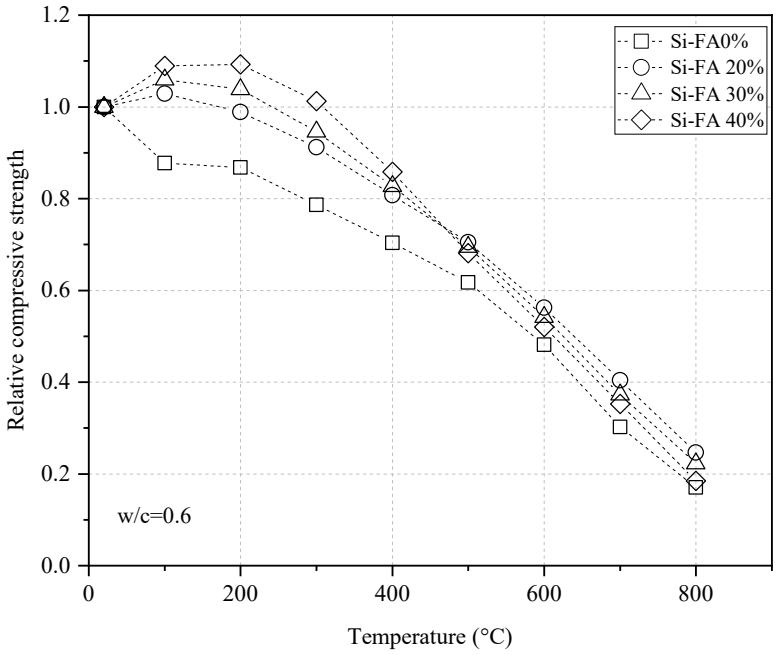

Figure 4-8. The influence of FA content on relative compressive strength of siliceous concrete with w/b of 0.6 exposed to high temperature using the proposed ANN model

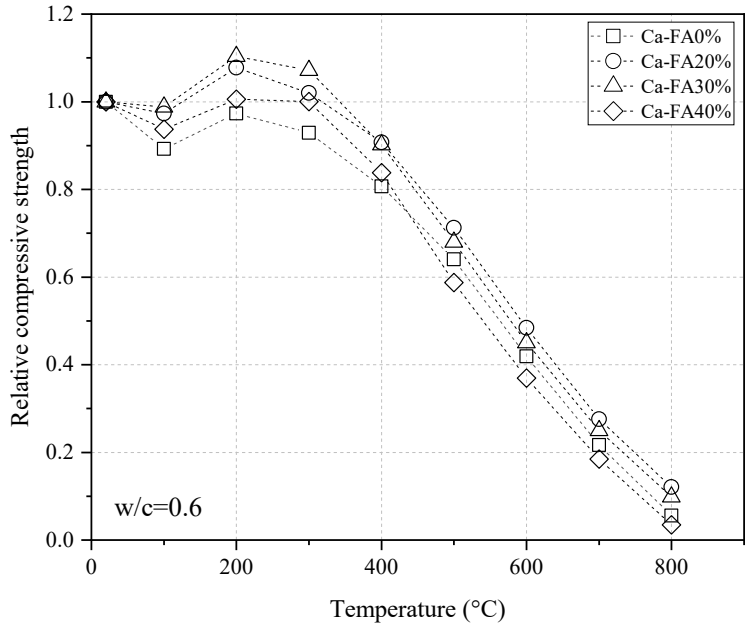

Figure 4-9. The influence of FA content on relative compressive strength of calcareous concrete with w/b of 0.6 exposed to high temperature using the proposed ANN model

4.1.1.3.3 The Effects of ground-granulated blast slag (GGBS)

The results of the ANN model for three concrete mixes with different levels of slag (0, 30 and 40%) for siliceous aggregate concrete with two w/b ratios (0.3 and 0.5) are depicted in Figure 4-10 and Figure 4-11, respectively. The data for calcareous concrete containing GGBS is not available in the literature, as represented in Figure 3-3. However, there are some studies in the literature, but the type of aggregate has not been specified.

Before 300 °C, there was no significant reduction except at 100 °C. The compressive strength decreased considerably for all concrete mixes with and without GGBS beyond 300 °C.

The replacement of cement with GGBS led to slightly better performance of concrete with w/b of 0.3 subjected to high temperature compared to OPC. This can be explained by the acceleration of the hydration reaction caused by the increase in temperature [58]. A similar observation was reported by Poon et al. [45] and Karahan et al. [58].

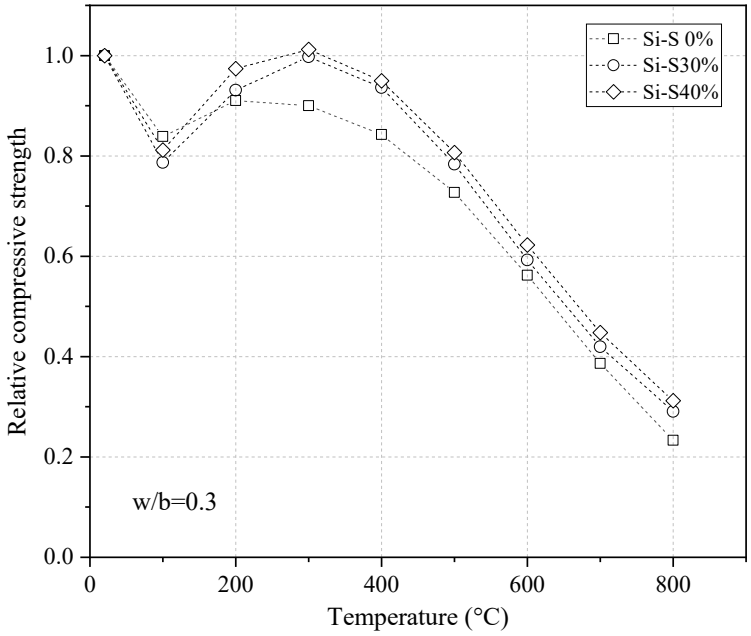

Figure 4-10. The influence of GGBS content on relative compressive strength of siliceous concrete with w/b=0.3 exposed to high temperature using the proposed ANN model

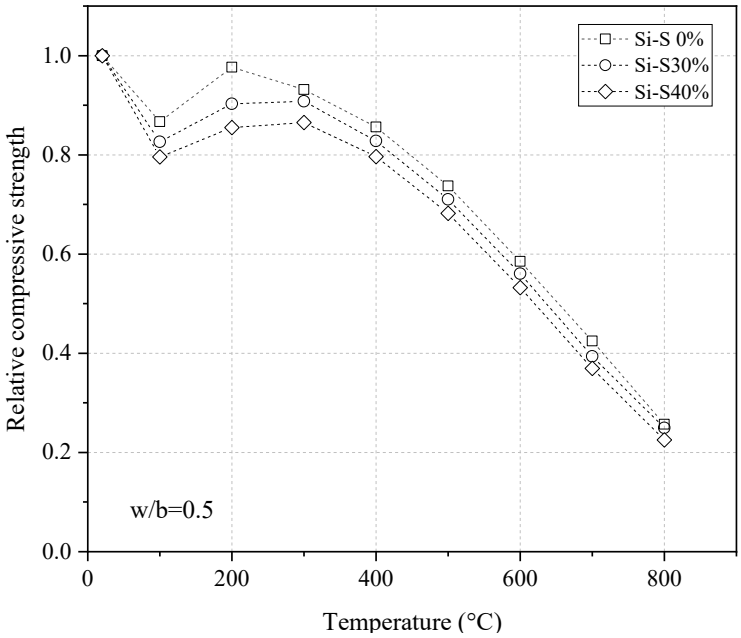

Figure 4-11. The influence of GGBS content on relative compressive strength of siliceous concrete with w/b=0.5 exposed to high temperature using the proposed ANN model

4.1.2 Tensile strength

The ratio of residual tensile strength of concrete at a given temperature to the tensile strength of concrete at room temperatures at two water to cement ratios of 0.3 and 0.5 for siliceous, calcareous and lightweight aggregate is plotted in Figure 4-12, Figure 4-13 and Figure 4-14, respectively. The concrete mix used in the parametric study on tensile strength is represented in Table 4-3.

Table 4-3. The concrete mix designs employed for parametric analysis of tensile strength

Number	Coarse Aggregate	Coarse aggregate (kg/m^3)	Fine aggregate (kg/m^3)	SF%	FA%	GGBS%	Cement (kg/m^3)	Water (kg/m^3)	w/c
1	Si	411	764	0	0	0	500	150	0.3
2	Si	1050	699	0	0	0	343	205	0.6
3	Ca	1168	615	0	0	0	500	149	0.3
4	Ca	1050	699	0	0	0	343	205	0.6
5	LWA	585	777	0	0	0	426	192	0.3
6	LWA	369	777	0	0	0	386	231	0.6

The proposed residual tensile strength model results were compared to the tensile strength of the concrete curve presented by Eurocode [73]. The results of Eurocode [73] show that the reduction of the tensile strength (under hot conditions) starts at 100 °C and continues until 600 °C. However, the types of aggregate have not been specified in the Eurocode [73]. The relative residual tensile strength estimated by the ANN model was greater than the Eurocode model [73] for both siliceous and calcareous concrete beyond 200 °C.

It was found that the concrete containing a lower w/c ratio exhibited a lower loss of tensile strength at high temperatures for siliceous and calcareous aggregate concrete compared to a higher level of w/c. This can be attributed to lower w/c caused by the decrease of porosity of ITZ led to higher bond strength at the paste–aggregate interface [72].

The lightweight concrete shows better performance than other aggregate types, as shown in Figure 4-14. The lightweight aggregate concrete loses less than 20% of its tensile strength at temperatures of 400 °C, while the tensile strength loss was about 40% for siliceous and calcareous concrete.

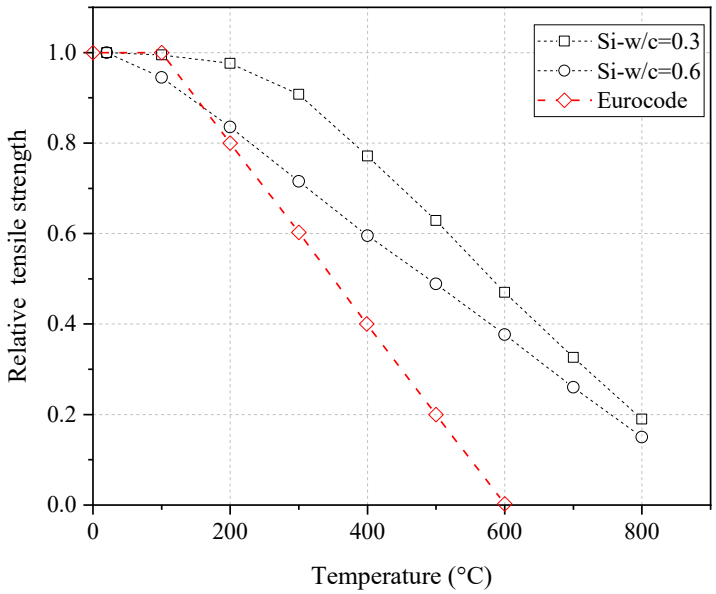

Figure 4-12. The comparison of the results of the ANN model for relative tensile strength of siliceous concrete at w/c of 0.3 and 0.6 at high temperatures with Eurocode [73] results

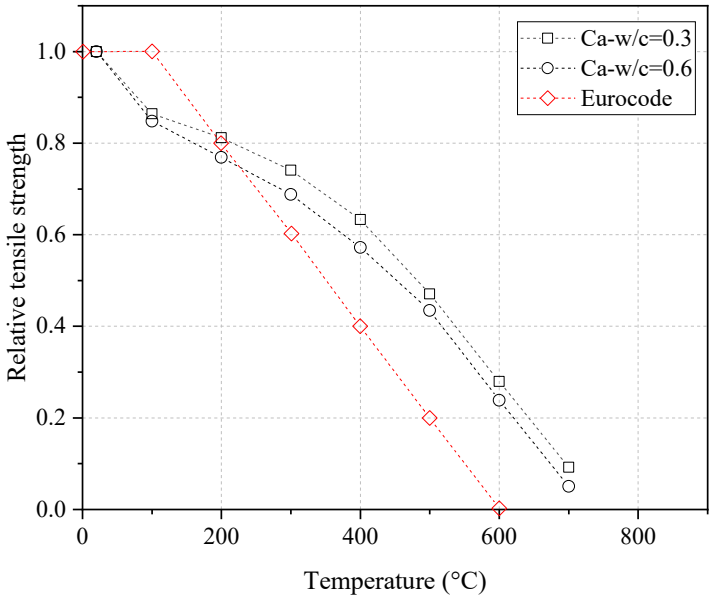

Figure 4-13. The comparison of the results of the ANN model for relative tensile strength of calcareous concrete at w/c of 0.3 and 0.6 at high temperatures with and of Eurocode [73] results

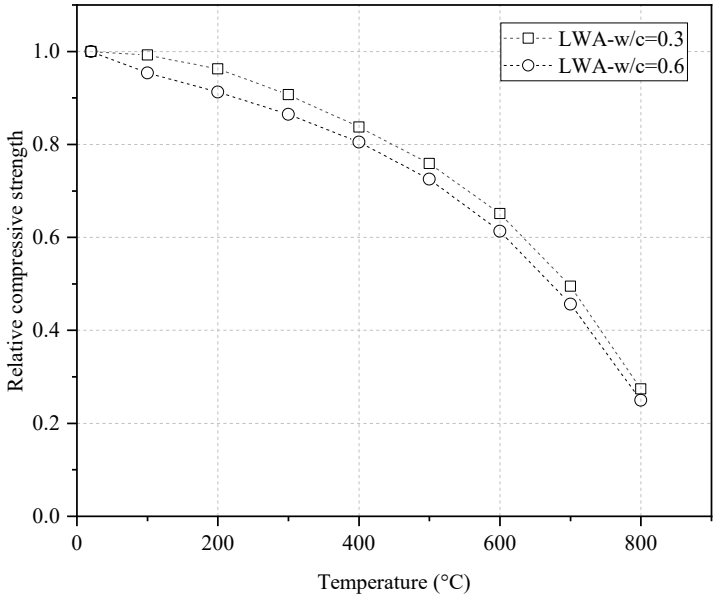

Figure 4-14. The results of the ANN model for tensile strength of lightweight concrete at w/c of 0.3 and 0.6 exposed to high temperature

4.1.3 Modulus of elasticity

The relative modulus of elasticity of concrete exposed to high temperatures for siliceous and calcareous aggregates was investigated using the ANN model compared to results obtained by Cruz [83] as presented by ACI 216R [82], as shown in Figure 4-15 and Figure 4-16. The concrete mixes used in analyzing the modulus of elasticity of concrete exposed to high temperatures are listed in Table 4-4. The network results indicated that the modulus of elasticity is more sensitive to high temperatures than compressive and tensile strength. The modulus of elasticity of siliceous concrete predicted by the ANN model was higher than the results of ACI 216R [81] regardless of the level of w/c, as depicted in Figure 4-15. In concrete containing calcareous aggregate, the modulus of elasticity declined more than in siliceous concrete.

In the case of calcareous aggregate, the output of the ANN model for concrete with w/c of 0.6 was in good agreement with the data obtained by ACI 216R [82], particularly beyond 400 °C.

Table 4-4. The concrete mix designs employed for parametric analysis on the modulus of elasticity

Number	Coarse Aggregate	Coarse aggregate(kg/m^3)	Fine aggregate(kg/m^3)	SF%	FA%	GGBS%	Cement (kg/m^3)	Water (kg/m^3)	w/c
1	Ca	459	646	0	0	0	500	150	0.3
2	Ca	1050	699	0	0	0	343	205.8	0.6
3	Si	411	764	0	0	0	500	150	0.3
4	Si	1050	699	0	0	0	343	205	0.6

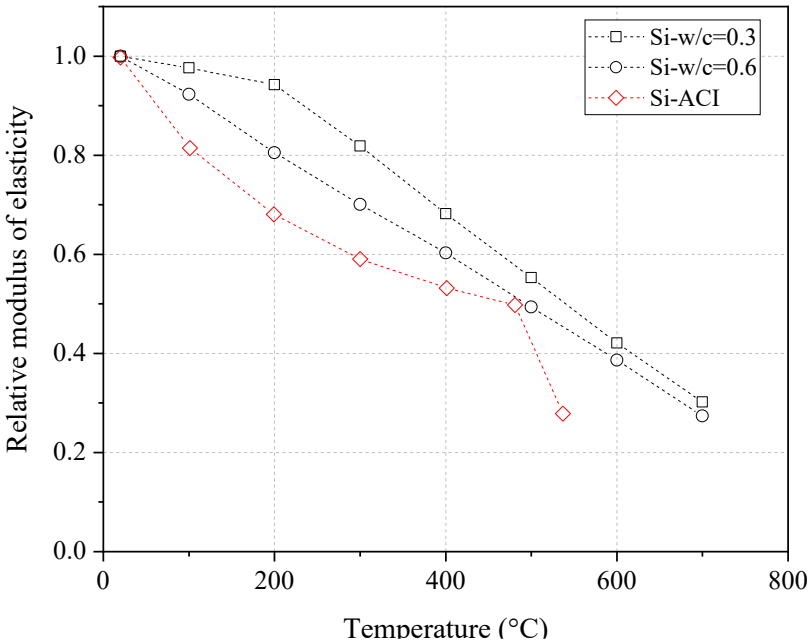

Figure 4-15. . The comparison of the results of the ANN model for relative modulus of elasticity of siliceous concrete at w/c of 0.3 and 0.6 at high temperatures with ACI 216R [82]results

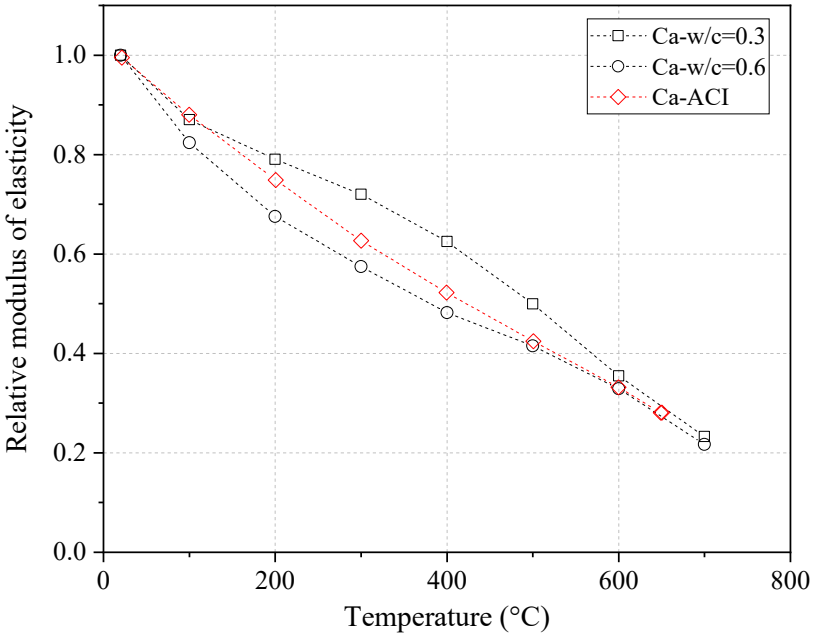

Figure 4-16 The comparison of the results of the ANN model for relative modulus of elasticity of calcareous concrete at w/c of 0.3 and 0.6 at high temperatures with ACI 216R [82] results

Chapter 5: Conclusions and Recommendations

The behaviour of concrete under high temperatures is complex and affected by several factors. The main purpose of this study was to predict the mechanical properties of concrete when subjected to high temperatures. A total of 500, 110 and 128 data points were gathered separately to establish the artificial neuron network (ANN) models to forecast the compressive strength, tensile strength and modulus of elasticity of concrete, respectively. Three distinct ANN networks were developed in the MATLAB environment to predict the mechanical characteristics of concrete exposed to high temperatures. Furthermore, a parametric study was conducted in order to evaluate the effect of input variables on the mechanical characteristic of concrete using suggested ANN models.

5.1 Conclusions

Based on analyzing the proposed ANN models, the following conclusions were drawn:

1. A network consisting of one hidden layer within 12 neurons was established to estimate the compressive strength of concrete exposed to high temperatures. This network with a mean squared error (MSE) of 0.004 and coefficient correlation (R) of 0.966 showed excellent accuracy and reliability in predicting the compressive strength of concrete.
2. The database contained experimental test results from three common test protocols: transient temperature, steady-state temperature, and residual tests. It was found that the reduction in the relative compressive strength of concrete for the transient test is lower than the steady-state and residual test for all aggregate types. A similar trend was reported by ACI 216.1 [74].

3. The lower water to cement ratio (w/c) resulted in less degradation of compressive strength of concrete exposed to high temperatures. However, the prediction of Eurocode [72] was on opposite.
4. The addition of silica fume (SF) has no positive effect on the compressive strength of concrete at high temperatures compared to ordinary Portland cement (OPC) concrete.
5. The incorporation of fly ash (FA) improves the compressive strength behaviour of siliceous concrete compared to OPC concrete.

   The siliceous aggregate concrete with a higher percentage of FA exhibited higher values of relative compressive strength up to 500 °C. In contrast, beyond this temperature, the concrete with a lower content of FA showed slightly higher strength.

   The calcareous aggregate concrete with FA up to 30% replacement ratio shows better results than OPC concrete at all temperatures.

   The presence of FA increases the relative compressive strength of concrete up to 300 °C. However, the compressive strength was reduced with temperature rise for all concrete mixtures.
6. There is no significant difference in relative compressive strength of siliceous concrete containing slag with different w/b ratios, but in siliceous concrete with w/b of 0.3, concrete containing 40% slag exhibits slightly better performance.
7. The ANN model comprised of one hidden layer with 15 neurons was selected for predicting the tensile strength of concrete. The MSE of 0.096 and R of 0.976

indicated the reliability of the model for the estimation of the tensile strength of concrete.

8. It was found that the concrete containing a lower w/c ratio exhibits a lower loss of tensile strength at high temperatures compared to a higher level of w/c regardless of aggregate type.
9. The tensile strength of lightweight concrete degrades less than siliceous concrete and calcareous concrete.
10. The ANN-based model with 12 neurons in the hidden layer shows the best performance in predicting the modulus of elasticity of concrete under high temperatures. The MSE and R were obtained as 0.0089 and 0.98, respectively, exhibiting the accuracy and reliability of the network for estimation of the modulus of elasticity of concrete exposed to high temperatures.
11. Based on analyzing the effect of the w/c ratio, it was observed that the lower w/c led to a smaller reduction of modulus of elasticity of concrete regardless of the type of aggregate.

5.2 Recommendations

Based on the findings of this study, there are some suggestions to improve the utilization of AAN as a powerful tool to evaluate the behaviour of concrete under high temperatures. The following key recommendations are made as follows:

1. Additional experimental studies are necessary to assess the behaviour of lightweight aggregates containing different SCM during and after exposure to high temperatures.

2. Overall, fewer studies have been carried out on the tensile strength and modulus of elasticity than compressive strength based on information collected from the literature. Therefore, additional research is recommended to evaluate the tensile strength and modulus of elasticity of concrete exposed to high temperatures.
3. A database can be developed and employ the ANN model approach to examine and analyze the other properties of concrete at high temperatures, such as flexural strength and creep.
4. Sufficient data is available in the literature regarding the thermal properties of concrete, including thermal expansion, specific heat, and thermal conductivity. ANN-based models can be established to evaluate the thermal characteristic of concrete.
5. Further experimental investigations are recommended on the calcareous aggregate concrete containing SCMs, particularly slag. Moreover, there are some studies in the literature, but the type of aggregate has not been identified. Thus, providing detailed information on types of aggregate would be helpful.

References

[1]. Wu, H., Lin, X., and Zhou, A., *A review of mechanical properties of fibre reinforced concrete at elevated temperatures.* Cement and Concrete Research, 2020. **135**: p. 106117.

[2]. Yazıcı, Ş., Sezer, G.İ., and Şengül, H., *The effect of high temperature on the compressive strength of mortars.* Construction and Building Materials, 2012. **35**: p. 97-100.

[3]. Mukherjee, A. and Biswas, S.N., *Artificial neural networks in prediction of mechanical behavior of concrete at high temperature.* Nuclear engineering and design, 1997. **178**(1): p. 1-11.

[4]. Nadeem, A., Memon, S.A., and Lo, T.Y., *Qualitative and quantitative analysis and identification of flaws in the microstructure of fly ash and metakaolin blended high performance concrete after exposure to elevated temperatures.* Construction and Building Materials, 2013. **38**: p. 731-741.

[5]. Chaabene, W.B., Flah, M., and Nehdi, M.L., *Machine learning prediction of mechanical properties of concrete: Critical review.* Construction and Building Materials, 2020. **260**: p. 119889.

[6]. Asteris, P.G., Skentou, A.D., Bardhan, A., Samui, P., and Pilakoutas, K., *Predicting concrete compressive strength using hybrid ensembling of surrogate machine learning models.* Cement and Concrete Research, 2021. **145**: p. 106449.

[7]. Ashteyat, A.M. and Ismeik, M., *Predicting residual compressive strength of self-compacted concrete under various temperatures and relative humidity conditions by artificial neural networks.* Computers and Concrete, 2018. **21**(1): p. 47-54.

[8]. Chan, S.Y.N., Peng, G.-f., and Chan, J.K.W., *Comparison between high strength concrete and normal strength concrete subjected to high temperature.* Materials and Structures, 1996. **29**(10): p. 616.

[9]. Naser, M., *Properties and material models for modern construction materials at elevated temperatures.* Computational Materials Science, 2019. **160**: p. 16-29.

[10]. Kodur, V., *Properties of concrete at elevated temperatures.* International Scholarly Research Notices, 2014. **2014**.

[11]. Arioz, O., *Effects of elevated temperatures on properties of concrete.* Fire safety journal, 2007. **42**(8): p. 516-522.

[12]. Ma, Q., Guo, R., Zhao, Z., Lin, Z., and He, K., *Mechanical properties of concrete at high temperature—A review.* Construction and Building Materials, 2015. **93**: p. 371-383.

[13]. Phan, L.T. and Carino, N.J., *Effects of Test Conditions and Mixture Proportions on Behavior of High-Strength Concrete Exposed to High Temperatures.* Materials Journal, 2002. **99**(1): p. 54-56.

[14]. Tanaçan, L., Ersoy, H.Y., and Arpacıoğlu, Ü., *Effect of high temperature and cooling conditions on aerated concrete properties.* Construction and Building Materials, 2009. **23**(3): p. 1240-1248.

[15]. Pliya, P., Hajiloo, H., Romagnosi, S., Cree, D., Sarhat, S., and Green, M., *The compressive behaviour of natural and recycled aggregate concrete during and after exposure to elevated temperatures.* Journal of Building Engineering, 2021. **38**: p. 102214.

[16]. Santos, C.C.d. and Rodrigues, J.P.C., *Residual mechanical properties of calcareous and granite aggregate concretes after fire.* Magazine of concrete research, 2014. **66**(16): p. 845-857.

[17]. Chandra Paul, S., Mbewe, P.B., Kong, S.Y., and Šavija, B., *Agricultural solid waste as source of supplementary cementitious materials in developing countries.* Materials, 2019. **12**(7): p. 1112.

[18]. Snellings, R., Li, X., Avet, F., and Scrivener, K., *Rapid, Robust, and Relevant (R3) reactivity test for supplementary cementitious materials.* ACI Materials Journal, 2019. **116**(4): p. 155-162.

[19]. Toutanji, H., Delatte, N., Aggoun, S., Duval, R., and Danson, A., *Effect of supplementary cementitious materials on the compressive strength and durability of short-term cured concrete.* Cement and Concrete Research, 2004. **34**(2): p. 311-319.

[20]. Behnood, A. and Ziari, H., *Effects of silica fume addition and water to cement ratio on the properties of high-strength concrete after exposure to high temperatures.* Cement and Concrete Composites, 2008. **30**(2): p. 106-112.

[21]. Ghandehari, M., Behnood, A., and Khanzadi, M., *Residual mechanical properties of high-strength concretes after exposure to elevated temperatures.* Journal of materials in Civil Engineering, 2010. **22**(1): p. 59-64.

[22]. Kim, S.S., Qudoos, A., Jakhrani, S.H., Lee, J.B., and Kim, H.G., *Influence of coarse aggregates and Silica Fume on the mechanical properties, durability, and microstructure of concrete.* Materials, 2019. **12**(20): p. 3324.

[23]. Mazloom, M., Ramezanianpour, A., and Brooks, J., *Effect of silica fume on mechanical properties of high-strength concrete.* Cement and Concrete Composites, 2004. **26**(4): p. 347-357.

[24]. Yogendran, V., Langan, B., Haque, M., and Ward, M., *Silica fume in high-strength concrete.* Materials Journal, 1987. **84**(2): p. 124-129.

[25]. Bhanja, S. and Sengupta, B., *Influence of silica fume on the tensile strength of concrete.* Cement and concrete research, 2005. **35**(4): p. 743-747.

[26]. Hooton, R., *Influence of silica fume replacement of cement on physical properties and resistance to sulfate attack, freezing and thawing, and alkali-silica reactivity.* materials Journal, 1993. **90**(2): p. 143-151.

[27]. Khedr, S. and Abou-Zeid, M., *Characteristics of silica-fume concrete.* Journal of Materials in Civil Engineering, 1994. **6**(3).

[28]. Golewski, G.L., *Green concrete composite incorporating fly ash with high strength and fracture toughness.* Journal of Cleaner Production, 2018. **172**: p. 218-226.

[29]. Siddique, R., *Performance characteristics of high-volume Class F fly ash concrete.* Cement and Concrete Research, 2004. **34**(3): p. 487-493.

[30]. Abubaker, F., Ghanim, H., and Abdalkader, A., *Effect of fly ash addition on mechanical properties of concrete* 2018.

[31]. Megat Johari, M.A., Brooks, J.J., Kabir, S., and Rivard, P., *Influence of supplementary cementitious materials on engineering properties of high strength concrete.* Construction and Building Materials, 2011. **25**(5): p. 2639-2648.

[32]. Lam, L., Wong, Y.L., and Poon, C.S., *Effect of Fly Ash and Silica Fume on Compressive and Fracture Behaviors of Concrete.* Cement and Concrete Research, 1998. **28**(2): p. 271-283.

[33]. Chidiac, S. and Panesar, D., *Evolution of mechanical properties of concrete containing ground granulated blast furnace slag and effects on the scaling resistance test at 28 days.* Cement and Concrete Composites, 2008. **30**(2): p. 63-71.

[34]. Güneyisi, E. and Gesoğlu, M., *A study on durability properties of high-performance concretes incorporating high replacement levels of slag.* Materials and Structures, 2008. **41**(3): p. 479-493.

[35]. Khatib, J.M. and Hibbert, J.J., *Selected engineering properties of concrete incorporating slag and metakaolin.* Construction and Building Materials, 2005. **19**(6): p. 460-472.

[36]. Aldea, C.-M., Young, F., Wang, K., and Shah, S.P., *Effects of curing conditions on properties of concrete using slag replacement.* Cement and concrete research, 2000. **30**(3): p. 465-472.

[37]. Siddique, R. and Kaur, D., *Properties of concrete containing ground granulated blast furnace slag (GGBFS) at elevated temperatures.* Journal of Advanced Research, 2012. **3**(1): p. 45-51.

[38]. Swamy, R.N. and Ammar, B., *Some Engineering Properties of Slag Concrete as Influenced by Mix Proportioning and Curing.* ACI Materials Journal, 1990. **87**(3).

[39]. Mustakim, S.M., Das, S.K., Mishra, J., Aftab, A., Alomayri, T.S., Assaedi, H.S., and Kaze, C.R., *Improvement in fresh, mechanical and microstructural properties of fly ash-blast furnace slag based geopolymer concrete by addition of nano and micro silica.* Silicon, 2021. **13**(8): p. 2415-2428.

[40]. Khan, M.I. and Siddique, R., *Utilization of silica fume in concrete: Review of durability properties.* Resources, Conservation and Recycling, 2011. **57**: p. 30-35.

[41]. Siddique, R., *Utilization of silica fume in concrete: Review of hardened properties.* Resources, Conservation and Recycling, 2011. **55**(11): p. 923-932.

[42]. Katkhuda, H., Hanayneh, B., and Shatarat, N., *Influence of Silica Fume on High Strength Lightweight Concrete.* International Journal of Civil and Environmental Engineering, 2009. **3**(10): p. 407-414.

[43]. Toutanji, H.A. and Bayasi, Z., *Effect of curing procedures on properties of silica fume concrete.* Cement and Concrete Research, 1999. **29**(4): p. 497-501.

[44]. Sancak, E., Sari, Y.D., and Simsek, O., *Effects of elevated temperature on compressive strength and weight loss of the light-weight concrete with silica fume and superplasticizer.* Cement and Concrete Composites, 2008. **30**(8): p. 715-721.

[45]. Poon, C.-S., Azhar, S., Anson, M., and Wong, Y.-L., *Comparison of the strength and durability performance of normal-and high-strength pozzolanic concretes at elevated temperatures.* Cement and concrete research, 2001. **31**(9): p. 1291-1300.

[46]. Phan, L.T., Lawson, J.R., and Davis, F.L., *Effects of elevated temperature exposure on heating characteristics, spalling, and residual properties of high performance concrete.* Materials and structures, 2001. **34**(2): p. 83-91.

[47]. Tanyildizi, H. and Coskun, A., *Performance of lightweight concrete with silica fume after high temperature.* Construction and Building Materials, 2008. **22**(10): p. 2124-2129.

[48]. Yu, L. and Pan, B., *Overview of High-temperature Deformation Measurement Using Digital Image Correlation.* Experimental Mechanics, 2021: p. 1-22.

[49]. Le, D.B., Tran, S.D., Torero, J.L., and Dao, V.T., *Application of digital image correlation system for reliable deformation measurement of concrete structures at high temperatures.* Engineering Structures, 2019. **192**: p. 181-189.

[50]. Khalaf, M.A., Ban, C.C., and Ramli, M., *The constituents, properties and application of heavyweight concrete: A review.* Construction and Building Materials, 2019. **215**: p. 73-89.

[51]. Cho, Y.K., Jung, S.H., and Choi, Y.C., *Effects of chemical composition of fly ash on compressive strength of fly ash cement mortar.* Construction and Building Materials, 2019. **204**: p. 255-264.

[52]. Papadakis, V.G., *Effect of fly ash on Portland cement systems: Part I. Low-calcium fly ash.* Cement and Concrete Research, 1999. **29**(11): p. 1727-1736.

[53]. Nochaiya, T., Wongkeo, W., and Chaipanich, A., *Utilization of fly ash with silica fume and properties of Portland cement–fly ash–silica fume concrete.* Fuel, 2010. **89**(3): p. 768-774.

[54]. Woszuk, A., Bandura, L., and Franus, W., *Fly ash as low cost and environmentally friendly filler and its effect on the properties of mix asphalt.* Journal of Cleaner Production, 2019. **235**: p. 493-502.

[55]. Supit, S.W., Shaikh, F.U., and Sarker, P.K., *Effect of ultrafine fly ash on mechanical properties of high volume fly ash mortar.* Construction and building materials, 2014. **51**: p. 278-286.

[56]. Hashmi, A.F., Shariq, M., and Baqi, A., *An investigation into age-dependent strength, elastic modulus and deflection of low calcium fly ash concrete for sustainable construction.* Construction and Building Materials, 2021. **283**: p. 122772.

[57]. Wang, W., Lu, C., Li, Y., and Li, Q., *An investigation on thermal conductivity of fly ash concrete after elevated temperature exposure.* Construction and Building Materials, 2017. **148**: p. 148-154.

[58]. Karahan, O., *Transport properties of high volume fly ash or slag concrete exposed to high temperature.* Construction and Building Materials, 2017. **152**: p. 898-906.

[59]. Khan, M.S. and Abbas, H., *Effect of elevated temperature on the behavior of high volume fly ash concrete.* KSCE Journal of Civil Engineering, 2015. **19**(6): p. 1825-1831.

[60]. Xu, Y., Wong, Y., Poon, C.S., and Anson, M., *Influence of PFA on cracking of concrete and cement paste after exposure to high temperatures.* Cement and Concrete Research, 2003. **33**(12): p. 2009-2016.

[61]. Nadeem, A., Memon, S.A., and Lo, T.Y., *The performance of fly ash and metakaolin concrete at elevated temperatures.* Construction and Building Materials, 2014. **62**: p. 67-76.

[62]. Tanyildizi, H. and Coskun, A., *The effect of high temperature on compressive strength and splitting tensile strength of structural lightweight concrete containing fly ash.* Construction and building materials, 2008. **22**(11): p. 2269-2275.

[63]. Nasser, K. and Marzouk, H. *Properties of mass concrete containing fly ash at high temperatures*. in *Journal Proceedings*. 1979.

[64]. Siddique, R., *Utilization (recycling) of iron and steel industry by-product (GGBS) in concrete: strength and durability properties.* Journal of Material Cycles and Waste Management, 2014. **16**(3): p. 460-467.

[65]. Siddique, R. and Bennacer, R., *Use of iron and steel industry by-product (GGBS) in cement paste and mortar.* Resources, Conservation and Recycling, 2012. **69**: p. 29-34.

[66]. Bilim, C., Atiş, C.D., Tanyildizi, H., and Karahan, O., *Predicting the compressive strength of ground granulated blast furnace slag concrete using artificial neural network.* Advances in Engineering Software, 2009. **40**(5): p. 334-340.

[67]. Li, Q., Li, Z., and Yuan, G., *Effects of elevated temperatures on properties of concrete containing ground granulated blast furnace slag as cementitious material.* Construction and Building Materials, 2012. **35**: p. 687-692.

[68]. Shumuye, E.D., Zhao, J., and Wang, Z., *Effect of fire exposure on physico-mechanical and microstructural properties of concrete containing high volume slag cement.* Construction and Building Materials, 2019. **213**: p. 447-458.

[69]. Savva, A., Manita, P., and Sideris, K., *Influence of elevated temperatures on the mechanical properties of blended cement concretes prepared with limestone and siliceous aggregates.* Cement and Concrete Composites, 2005. **27**(2): p. 239-248.

[70]. Tufail, M., Shahzada, K., Gencturk, B., and Wei, J., *Effect of elevated temperature on mechanical properties of limestone, quartzite and granite concrete.* International Journal of Concrete Structures and Materials, 2017. **11**(1): p. 17-28.

[71]. Masood, A., Shariq, M., Alam, M.M., Ahmad, T., and Beg, A., *Effect of Elevated Temperature on the Residual Properties of Quartzite, Granite and Basalt Aggregate Concrete.* Journal of The Institution of Engineers (India): Series A, 2018. **99**(3): p. 485-494.

[72]. Xing, Z., Beaucour, A.-L., Hebert, R., Noumowe, A., and Ledesert, B., *Influence of the nature of aggregates on the behaviour of concrete subjected to elevated temperature.* Cement and concrete research, 2011. **41**(4): p. 392-402.

[73]. EN, C., *1-2: Design of concrete structures-Part 1-2: General rules-Structural fire design.* European Committee for Standardization, Brussels, Belgium, 2004. **1**(2): p. 1.

[74]. 216.1, A., *Code Requirements for Determing Fire Resistance of Concrete and Masonry Construction Assemblies*. 2014: American Concrete Inst.

[75]. Abrams, M.S., *Compressive strength of concrete at temperatures to 1600F.* Special Publication, 1971. **25**: p. 33-58.

[76]. Cheng, F.-P., Kodur, V., and Wang, T.-C., *Stress-strain curves for high strength concrete at elevated temperatures.* Journal of Materials in Civil Engineering, 2004. **16**(1): p. 84-90.

[77]. Hossain, K.M. and Lachemi, M., *Mixture design, strength, durability, and fire resistance of lightweight pumice concrete.* ACI Materials Journal, 2007. **104**(5): p. 449.

[78]. Roufael, G., Beaucour, A.-L., Eslami, J., Hoxha, D., and Noumowé, A., *Influence of lightweight aggregates on the physical and mechanical residual properties of concrete subjected to high temperatures.* Construction and Building Materials, 2021. **268**: p. 121221.

[79]. Sollero, M.B.S., Moreno Junior, A.L., and Costa, C.N., *Residual mechanical strength of concrete exposed to high temperatures – international standardization and influence of coarse aggregates.* Construction and Building Materials, 2021. **287**: p. 122843.

[80]. Abid, M., Hou, X., Zheng, W., and Waqar, G.Q., *Mechanical properties of steel fiber-reinforced reactive powder concrete at high temperature and after cooling.* Procedia engineering, 2017. **210**: p. 597-604.

[81]. Khaliq, W. and Kodur, V.K.R., *Effect of High Temperature on Tensile Strength of Different Types of High-Strength Concrete.* ACI Materials Journal. **108**(4).

[82]. ACI, *ACI/TMS 216R-89*, in *Guide for determining the fire endurance of concrete elements*. 1989, American Concrete Institute: American Concrete Institute.

[83]. Cruz, C.R., *Elastic properties of concrete at high temperatures*. 1966.

[84]. Nathani, N. and Singh, A., *Foundations of Machine Learning*, in *Introduction to AI Techniques for Renewable Energy Systems*. 2021, CRC Press. p. 43-64.

[85]. Naser, M., *Mechanistically informed machine learning and artificial intelligence in fire engineering and sciences.* Fire Technology, 2021: p. 1-44.

[86]. Salehi, H. and Burgueño, R., *Emerging artificial intelligence methods in structural engineering.* Engineering structures, 2018. **171**: p. 170-189.

[87]. Balyen, L. and Peto, T., *Promising artificial intelligence-machine learning-deep learning algorithms in ophthalmology.* The Asia-Pacific Journal of Ophthalmology, 2019. **8**(3): p. 264-272.

[88]. DeRousseau, M., Kasprzyk, J., and Srubar III, W., *Computational design optimization of concrete mixtures: A review.* Cement and Concrete Research, 2018. **109**: p. 42-53.

[89]. C A Padmanabha Reddy, Y., Viswanath, P., and Eswara Reddy, B., *Semi-supervised learning: a brief review.* 2018, 2018. **7**(1.8): p. 5.

[90]. Abiodun, O.I., Jantan, A., Omolara, A.E., Dada, K.V., Mohamed, N.A., and Arshad, H., *State-of-the-art in artificial neural network applications: A survey.* Heliyon, 2018. **4**(11): p. e00938.

[91]. Roshani, M.M., Kargar, S.H., Farhangi, V., and Karakouzian, M., *Predicting the effect of fly ash on concrete's mechanical properties by ann.* Sustainability, 2021. **13**(3): p. 1469.

[92]. Boğa, A.R., Öztürk, M., and Topcu, I.B., *Using ANN and ANFIS to predict the mechanical and chloride permeability properties of concrete containing GGBFS and CNI.* Composites Part B: Engineering, 2013. **45**(1): p. 688-696.

[93]. Ince, R., *Prediction of fracture parameters of concrete by artificial neural networks.* Engineering Fracture Mechanics, 2004. **71**(15): p. 2143-2159.

[94]. Sarıdemir, M., *Predicting the compressive strength of mortars containing metakaolin by artificial neural networks and fuzzy logic.* Advances in Engineering Software, 2009. **40**(9): p. 920-927.

[95]. Behnood, A. and Golafshani, E.M., *Predicting the compressive strength of silica fume concrete using hybrid artificial neural network with multi-objective grey wolves.* Journal of Cleaner Production, 2018. **202**: p. 54-64.

[96]. Atici, U., *Prediction of the strength of mineral admixture concrete using multivariable regression analysis and an artificial neural network.* Expert Systems with applications, 2011. **38**(8): p. 9609-9618.

[97]. Chopra, P., Sharma, R.K., and Kumar, M., *Prediction of compressive strength of concrete using artificial neural network and genetic programming.* Advances in Materials Science and Engineering, 2016. **2016**.

[98]. Ahmad, A., Ostrowski, K.A., Maślak, M., Farooq, F., Mehmood, I., and Nafees, A., *Comparative Study of Supervised Machine Learning Algorithms for Predicting the Compressive Strength of Concrete at High Temperature.* Materials, 2021. **14**(15): p. 4222.

[99]. Abbas, H., Al-Salloum, Y.A., Elsanadedy, H.M., and Almusallam, T.H., *ANN models for prediction of residual strength of HSC after exposure to elevated temperature.* Fire safety journal, 2019. **106**: p. 13-28.

[100]. TÜRKMEN, İ., BİNGÖL, A., TORTUM, A., Demirboga, R., and Guel, R., *Properties of pumice aggregate concretes at elevated temperatures and comparison with ANN models.* 2017.

[101]. Moradi, M., Daneshvar, K., Ghazi-Nader, D., and Hajiloo, H., *The prediction of fire performance of concrete-filled steel tubes (CFST) using artificial neural network.* Thin-Walled Structures, 2021. **161**: p. 107499.

[102]. Öztaş, A., Pala, M., Özbay, E.a., Kanca, E., Caglar, N., and Bhatti, M.A., *Predicting the compressive strength and slump of high strength concrete using neural network.* Construction and building materials, 2006. **20**(9): p. 769-775.

[103]. Haykin, S. and Lippmann, R., *Neural networks, a comprehensive foundation.* International journal of neural systems, 1994. **5**(4): p. 363-364.

[104]. Topçu, İ.B. and Sarıdemir, M., *Prediction of rubberized concrete properties using artificial neural network and fuzzy logic.* Construction and Building Materials, 2008. **22**(4): p. 532-540.

[105]. Mansour, M.Y., Dicleli, M., Lee, J.-Y., and Zhang, J., *Predicting the shear strength of reinforced concrete beams using artificial neural networks.* Engineering Structures, 2004. **26**(6): p. 781-799.

[106]. Demir, F., *Prediction of elastic modulus of normal and high strength concrete by artificial neural networks.* Construction and Building Materials, 2008. **22**(7): p. 1428-1435.

[107]. Çelik, Ö., Teke, A., and Yıldırım, H.B., *The optimized artificial neural network model with Levenberg–Marquardt algorithm for global solar radiation estimation in Eastern Mediterranean Region of Turkey.* Journal of cleaner production, 2016. **116**: p. 1-12.

[108]. Zhang, J.-R., Zhang, J., Lok, T.-M., and Lyu, M.R., *A hybrid particle swarm optimization–back-propagation algorithm for feedforward neural network training.* Applied Mathematics and Computation, 2007. **185**(2): p. 1026-1037.

[109]. Elbahy, Y.I., Nehdi, M., and Youssef, M.A., *Artificial neural network model for deflection analysis of superelastic shape memory alloy reinforced concrete beams.* Canadian Journal of Civil Engineering, 2010. **37**(6): p. 855-865.

[110]. Moradi, M., Khaleghi, M., Salimi, J., Farhangi, V., and Ramezanianpour, A., *Predicting the compressive strength of concrete containing metakaolin with different properties using ANN.* Measurement, 2021. **183**: p. 109790.

[111]. Silva, F.A., Delgado, J.M., Cavalcanti, R.S., Azevedo, A.C., Guimarães, A.S., Lima, A.G., and Uva, G., *Use of Nondestructive Testing of Ultrasound and Artificial Neural Networks to Estimate Compressive Strength of Concrete.* Buildings (2075-5309), 2021. **11**(2).

[112]. Benardos, P.G. and Vosniakos, G.C., *Optimizing feedforward artificial neural network architecture.* Engineering Applications of Artificial Intelligence, 2007. **20**(3): p. 365-382.

[113]. Liu, Q.-f., Iqbal, M.F., Yang, J., Lu, X.-y., Zhang, P., and Rauf, M., *Prediction of chloride diffusivity in concrete using artificial neural network: Modelling and performance evaluation.* Construction and Building Materials, 2021. **268**: p. 121082.

[114]. Golafshani, E.M., Behnood, A., and Arashpour, M., *Predicting the compressive strength of normal and High-Performance Concretes using ANN and ANFIS hybridized with Grey Wolf Optimizer.* Construction and Building Materials, 2020. **232**: p. 117266.

[115]. Ramadan Suleiman, A. and Nehdi, M.L., *Modeling Self-Healing of Concrete Using Hybrid Genetic Algorithm–Artificial Neural Network.* Materials, 2017. **10**(2): p. 135.

[116]. Šipoš, T.K., Miličević, I., and Siddique, R., *Model for mix design of brick aggregate concrete based on neural network modelling.* Construction and building materials, 2017. **148**: p. 757-769.

[117]. Getahun, M.A., Shitote, S.M., and Abiero Gariy, Z.C., *Artificial neural network based modelling approach for strength prediction of concrete incorporating agricultural and construction wastes.* Construction and Building Materials, 2018. **190**: p. 517-525.

[118]. Tran, V.-L., Thai, D.-K., and Nguyen, D.-D., *Practical artificial neural network tool for predicting the axial compression capacity of circular concrete-filled steel tube columns with ultra-high-strength concrete.* Thin-Walled Structures, 2020. **151**: p. 106720.

[119]. Yüzer, N., Akbaş, B., and Kızılkanat, A.B. *Predicting the compressive strength of concrete exposed to high temperatures with a neural network model*. in *TÇMB, 3rd International Symposium Sustainability in Cement and Concrete, İstanbul*. 2007.

[120]. Goh, A.T., *Back-propagation neural networks for modeling complex systems.* Artificial intelligence in engineering, 1995. **9**(3): p. 143-151.

[121]. Fu, Y., Wong, Y., Poon, C.S., and Tang, C., *Stress–strain behaviour of high-strength concrete at elevated temperatures.* Magazine of Concrete Research, 2005. **57**(9): p. 535-544.

[122]. Chan, Y.N., Peng, G.F., and Anson, M., *Residual strength and pore structure of high-strength concrete and normal strength concrete after exposure to high temperatures.* Cement and Concrete Composites, 1999. **21**(1): p. 23-27.